aerospace

MDPI

Review

Review of Rotary-Wing Morphing Actuation Systems

Mars Burke * and Alvin Gatto

Mechanical and Aerospace Engineering Department, College of Engineering, Design and Physical Sciences, Brunel University of London, Uxbridge, London UB8 3PH, UK; alvin.gatto@brunel.ac.uk
* Correspondence: mars.burke@brunel.ac.uk

Abstract

A review of morphing actuation systems in relation to rotary-wing aerial platforms is presented. The research highlights an inadequate maturation of rotary actuation systems, characterised by a scarcity of (1) comprehensive full-scale experimental research relative to non-rotary (fixed-wing) systems, (2) techniques used for rotary actuation systems and (3) implementation of full-chord morphing systems, with existing research only utilising partial-chord actuation techniques. Additionally, another notable shortcoming is presented to be the lack of comprehensive proportional investigation in the proposed five-step development process for rotary actuation designs. A comprehensive critical review is offered, covering the following challenges of progressing through this development process for rotary actuation systems from conceptual design to production: (1) numerical and computational studies, (2) small-scale wind-tunnel testing, (3) full-scale wind-tunnel testing, (4) demonstrator, and ultimately (5) fabrication for industrial implementation. The review examines several existing rotary actuation systems, including (but not limited to) leading-edge, trailing-edge and Gurney flaps; active twist; chord extension; variable span and camber systems. Comparisons are made between rotary morphing actuation systems and their non-morphing counterparts, highlighting the distinct difficulties encountered by rotary-wing systems due to the more complex and challenging operational conditions found in rotorcraft. The review reveals that a significant portion of existing research on rotary-wing systems has focused only on early-stage development, including computational modelling and sub-scale wind-tunnel experiments, underscoring the necessity for more comprehensive full-scale testing and prototype evaluation given that only a small number of studies have progressed to full-scale wind-tunnel testing or actual prototype evaluation, with only one example identified as having been tested on a production helicopter. In addition, a comparative Technology Readiness Level (TRL) assessment is presented for both rotary-wing and fixed-wing morphing actuation systems, enabling a structured evaluation of relative technology maturity, experimental validation depth, and proximity to operational implementation. Building upon this assessment, a morphing Actuation Concept-Transfer Feasibility (ACTF) study is also provided, examining the potential for adapting mature fixed-wing morphing actuation technologies for application in rotary-wing environments, while identifying the key structural, aerodynamic, and operational constraints that currently limit direct technology transfer. This study addresses and proposes opportunities for a novel rotary actuation system design and concludes by suggesting the potential for future research on more effectual systems to include full-chord configuration over larger spanwise blade footprints with innovative actuation mechanisms that could be utilised and progressed through all development stages from numerical studies to full-scale fabrication.

Academic Editor: Ioannis Goulos

Received: 20 January 2026
Revised: 15 February 2026
Accepted: 18 February 2026
Published: 23 March 2026

Keywords: actuation systems; rotary morphing; adaptive structures; rotational aerodynamics; rotorcraft morphing

1. Introduction

The concept of morphing in aviation is not new. The Wright Flyer, a pioneering aircraft that marked the beginning of modern aviation, utilised wing morphing through a system of cables and pulleys for roll control [1]. This simple yet ingenious mechanism was effective due to the combination of the low flight speed of the craft and the use of flexible wings, establishing morphing as feasible in the early days of powered flight. However, as aircraft performance demands grew (i.e., requiring greater speed, altitude, and range), the need for more rigid structures became essential. As a result, morphing techniques largely fell out of favour, given their inability to withstand more demanding external forces and moments. Nevertheless, morphing technology has gradually re-emerged and evolved over the last century. Despite this renewed focus, few full-scale morphing concepts have been widely adopted, with actuation methodologies beyond traditional hydraulic and electric systems remaining scarce.

This review seeks to address a gap in the current rotary morphing actuation system literature by providing a targeted examination of morphing technologies, particularly with an emphasis on rotary actuation mechanisms and techniques. It aims to offer meaningful comparisons, highlighting key advantages and disadvantages, while also identifying areas where implementation and technical understanding may still be lacking. This focused approach is intended to support broader efforts in exploring the full scope of morphing actuation concepts, which is not currently covered within the existing literature.

As outlined by [2], a set of conflicting requirements exists that needs careful examination, particularly in the context of morphing actuation systems. These systems integrate various sub-elements within a structural framework to provide adaptive capabilities in response to external changes while maintaining adequate structural integrity. Overall, morphing systems generally consist of five essential elements (as illustrated in Figure 1): a skeletal structure, an actuation system, a skin, a sensor network, and a control system. Among these, the interactions between the skin–skeleton and skeleton–actuation elements are particularly crucial, presenting significant challenges when studied collectively. The skeletal structure and actuation system are inherently linked, with the skeleton maintaining the shape during transitions and the actuation system facilitating the deformation. These interactions typically involve complex interconnections that define the system's overall kinematics. As such, the effectiveness of any morphing design heavily depends on the type, configuration, and power requirements of the actuation mechanism. Additionally, in many examples, the actuation system is load-bearing given its integration with the skeletal structure itself, particularly in simpler kinematic chains where it can carry up to 100% of the load. Traditional components like flaps, slats, and ailerons fall into this category, where innovation is primarily focused on integrating actuators within the main body, ensuring near-seamless operation. However, this leads to the mentioned paradox: greater numbers of actuators ensure even load distribution and effective operation but at the cost of complexity, integration challenges, and maintenance requirements. Conversely, fewer actuators simplify the system but may compromise performance and reliability. Resolving this paradox remains a critical gap in the fundamental understanding of any integrated actuation system.

As described by [2] and as illustrated in Figure 2, this paradox is highlighted by comparing the two systems: the first with few actuators and the other with many. The

former offers benefits such as lower weight, reduced risk of failure, and longer inspection intervals but has limited geometric flexibility and requires larger unit volumes. In contrast, the latter enhances geometric adaptability with reduced unit volume but increases overall weight, risk of failure, and maintenance demands. The primary purpose of any actuation system is to enable controlled deformation of a structure, a function utilised across various industries, particularly aerospace and robotics. Actuation hardware and systems can vary widely in form, size, and capability, employing technologies underpinned by electric, pneumatic, hydraulic, magnetic, thermal, and mechanical methods. These systems often include additional components that work together to achieve the desired deformation, speed, and control, complementing the core actuator by sensing the current state and providing necessary control adjustments. One of the main aims of this work is to highlight the ongoing challenges and opportunities within this field, aiming to address the existing gaps requiring more focus and advance underlying understanding. The current literature's rotary-wing morphing examples appear to suggest that the term "morphing" is referred to in the broader terms as any means that increases performance (e.g., envelope expansion, control load adjustment, etc.) or lowers vibrations or noise.

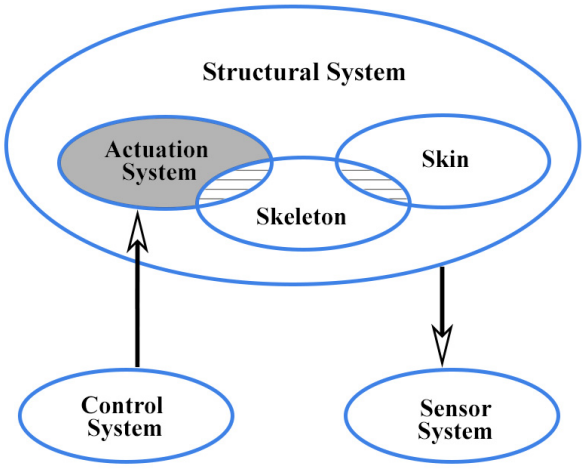

Figure 1. Illustration highlighting how the actuation system fits within a generic adaptive structure [2].

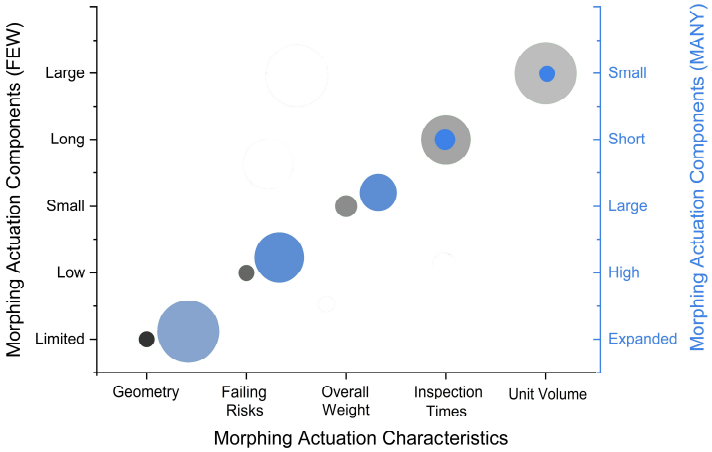

Figure 2. Qualitative comparison of two sets of morphing actuation configurations, one with "few" components and the other with "many," and how the number of components affects characteristics like geometry, weight, inspection times, size, and volume.

As a result, a wide range of research from numerical concepts to flight testing (including whirl stand and wind-tunnel tests) is reviewed and presented in order to identify

the gaps in rotary morphing actuation technologies. Consistent with existing research [2], multiple technologies have been studied and continue to be examined for rotary morphing actuation, and they are primarily grouped into seven main categories: (1) flaps (trailing-edge flaps, Gurney flaps, and leading-edge flaps); (2) active or variable twist; (3) variable span; (4) variable chord; (5) variable camber; (6) variable nose droop; (7) variable speed. All of these approaches, each with distinct design considerations and performance trade-offs, are considered in this review, along with their corresponding adapted actuation system(s).

2. Literature Review

2.1. Scope, Methodology and Literature Characteristics of This Review

Literature acquisition and data sets: The literature supporting this review was assembled from the primary publication streams used in rotorcraft research, drawing from peer-reviewed indexed journals, technical societies, and specialist conference proceedings. Key sources included the Journal of the American Helicopter Society, AIAA journals and conference papers, the Journal of Intelligent Material Systems and Structures, Progress in Aerospace Sciences, CEAS Aeronautical Journal, The Aeronautical Journal (Cambridge/Royal Aeronautical Society), SPIE Smart Structures and Materials proceedings, and the European Rotorcraft Forum, supplemented by relevant dissertations and technical reports from NASA, the U.S. Army AFDD, DLR, Penn State ARL, and ONR programmes. Across the entire set, approximately 40–45% of references were rotorcraft-specific, 30–35% focused on smart-material or adaptive-structure actuation, 15–20% originated from fixed-wing morphing studies used deliberately as comparators for assessing technology readiness gaps in rotary-wing morphing platforms, and the remaining 5–10% consisted of textbooks, theses and early conceptual studies foundational to modern rotary morphing approaches.

Time span of investigations: The earliest studies included date back to the 1940s, such as the variable-diameter rotor (VDR) and early trailing-edge servo-flap implementations, which represent the first mechanically actuated rotor morphing devices. The most recent works extend to 2025, encompassing high-bandwidth piezoelectric flaps, variable-twist SMA-driven demonstrators, compliant leading-edge morphing systems, variable-span rotor concepts, and recent analyses of integrated actuation and aeroelastic architectures for next-generation rotorcraft.

Inclusion criteria: Studies were included if they met one or more of the following conditions:

1. Primary focus on rotary systems, including helicopter main rotors, tail rotors and high-thrust rotors for e/VTOL platforms.
2. Clear description of actuation technology, structural integration, or morphing mechanism (piezoelectric, SMA, magnetostrictive, pneumatic, compliant and adaptive structures, electromechanical, etc.).
3. Provision of quantitative performance parameters, including flap deflection, twist amplitude, bandwidth, force output, aerodynamic coefficients, or vibration/noise metrics.
4. Experimental, numerical, computational, aeroelastic, or wind-tunnel test validation relevant to rotary systems.
5. Inclusion of fixed-wing morphing studies only when they clarified technology readiness gaps, demonstrated mechanisms later repurposed for rotary systems, or provided transferable actuation architectures (e.g., MFC/SMA mechanisms first demonstrated in fixed-wing platforms).

Finally, while vibration and BVI noise reduction have been the dominant objectives of rotor morphing research, the aerodynamic implications and performance-based evaluations remain comparatively under-reported. This review therefore intends to place greater emphasis on aerodynamic consequences (where possible), informed by the comparative tables developed in this work.

2.2. Trailing Edge, Leading Edge and Gurney Flaps

A morphing rotor blade is not a new or novel idea. The prototype Kaman K-125 first flew with servo flaps in 1947, making it the first example in the broadest definition. The servo flaps, which were set at a 3/4 blade radius, enacted localised twist deformation, changing its shape. Since 1947, when Charles Kaman, founder of Kaman Helicopters, used flaps for primary control of the K-125, they have been subsequently used in helicopter production. The servo flap design itself was simple, consisting of a fully exposed flap attached to the trailing edge of the blade. Given that by design it was aerodynamically balanced, the exposed servo flap facilitated very low control moments. However, the drag created by supporting brackets, the control rod, and the servo flap itself posed a significant disadvantage. As such, plain flaps incorporated within the trailing edge and similar in design to an aileron on a fixed-wing platform are the modern-day evolution. Such systems have been shown to not only reduce noise and vibration [3–5] but also increase performance [6]. This category of trailing-edge morphing systems frequently employs piezoelectric actuators for "on-blade actuation" due to their simplicity, bandwidth, and effectiveness. Based on the use of the piezo effect, and as described by Chopra [7], these systems make use of the application of a voltage to a piezoceramic element to induce in-plane strain. In most examples, utilising piezo-bender or piezo-stacking devices amplifies the displacement effect. Research within this specific category spans benchtop to wind-tunnel testing; however, it predominantly focuses on miniature or scaled models [8–19]. Two previous studies concerning the latter and tested in a wind tunnel were the L–L amplification piezo-stack actuator [20–22] and X-frame actuator [23–25], achieving up to a 10 dB noise reduction [25]. Comparable studies [19–30] also investigated piezo-stack configurations with others using more exotic piezo-stack/mechanical combinations [31–46].

Within the scope of these studies, O. Dietrich et al. [4] investigated a range of trailing-edge flap radial locations and blade lift conditions. In these numerical studies, the flap/blade chord ratio was varied from 10% to 30% with the value of 10% found to achieve the majority of required hub load controllability. Doubling further to 20% resulted in an extra one-third increase with a further dimensioning increase at 30%. The adaptive dynamic systems (ADASYS) rotor used could be equipped with up to three actuation sections (each with a 5.4% blade span footprint) located at r/R = 0.718, 0.773, and 0.827 respectively, with optimal design identified as a flap chord ratio of 15.6%, a flap span ratio of 10.9% and a flap centre position of r/R = 0.745 as illustrated in Figure 3. The aerodynamic observations associated with the actuator design and technique were inherently limited, given the study's emphasis on noise and vibration reduction. That said, the additional lift coefficient (ΔC_L) generated by flap deflection was shown to remain $\lesssim$0.3 for trailing-edge flap angles of approximately +5° above the baseline configuration. At Mach 0.33, the (ΔC_L) increase was ~0.2, rising to ~0.3 at Mach 0.74.

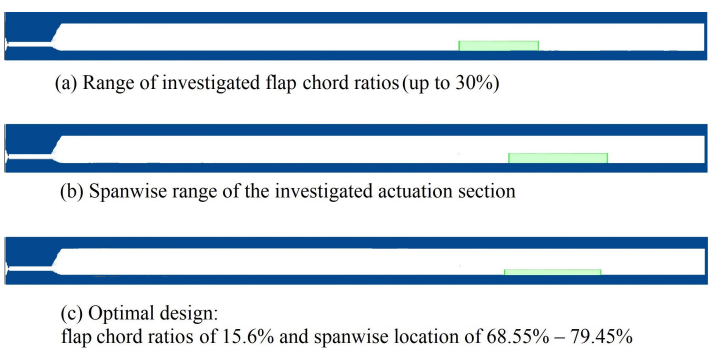

Figure 3. Schematic representation of the rotor blade with (**a**) range of investigated flap chord ratios, (**b**) spanwise range of the investigated actuation system and (**c**) optimal design [4].

Hall and Prechtl [10], developed a piezoelectric servo flap driven by an eight-layer, length-stepped APC-850 bender coupled to the trailing-edge flap through a three-flexure Delrin mechanism that removed hinge friction and backlash (Figure 4). The tapered multilayer design was selected because a uniform bender was limited to ≈56% efficiency, whereas the optimised geometry achieved ≈71% efficiency (near the 75% theoretical limit) while meeting the required 0.06 in^2 cross-section (actual: 0.10 in^2 including electrodes). Bench tests measured 11.5° flap motion at 10 Hz using only six active layers, whilst scaling to eight layers would return ≈12.5° free deflection at 10 Hz. With a measured tip stiffness of 113 $lb{\cdot}in^{-1}{\cdot}in^{-1}$, this corresponded to ≈4.5° aerodynamic deflection at 10 Hz at 90% span for the Mach-scaled rotor, increasing to ≈6.7° when electric fields were raised from 40/20 to 60/30 $V{\cdot}mil^{-1}$. The experimental data suggested that properly scaling and impedance matching the actuator can result in flap deflections greater than 5° while operating at the 90% span location on an operational helicopter. Hall and Prechtl also examined bending modes: the first bending mode was ≈90 Hz (≈6.9 rev^{-1} at 780 RPM); therefore, the bandwidth of the actuator was deemed more than adequate for applications such as HHC.

Key advantages included compact blade integration, high force density, friction-free flexures, and a ~27% bender-efficiency increase (56% → 71%), along with demonstrated ≈±5° usable authority and mode frequencies compatible with advanced rotor control. Limitations involved hysteresis, creep, nonlinear strain–voltage response, and sensitivity to bonding stiffness, which reduced the natural frequency from the predicted 125 Hz to 90 Hz (a major drawback since a lower natural frequency reduces dynamic bandwidth, brings the actuator's resonance closer to the operational harmonic range, and limits the phase margin for closed-loop rotor control). Additional drawbacks were the high-voltage drive levels (up to 300/150 V) and fabrication challenges associated with multilayer piezo-stacks and precise flexure machining. No performance or aerodynamic implications were investigated in this study. Overall, Hall and Prechtl showed that the tapered multilayer bender with a flexure-coupled flap could realistically deliver >5° flap motion at >10 rev^{-1}, making it a credible actuator architecture for active rotorcraft vibration and load control.

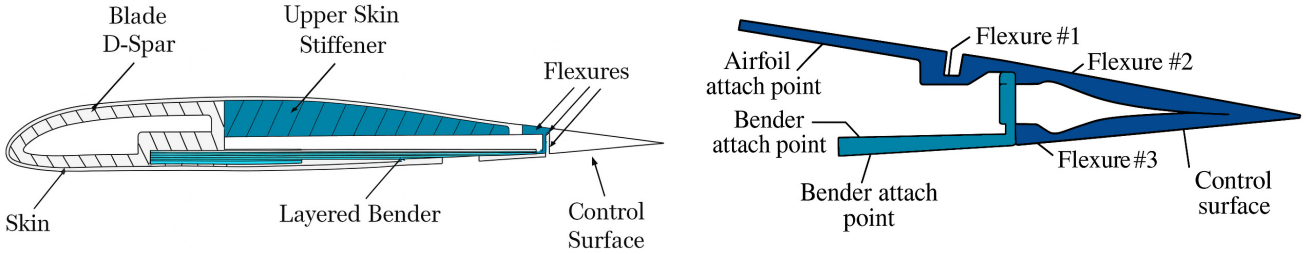

(**a**) (**b**)

Figure 4. Illustrating (**a**) the airfoil section incorporating a piezoelectric bender and (**b**) the design of the flexure mechanism [10].

Fulton and Ormiston [13] carried out an experimental study on a small-scale, two-bladed rotor fitted with on-blade trailing-edge elevons actuated by piezoceramic bimorphs, with the aim of characterising the aeroelastic and structural-dynamic response of the actuators under representative hover loading. The system used 10%-chord elevons of 0.12 R span located at 0.75 r/R, driven by a pair of PZT bimorph cantilevers installed within the blade section. Each bimorph, constructed from parallel-poled PZT-5A layers bonded around a metallic shim, was clamped to the blade spar and coupled to the elevon through low-friction Delrin bearings, slotted fibreglass lever arms, and steel-pin linkages to provide mechanically amplified rotation (Figure 5). The actuators were supplied by Trek high-voltage amplifiers delivering up to 110 Vrms AC with a DC bias to prevent

depolarisation and were exercised using fixed-frequency dwell commands from 5 to 100 Hz as well as logarithmic sine sweeps spanning 1–105 Hz.

The actuation system successfully achieved $\pm 5^{\circ}$ elevon deflection at 760 RPM, surpassing the design goal and confirming the feasibility of smart-material-driven control surfaces in a rotating environment. Elevon authority exhibited the expected quadratic degradation with rotor speed due to increasing aerodynamic hinge moments. However, the elevon pitching-moment coefficient was found to be dramatically lower than thin-airfoil theory predictions: the measured value (~0.25 rad^{-1}) was only ≈45% of the theoretical 0.55 rad^{-1}, a consequence attributed to low Reynolds number effects (~4×10^5) at the active radial station [13]. The approach demonstrated several advantages, including reliable smart-material actuation under centrifugal loading, compact integration without external linkages, high bandwidth, and clean excitation of blade modes for system identification. Its limitations were equally evident: a strong Reynolds number-dependent loss of elevon authority, reversal effects near operating speed, added structural mass of roughly 34% in the active section, and deflection levels well below the 15–20° typically required for primary control without a swashplate [13]. Performance also remained sensitive to friction, available voltage margin, and blade-to-blade variability. Overall, the study shows that PZT-actuated elevons can produce useful aerodynamic control for vibration-related higher harmonic tasks, though significant aerodynamic and structural constraints remain before application to full-authority rotor control.

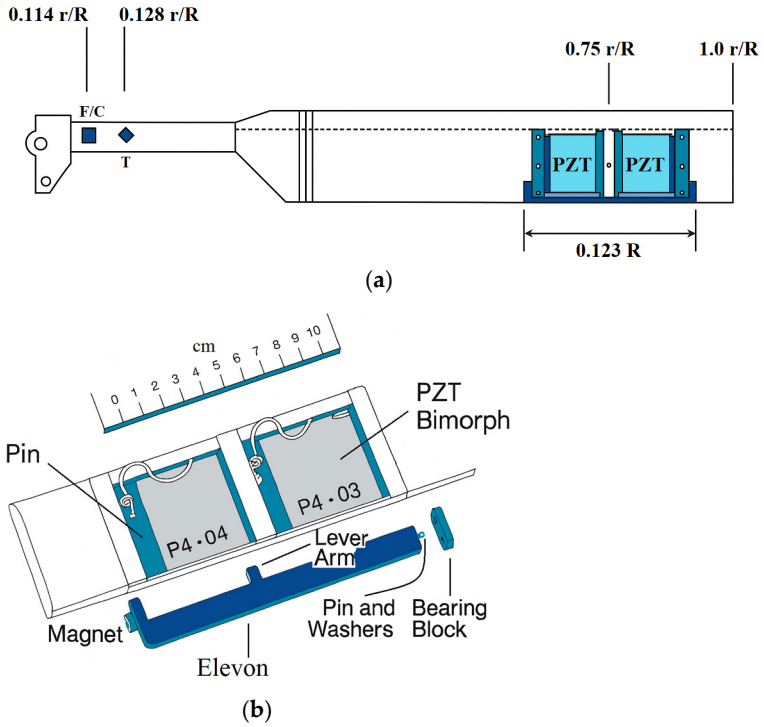

Figure 5. (**a**) Blade planform showing flap (f), chord (c), and torsion (T) strain gauge locations on root flexure, as well as transition, constant blade, and active elevon sections (approximate scale). (**b**) Active elevon section of blade with access panel removed and elevon and hinge pin bearing blocks disassembled [13].

Lee and Chopra [20] developed a piezo-stack-driven trailing-edge flap actuator intended for rotating-blade deployment, motivated by the need for high-force, high-bandwidth smart-material actuation for individual blade control and higher harmonic vibration reduction. The system employed P-804.10 piezo-stacks selected from eleven candidates for their superior force–stroke characteristics under static and dynamic loading

up to 10 ksi and coupled them to the flap through the L–L double-lever amplification mechanism (Figure 6). This architecture (kinematically equivalent to a Watt II six-bar linkage) combined an inner and outer lever (each targeting ~6× amplification) with an elastic coupling that provided preload and returning force. Although the ideal amplification approached 30×, the first prototype achieved a measured factor of 19.4 owing to elastic deformation at endcaps, hinge shafts, and internal interfaces. Bench and spin testing showed ~20 mil free stroke at 100 Vp-p, <10% loss at ~600 g, and a stable response to 50 Hz, confirming feasibility but revealing compliance losses. The second prototype, using five stacks, spherical endcaps, improved Timetal 6-4 and stainless housings, and needle-roller bearings, produced 1.87 mm free stroke at 120 Vp-p, uniform behaviour to 150 Hz, and ~13% loss at 700 g, with no degradation at 115% overload. Under a representative aerodynamic spring load (~40–50 lb/in), the actuator retained ~70% of its free stroke. The assembly remained blade-compatible (~7.2 in × 2.8 in × 0.75 in) and was integrated into a NACA 0012 section for wind-tunnel evaluation. The P-804.10 stack was selected for its required hinge-moment capability, stable strain output across −24 to 120 V, and stiffness on the order of 4.2–4.9 × 10^6 psi, outperforming sheet actuators that lacked force by roughly an order of magnitude.

Advantages included high amplification approaching design intent, >150 Hz bandwidth, robust operation to 700 g, and compact integration without external linkages. Limitations involved deformation-driven efficiency losses in early builds, mass growth from 1.4 to ~2 lb, sensitivity to hinge-offset choices, and stiffness shifts under non-ideal boundary conditions. Overall, the results showed that a piezo-stack-driven L–L mechanism can deliver the stroke, force, and bandwidth needed for high-authority trailing-edge flap control on rotating blades, representing one of the first experimentally validated smart-material actuator systems capable of operating under realistic centrifugal environments.

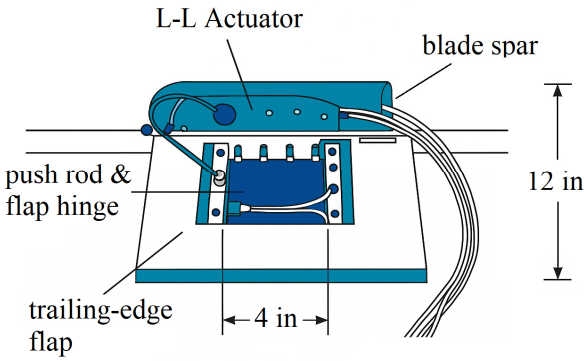

Figure 6. Blade section with trailing-edge flap actuated by the second prototype L–L actuator [20].

Hall and Prechtl [23] investigated a Mach-scaled CH-47D rotor blade incorporating an embedded X-Frame actuator to drive a slotted trailing-edge servo flap via a pushrod, with the aim of confirming stroke, robustness, and bandwidth under model-scale loading. The actuation mechanism consisted of two EC-98 PMN-PT stacks arranged between two crossed frame members joined by a flexural pivot; as the stacks extended, the frames rotated relative to one another, and the shallow stack-frame angle produced the required geometric stroke amplification at the output end. Within the blade, the actuator was mounted using an outboard bolted restraint paired with a spanwise flexure to balance centrifugal loads, while an inboard sliding restraint provided chordwise and flapwise constraint but spanwise freedom (Figure 7). Actuation loads were transmitted through an 0–80 threaded control rod and clevis-horn interface, with a graphite reaction rib reacting to actuation forces and a pre-stress wire functioning simultaneously as the flap shaft, thrust bearing, and actuator preload.

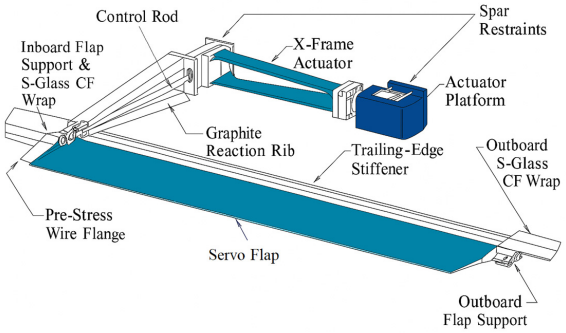

Figure 7. Rotor blade actuation system [23].

Shake-table tests across 7.1–69 g and 22.5–135 Hz, with actuation at 3–67.5 Hz, showed negligible change in stroke: for ~400 V excitation, peak-to-peak deflection remained ~14.3–15.3 mil, with only minor 90 Hz ripple at the highest acceleration levels. When installed in the blade, hinge and clevis friction increased hysteresis and reduced free deflection by ~4°, a loss expected to decrease to ~2° under aerodynamic loading. The actuator alone exhibited a ~650 Hz natural frequency; once coupled to the flap and blade, two modes appeared: a heavily damped ~140 Hz mode influenced by flap inertia and friction and a ~180 Hz mode corresponding to the first torsional mode of the free-root blade. The overall bandwidth exceeded 6/rev, satisfying CH-47 requirements for 4/rev control.

The system's advantages included high amplification in a compact configuration, stable performance across the full acceleration range, and bandwidth compatible with Mach-scale vibration-control objectives. Principal limitations were friction-induced hysteresis, sensitivity to hinge-line fabrication constraints, and incomplete representation of flap inertia in benchtop testing. No performance or aerodynamic implications were investigated in this study. Overall, the X-Frame actuator exhibited the necessary authority and robustness for trailing-edge flap control and was judged capable of maintaining performance under full-scale centrifugal loading.

Straub et al. [30] demonstrated a smart-material actuation system for the MD900 bearingless rotor, integrating a PE-driven trailing-edge flap for high-bandwidth vibration/noise control and an SMA-driven trim tab for quasi-static tracking. The PE actuator used two biaxial PMN–PZT stacks in push–pull, linked through a refined two-stage amplification mechanism (later reduced to a single-stage flexure; Figure 8), enabling large stroke under ≈90 g dynamic and 655 g steady loads. Design revisions improved stack seats, elimination of the second stage and an updated inboard mount increased output by ≈70%, and force–displacement tests indicated required stroke could be met with emerging high-voltage stacks. Bench, shaker, and vacuum spin tests verified stroke, force, and thermal robustness, though early prototypes underperformed relative to predictions.

The SMA system employed two NiTi–10Cu torsion tubes (driver and bias) with combining gears and an active SMA lock for power-off hold. Material testing confirmed the superior cyclic stability of NiTi–10Cu, and successive prototypes improved packaging, tube attachment, and control/sensing. Static–dynamic tests met torque and deflection requirements; bandwidth remained thermally limited, with enhanced cooling (centrifugal pumping, fins, and thermoelectrics) identified as necessary for higher frequency actuation. Flap geometry optimisation (CFD + 0.3 m TCT tests) identified a 25%-chord integral flap, 40% overhang, and 0.1 in LE radius as the configuration providing the lowest measured hinge-moment levels and the highest actuation leverage of all geometries examined. Structural tests confirmed torsional and pitch stiffness assumptions. Aeroelastic simulations predicted >80% vibratory-load reduction with <2° multicyclic flap inputs and ≈5 dB BVI noise reduction with 2°@4/rev, with potential for ≈10 dB using closed-loop control.

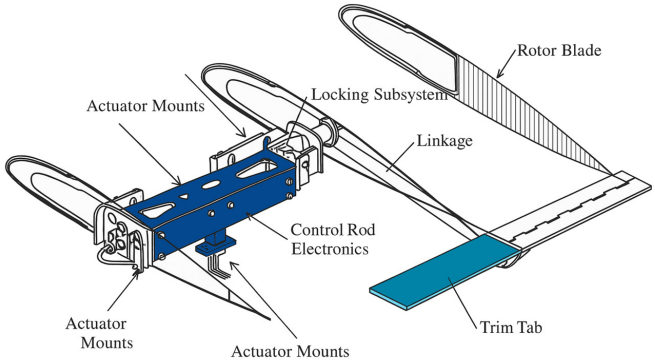

Figure 8. Blade–tab–actuator integration [30].

Advantages included high energy density, compact in-blade integration, modular architecture, limited-authority fail-safe behaviour, and robustness across bench/shake/spin tests. Limitations involved early performance shortfalls, friction sensitivity, high-voltage requirements for PE stacks, SMA bandwidth constraints, and strict MD900 integration envelopes and no further performance or aerodynamic implications were investigated in this study. Overall, the SMART rotor results showed that embedded PE and SMA actuation could deliver the authority, bandwidth, and durability needed for in-blade active control, with successful whirl-tower validation confirming feasibility for future rotorcraft.

Bernhard and Chopra [31] developed and evaluated an active trailing-edge flap system for helicopter rotors using a piezo-induced bending–torsion coupled beam. Two flap types were examined: (1) an integral flap, directly attached to the actuator tip (mechanically simple but limited because flap deflection was capped by the twist achievable over the actuator length) and (2) a plain hinged flap driven via a lever arm, which allowed optimisation through hinge-moment amplification. A drawback of the structural-coupling actuator approach was its low mechanical efficiency (~10%) [31]. Their design studies on small-scale rotor blades (Mach 0.25) showed that, within the thin blade profile, a 546 mm actuator could theoretically provide $\pm 16^\circ$ flap deflection for a 20% chord, 10% span hinged flap using a 12.5:1 amplification ratio. The integral flap, however, achieved only $\pm 2.1^\circ$ for a 20% chord, 20% span configuration. A proof-of-concept beam generated $\pm 0.45^\circ$ twist at 315 V/mm with negligible bending, matching analysis within 12.5%. When integrated into a 1/8th-scale blade with a 20% chord, 3% span flap at 0.9R (Figure 9), the actuator produced $\pm 1.25^\circ$ twist at zero RPM and $\pm 2^\circ$ flap motion in hover at 900 RPM and up to 8° collectively, using only 50% of the PZT voltage limits, indicating substantial remaining authority. Overall, the work demonstrated the feasibility of a compact, structurally coupled piezoelectric twist actuator for smart-rotor trailing-edge flaps, particularly valuable for small-scale rotor tests.

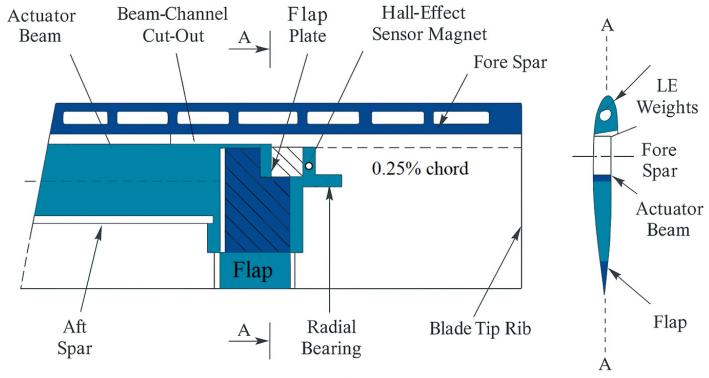

Figure 9. Detail schematic of the rotor blade with the integral trailing-edge flap (20% chord, 3% span) [31].

Clement et al. [33] developed an active rotor blade trailing-edge flap system actuated by serial/parallel piezoceramic C-block stacks, each stack containing eight PZT-5H half-tube C-blocks in series, with two stacks arranged in a parallel (pull–pull) configuration (Figure 10). Two C-block actuators drove a balanced active rotor blade flap to suppress the vibrations of a helicopter rotor blade. The curved unimorph geometry provided internal mechanical leverage, yielding 2.7× higher force and ≈8% higher mechanical work than an equivalent straight bender. Static testing demonstrated predictable performance: the 92–101 μm free deflection at 150 V was slightly lower than analytical predictions (within ≈5%), and the 9.2–10.1 N blocking force was also just below the model (within ≈2.6%), confirming strong model–experiment agreement while still delivering high force output for a piezoceramic actuator of this size.

Advantages of the actuation system included high authority in a compact form, strong model–experiment agreement, and excellent dynamic performance. Flap motion remained ≥8° peak-to-peak (pp) from 0 to 40 Hz, reaching 11.6–13.6° pp at 40 Hz and extrapolating to ≈20° pp at the 340V limit. Disadvantages included sensitivity to bond-line thickness (~40% variation), which alters stiffness and output, as well as creep (slow, time-dependent, nonlinear change in deformation when a constant voltage or load is applied), hysteresis (output lags and differs for rising vs. falling voltage), and friction losses, which reduced integrated quasi-static flap motion from 9.6° pp (static) to 8.4° pp. Dynamic performance was also influenced by preload-induced frequency shifts, requiring careful tuning to avoid adverse mode interactions. Overall, Clement et al. demonstrated that C-block piezoceramic actuators provide the bandwidth, authority, and robustness needed for active rotor blade trailing-edge flap systems, with strong performance margins despite some fabrication and dynamic sensitivities.

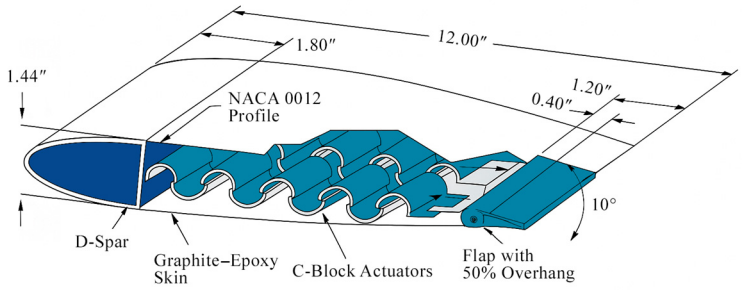

(**a**)

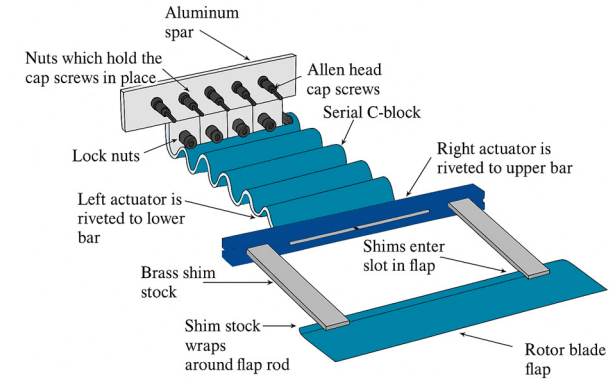

(**b**)

Figure 10. (**a**) Active flap system design. (**b**) Integration of actuators with blade section [33].

Similarly, Fenn et al. [47] investigated the applicability of magnetostrictive actuators (specifically Terfenol-D) to reduce helicopter vibration by actuating trailing-edge flaps on the UH-60A Black Hawk rotor blade. These actuators leverage the material's ability to deform under a magnetic field, effectively converting linear motion into rotational movement for flap control. They also used a Terfenol-D rod enclosed by an electric coil surrounded by a permanent magnet. When current passes through the coil, it generates a magnetic field that induces strain in the Terfenol-D rod, producing linear motion. This motion is translated into flap rotation via mechanical linkages. Several actuators were placed along the span, each controlling specific flap segments to reduce vibration (Figure 11). The baseline design used 17.5% chord flaps spanning $0.52 < r/R < 0.98$ with each actuator including two magnetostrictive struts producing chordwise motion that, with appropriate lever arms, rotated the flap. Struts were configured to maximise energy efficiency and fit within the existing blade structure, with a total of 24 actuators (weight ~95 lbs or 0.5% total gross weight). Overall, this work demonstrated ~90% reduction in vibration whilst reducing maintenance needs.

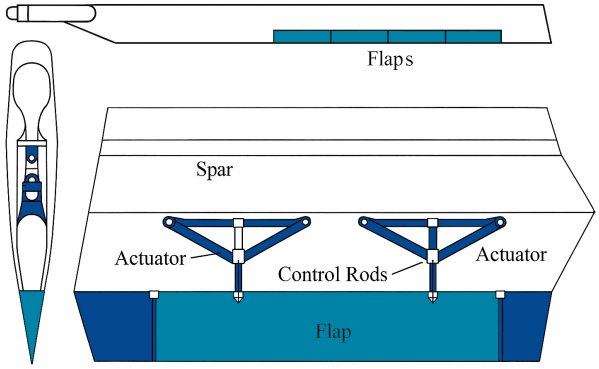

Figure 11. Schematic of the magnetostrictive actuator and TE flaps [47].

While piezo-based trailing-edge flaps have been deployed within rotary-wing applications, it is of note that a variety of techniques have also been explored for fixed-wing platforms. These include similar piezo-stack use [48–62], more traditional motor and cam systems [48,49], and magnetostrictive-based examples [49,50] as well as electromagnetic and electromechanical [50,51,56–58], hydraulic [53], hybrid piezoelectric [54,55], and traditional pneumatic systems [59–62]. Section 3.3 covers each of these in more detail.

Bothwell et al. [63] investigated the magnetostrictive variant in combination with an extension–torsion composite coupling to actuate a trailing-edge flap in an attempt to actively control vibration. Constructed from a Terfenol-D rod surrounded by an electric coil and a permanent magnet, when the coil is energised, an induced strain develops within the rod. Imparting rod pre-stress was identified to enhance the bidirectional motion capabilities of the setup, with both twist and axial displacement used. Figure 12 provides further context. To enact twist, the end of a Kevlar–epoxy composite tube was fixed to the actuator core with a low-melting-point alloy, enabling free rotation with commanded axial force generation. A bidirectional twist magnitude of ~0.19 was demonstrated but this variant was found to be inferior to the use of piezo-stacks deployed in a similar manner, with the latter producing superior induced twist and force magnitudes (i.e., ~0.62 degrees and 51.4 lb respectively), about three times the output of the magnetostrictive variant.

Here, the piezo-stack actuator consisted of many thin PZT layers bonded mechanically in series, each layer straining in its thickness direction (d_{33}-mode) under applied electric field; the cumulative through-thickness expansion generated a high-force, low-stroke axial extension, maintained in compression by a pre-stress frame to protect the brittle ceramic and allow controlled bidirectional actuation. Beyond the baseline comparison, Bothwell,

Chandra, and Chopra [63] showed that the magnetostrictive actuator produced roughly 190 lb of force and 1.25 mil of free stroke (generated only 0.089–0.102° of twist in a [20/-70]s tube and about 0.19–0.20° in the more responsive $[11]_2$ tube), and a two-ply Kevlar–epoxy lay-up was designed to convert axial loading into twist more effectively. When the same tubes were driven by a piezoelectric stack, the results improved markedly. A representative stack (787 lb block force; 3.54 mil stroke at 1000 V) produced 0.34°/45 lb in the [20/-70]s tube and 0.62°/51.4 lb in the $[11]_2$ tube, showing a consistent threefold increase (3:1) in twist and force compared to the magnetostrictive device. Here the [20/-70] denotes extension–torsion coupling and $[11]_2$ refers to a two-ply unidirectional Kevlar–epoxy lay-up at 11°, selected for its high extension–torsion coupling (not to be confused with a reference/citation).

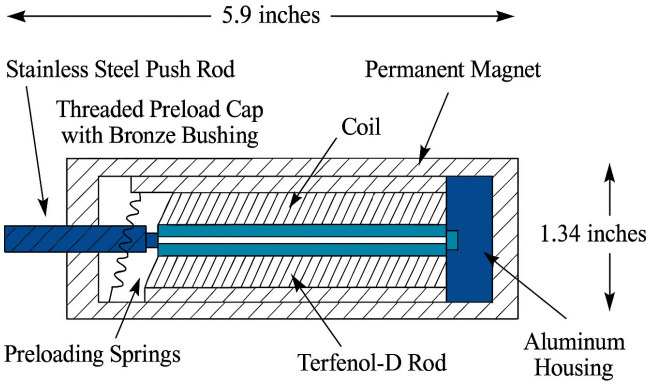

Figure 12. Schematic of the magnetostrictive actuator [63].

Duvernier et al. [64] focused on exploring an electromagnetic actuator for controlling a similar trailing-edge flap to again reduce noise and vibration. This actuator used a variable electromagnetic field created by a coil together with permanent magnets to produce a linear displacement with near-consistent force across its entire stroke. A Terfenol-D rod was again encased within the electric coil with overall mass being 1.4 kg. Both static and dynamic testing was conducted using a PWM switching amplifier powered by a 48VDC supply to allow for precise control and monitoring (i.e., position, speed, input current, etc.). While the system faced various challenges (i.e., friction hysteresis, magnetic stiffness, high mass, fatigue, etc.), the tests showed that the actuator could deliver stable and repeatable force over its operating range and maintain nearly constant output across the stroke, which was a clear operational benefit. However, the weight penalty, energy losses, and hysteresis-driven control difficulties heavily restricted achievable flap authority and limited its suitability for higher-frequency actuation. Overall, the study demonstrated that although electromagnetic actuation was feasible and functionally reliable, its mass, stiffness effects, and durability concerns made it less attractive than lighter, higher-bandwidth smart-material solutions for integration into rotor blade trailing-edge flap systems.

An active trailing-edge flap (TEF) system using Pneumatic Artificial Muscles (PAMs) was tested on a Bell 407 scale rotor model by Woods et al. [65]. This system aimed for large deflections (±20 degrees) at 1 rev/s as a primary control system and smaller deflections up to 5 rev/s for vibration mitigation. The setup included an antagonistic pair of PAMs at the root of each blade, connected to the flap via a bell crank and linkage system, ultimately converting force into flap rotational motion (Figure 13). Tested at flight speeds up to Mach 0.3 with actuation frequencies from 0.1 to 40 Hz, this system achieved nearly ±40° of flap deflection over a pitch angle range from −6° to 9° and demonstrated significant control authority and performance potential despite highlighted response time limitations and durability concerns.

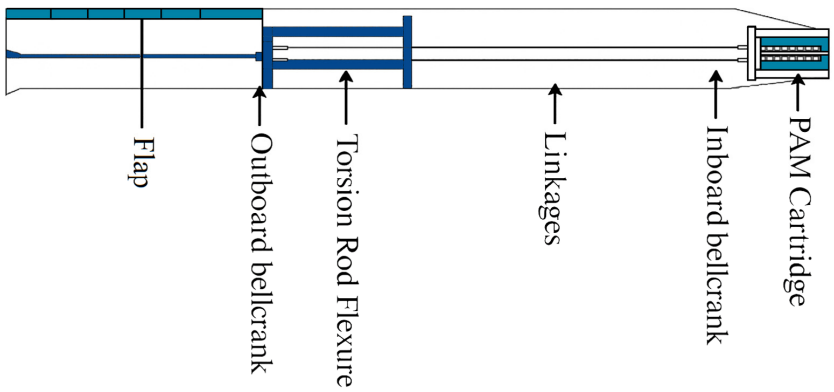

Figure 13. Schematic of the PAM-TEF actuator [65].

The use of actively deployed Gurney flaps within rotary-wing platforms is also prevalent in training-edge devices. As highlighted by Concilio et al. [2], approximately 2% of the chord length is sufficient for an increase in airfoil $C_{L\text{-}Max}$ of up to 30% and ultimately for an improvement in overall performance [2,66,67]. Along this theme, Woodgate et al. [68] also demonstrated that compared to fixed-wing use, the application of a Ggurney flap for rotary-wing applications was much more challenging and complicated, particularly if high-fidelity data was desired. The overall methodology utilised detailed simulations in an attempt to optimise the size, location, and length parameters of a Gurney flap installation. Results demonstrated an increase in rotor thrust of ~7.4% in selected configurations but with the side effect of an average ~20% increase in nose-down around the azimuth requiring careful design consideration to mitigate adverse effects on blade stability and control.

A variable boundary condition technique was also considered, in which dynamic adjustment of the flap position to better optimise aerodynamic performance was also considered. During this investigation, the Gurney flap was modelled as a thin surface integrated into the mesh itself, with movement controlled by altering boundary conditions rather than physical mesh deformation. The computational setup employing the variable boundary condition approach proved effective, enabling flap motion to be represented without mesh deformation while preserving solution fidelity. Overall, both methodologies indicated that while the use of such flaps could enhance lift and thrust, they also could introduce significant drag and pitching moments that needed careful consideration.

Gagliardi and Barakos [69] further investigated the use of deployable trailing-edge flaps to improve hover performance of low-blade-twist configurations, aiming to combine the low-blade-twist advantages for forward flight with those of the highly twisted blade benefits in a hover flight regime. Using a combination of blade element modelling and high-fidelity RANS CFD, they assessed various fixed-flap configurations, focusing on blade spanwise location, chord, deflection angle, and span.

They found the optimal design was an inboard slotted flap at 24% span, 32% chord, and 10° deflection located at 48% of the blade radius (Figure 14), which improved the figure of merit by up to 4.7%, matching the performance of a blade with 6° more twist. Further outboard combinations showed limited or even negative effects, particularly in high-thrust scenarios, with a blended, more inboard flap suitable for practical applications. This particular configuration was found to achieve up to an additional 6.5% performance gain, matching the performance of a $-10°$ twisted blade with a reduced trim angle of up to 1°. The study in particular highlighted the potential of passive flap integration to enhance hover performance without unduly compromising forward flight performance, although increased wake interactions and structural complexity were cited as notable challenges requiring further consideration.

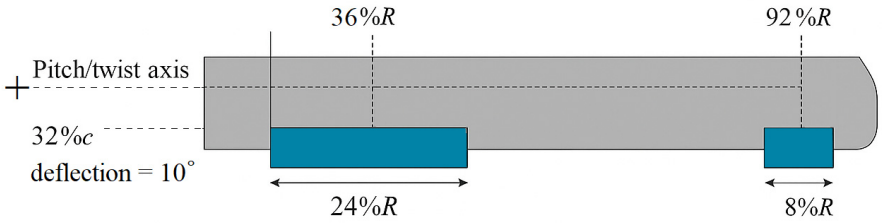

Figure 14. Schematic and deployment schedule for trailing-edge flap in hover [69].

Kim, Wang, and Smith [70] developed a resonant trailing-edge flap actuation system using a piezoelectric induced-shear tube actuator to enhance helicopter rotor vibration control (Figure 15). By tuning the actuator–flap system to resonate at 4/rev (26.6 Hz), they significantly increased flap authority (achieving up to 4.5° deflection, a 2.1–3.5× improvement over non-resonant setups). A digital signal processor (DSP) was used to emulate a high-voltage electric network, broadening bandwidth and improving robustness. An adaptive controller effectively tracked phase variations near resonance. The system showed strong potential for multi-flap higher harmonic control (HHC), though concerns remain around fatigue and heating under resonant operation.

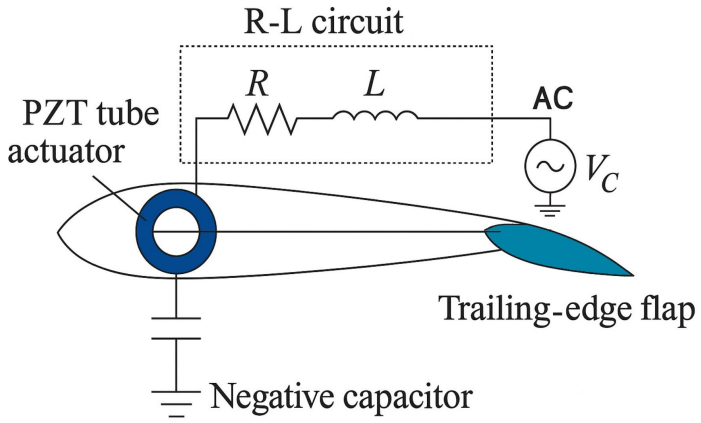

Figure 15. Schematic of the PZT tube actuator with circuitry [70].

Chia et al. [71] developed a coupled aeroelastic–acoustic framework known as AVINOR/HELINOIR to simulate and control in-plane rotorcraft noise. This framework utilised on-blade trailing-edge plain flaps actuated via higher harmonic control (HHC). The system employed adaptive, closed-loop control based on feedback from either far-field or near-field microphones. The optimal performance was achieved using a 20%-chord flap. Two configurations were studied: a single-flap setup with a 0.12R span, centred at 0.75R, and a dual-flap system consisting of two 0.06R flaps at 0.72R and 0.92R (Figure 16). The dual-flap setup provided broader noise reduction coverage and reduced vibration penalties compared to the single-flap setup. The left boom was identified as the optimal onboard feedback location, achieving up to 6 dB in-plane noise reduction, which is comparable to far-field results. However, all configurations resulted in trade-offs. Significant out-of-plane noise increases (up to 18 dB) and vibration penalties were observed; in particular, the vertical hub shear increased by 14% with far-field feedback and 47.1% with the near-field left boom. The study demonstrated that actively controlled flaps can effectively generate anti-noise loading to suppress in-plane noise but at the cost of increased structural loads and potential performance penalties. Additionally, the system adds complexity through controller tuning and actuator saturation constraints, and its effectiveness is sensitive to sensor placement and specific flight conditions.

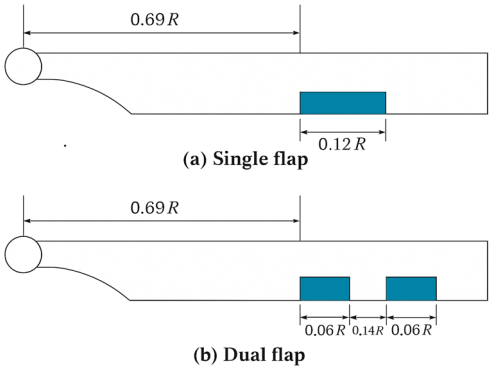

Figure 16. Schematic configurations of the plain flap on the rotor blade [71].

Feinerman et al. [72] conducted an experiment to investigate the use of passive leading-edge serrations on rotor blades to reduce blade–vortex interaction (BVI) noise. They used a controlled gust-based simulation, known as the Blade-Controlled Disturbance Interaction (BCDI), in a hover test environment (Figure 17). The experiment compared a serrated blade with a sinusoidal leading-edge geometry to a conventional straight-edge blade at full-scale tip Mach numbers. The results showed a peak-to-peak noise reduction of up to 3 dB in the primary radiation direction for parallel BVIs. However, broader but smaller reductions were observed in oblique interactions. The serrations altered the phasing of the spanwise acoustic sources, leading to partial destructive interference and widened acoustic pulses. Theoretical modelling supported the experimental findings, highlighting phase cancellation as the primary mechanism. Nevertheless, the design has some disadvantages, including limited effectiveness of noise reduction, primarily near peak radiation directions, and non-optimal aerodynamic response of the serrated blade, which may introduce performance penalties or aerodynamic inefficiencies. The design was also sensitive to the type and geometry of BVI encounter, suggesting that more refined or adaptive geometries may be necessary for operational effectiveness.

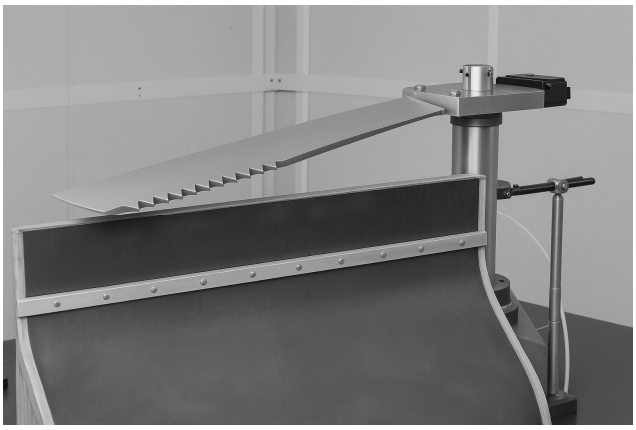

Figure 17. Schematic representation of the gust generator nozzle, testing rig and serrated rotor blade [72].

2.3. Active and Variable Twist

Active flap actuation systems attenuate rotor forces in two ways: a direct lift increase due to flap deflection and increased pitching moment, which causes the rotor blade to twist elastically. Direct active adjustments of the blade twist are another approach to achieve this type of rotor force management. This blade twist variation can be dynamic (N − 1, N, N + 1/rev frequencies) or quasi-static (N − 1, N, N + 1/rev frequencies (change per flight condition)). While dynamic twist adjustments are designed to minimise rotor system noise

and vibration [26,73,74], quasi-static twist changes can be employed for both performance and potentially vibration reduction [75–79]. Keys, Tarzanin and McHugh [77] focused on the quasi-static twist actuation method to improve both the performance and vibrations of helicopter rotors.

A test was conducted on a 10 ft diameter, four-bladed rotor with Mach-scaled composite blades (blades designed and constructed to replicate the aerodynamic and dynamic characteristics of full-scale blades). The blades, initially with a linear twist of approximately 11.5°, were retwisted to 17.3°. The rotor had a thrust-weighted solidity (σ_T) of 0.1383, a tip taper of 0.6 starting at 95% of the rotor radius, and a quarter chord sweep of 30° at the last 5% of the blade tip. The quasi-static twist aimed to redistribute the aerodynamic loads along the blade span, reducing the high negative angles of attack encountered on the advancing blade tip during forward flight. This modification improved hover and low-speed performance by creating a more uniform downwash velocity, thus reducing the induced power required. The results showed that increasing the twist from 11.5° to 17.3° resulted in a 2.4% increase in figure of merit (FoM) during hover, translating to improved efficiency. On the contrary, in terms of vibration results, the twist modification had a significant impact. The 17.3° twist blade exhibited increased 4/rev hub vibratory loads, with increases ranging from 37.3% to 126% depending on the force components. The flap bending loads increased by 11.3% to 32.4%, chord bending at 0.45R showed a 45% increase, and blade torsion increased by 6% to 11%. Despite the increase in vibratory loads, the overall performance enhancement due to improved aerodynamic efficiency during hover and low-speed flight was deemed beneficial.

The development of a system that can overcome the aerodynamic and dynamic forces faced by the blade while retaining structural integrity is a key issue as active-twist technologies modify the planform of the rotor blade. Because the actuation materials only carry a small portion of the intended load, blade weight suffers. A study by M. Mistry et al. [80] suggested an active rotor blade twist of 12 to 32% of the outboard section (rotor tip) for optimum performance. According to a thorough computational study [81] of the Hover Tip Vortex Structure Test (HOTIS) experiment's best optimised twist angle and locations for rotor blades, the best solution occurs when the difference in the blade twist at r/R = 0.875 from the baseline Liθ1 is around 1–3 degrees and the difference in the blade twist at r/R = 1.0 from the baseline is an Liθ2 of negative value. In particular, in the case of Liθ1 = 2.0 and Liθ2= 3.7 deg, a maximum value of the figure of merit (thrust efficiency under hover conditions) approximately 1.5% higher than the baseline design was achieved. This configuration seems to have weakened the tip vortex strength of the modified blade twist compared to that of the baseline.

Another pivotal investigation that contributed significantly to the development of active/adaptive rotors was by Proctor (1997). Proctor's work [82] marked a critical milestone in the advancement of adaptive rotor technologies. His work demonstrated the use of large solid-state piezoelectric servopaddles, which could achieve deflections up to ±11° (22° peak-to-peak), for adaptive flight control in a rotorcraft. This was one of the first significant demonstrations of morphing rotor technology applied in a flight control context, moving beyond the earlier focus on main rotor blade actuation. Proctor's system introduced active servopaddle flight control, achieving full flight control at speeds exceeding 2/rev. His groundbreaking approach is widely cited as a benchmark in adaptive rotorcraft innovations.

One other notable advancement in adaptive flight control technology utilising piezoelectric actuators was seen with the XQ-138 programme [83], developed by Micro Autonomous Systems (MASs) Corp. The piezoelectric actuators enabled efficient hovering and high-speed transitions in rotorcraft. These actuators converted electrical signals into

mechanical strain, allowing for real-time rotor blade adjustments. Based on US Patent 6,502,787, this actuation system allowed for active load control, improving hover efficiency and allowing speeds of up to 250 knots (≈288 mph/≈463 km/h), while maintaining both fuel efficiency and manoeuvrability. The XQ-138's adaptive flight control system not only reduced mechanical complexity but also offered high-precision control, making it a significant step forward compared to traditional rotorcraft systems. This technology is currently in serial production but remains limited in availability due to its military applications, with special forces from several armed forces around the world using it.

2.3.1. High-Frequency Actuation (Surface-Mounted vs. Internally Mounted)

The literature suggests that surface-mounted actuation systems and internal actuation systems are two subtypes of high-frequency actuation (active-twist rotor) systems/designs [2]. The primary idea of surface-mounted active-twist technologies is to create a shear in the blade, resulting in cross-sectional twist. To achieve this result, piezoceramics must be used to generate longitudinal strain at 45 degrees from the spanwise axis of the blade. Given that piezoceramic sheets create strain along both planar directions when a field of thickness is applied, the first difficulty that needed to be solved was introducing directional strain. Barrett and Chopra's [84] directionally attached piezoelectrics (DAPs) idea was the first recorded effort of a piezo-actuated active-twist rotor blade concept and the starting point for many of the designs that followed [7,85–87]. It was discovered that by employing components with high aspect ratios bonded to the substrate through a thin bank of adhesive, it was possible to inject the majority of the strain created by the piezoelectrics along a predefined path. The testing of these concepts revealed that active-twist technology has a considerable influence on vibratory rotor loads. Parallel to the DAP efforts, MIT researchers were working on the next generation of piezo-actuators, the interdigitated electrode–piezo fibre composites (IDEPFCs), also known as active fibre composites (AFCs). These are made up of piezo fibres with circular cross-sections sandwiched between two layers of interdigitated electrode circuits [88]. Because the interdigitated electrodes allow for equal distribution of the electric field and the piezo fibres function in the more efficient d33 mode, this approach improves actuation strain capability. These were employed in a number of research projects [88–92], most notably NASA/Army/MIT; the active-twist rotor (ATR) and the Boeing advanced material rotor (AMR).

The study [74] revealed that the amount of power required for efficient vibration reduction was a major concern during the development of the active vibration suppression system. With the blade capable of creating a tip twist magnitude of up to 1.5 degrees, the relative insensitivity of the blade actuation as a function of operating state (forward velocity and blade pitch) was demonstrated [93,94]. This discovery demonstrates the significant advancement in actuation performance of the AFC actuation technology over the conventional piezo sheet-driven (DAP) first-generation active-twist rotor blades in less than ten years. The main distinction is that the fibres have a rectangular cross-section created by slicing piezo sheets into thin strips. This method results in more consistent cross-sections and fibre spacing. Such actuators have been employed by NASA Langley, DLR, and others [95–107].

Other actuation solutions incorporated inside the blade have also been investigated by researchers; Bernhard and Chopra [108,109] through a smart active blade tip, which is a bend–twist-linked beam that runs along the blade span (SABT) and Rochettes et al. [110] through a novel active twist rotor blade. Extension–twist-linked composites and actuators were considered by DLR [95,97] (Figures 18 and 19). ONERA explored the TWIstable section closed by actuation (TWISCA) idea [111], which made use of the feature that open-section beams experience cross-sectional warping when subjected to torsional strain. When

compared to MFC actuators (operation voltage 500 V to +1000 V), this actuator system design (operating voltage 20 V to 120 V) showed better active-twist performance per active area, according to this experiment. A shear-introduced twist actuation methodology (AT2), along with the active-twist blade (ATB) actuation method (AT1) were investigated and compared in a study [98]; see (Figure 20).

The shear-introduced twist actuation method functioned by means of piezoelectric actuators embedded into the blade skin, which caused the blade to twist (an introduction of strain in the 45° direction caused a closed cell to twist). Most of the characteristics of the blades were taken from the well-known BO105 model rotor blade. Both ideas have been shown to function while subjected to centrifugal loads; the findings further showed that the shear actuation introduction presented somewhat better results, since there was a better match in the stiffness correlation between the actuator and passive structure. On the negative side, failure safety is one issue that the experimental investigations also revealed will arise during operation. Additionally, the study revealed that even though there are significant efforts being made to create actuators that are better (in terms of electrical shortages), there needs to be a concept for repairing any active-twist blades that will be used in actual helicopter operations.

Figure 18. (**Left**) Top view of the active-twist blade. (**Right**) Detailed view of the multilayer actuators integrated into the blade skin [95] (Image: DLR, CC-BY 3.0 and ERF2014).

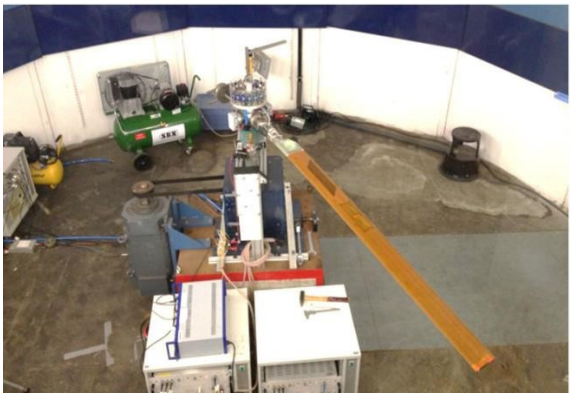

Figure 19. Blade mounted in the test rig [95] (Image: DLR, CC-BY 3.0 and ERF2014).

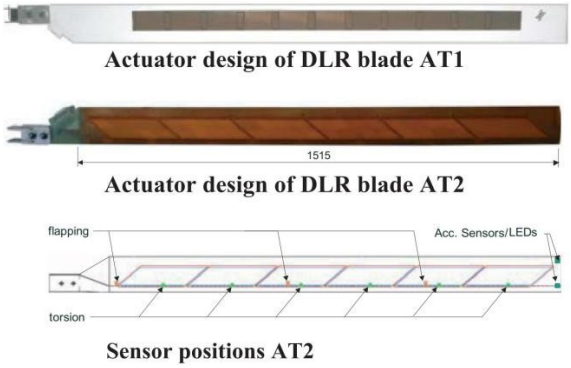

Figure 20. Actuator design blades demonstrating two totally different concepts for the generation of active twist. One is using shear introduction into the blade skin (AT2), and the other one is using a cut section, which is filled by actuation (AT1) [98] (Image: DLR, CC-BY 3.0).

Bernhard and Chopra [108] experimentally investigated a Mach-scale active-twist rotor actuated by a novel internal piezoelectric bending–torsion beam, designed to provide on-blade twist for vibration control in hover. The actuation system used a segmented composite beam embedded along the blade span inside the spar. Each segment had alternating ±45° graphite–epoxy layers and surface-bonded PZT-5H piezoceramic patches. When voltage was applied, the PZT elements caused the beam segments to bend, and due to the specific fibre orientation, this bending was coupled with twisting. As the segments bent in a sinusoidal pattern along the span, their combined motion generated overall blade twist (Figure 21). This allowed the entire blade to twist without using external flaps or mechanical linkages. In hover tests at 2000 rpm (tip Mach 0.47), the system achieved tip twist amplitudes up to ±2.2°, with thrust variations corresponding to over 10% control authority at 3/rev (150 V RMS). Key benefits included clean aerodynamic integration, good twist authority, and compact design. However, drawbacks included a large mass increase; actuation hardware added approximately 48% to blade mass, limiting rotor speed, and piezoelectric material degradation (e.g., cracking and reduced current draw) affected long-term reliability. The study demonstrated the feasibility of internal twist actuation and highlighted opportunities for improved efficiency and durability through better materials and design optimisation.

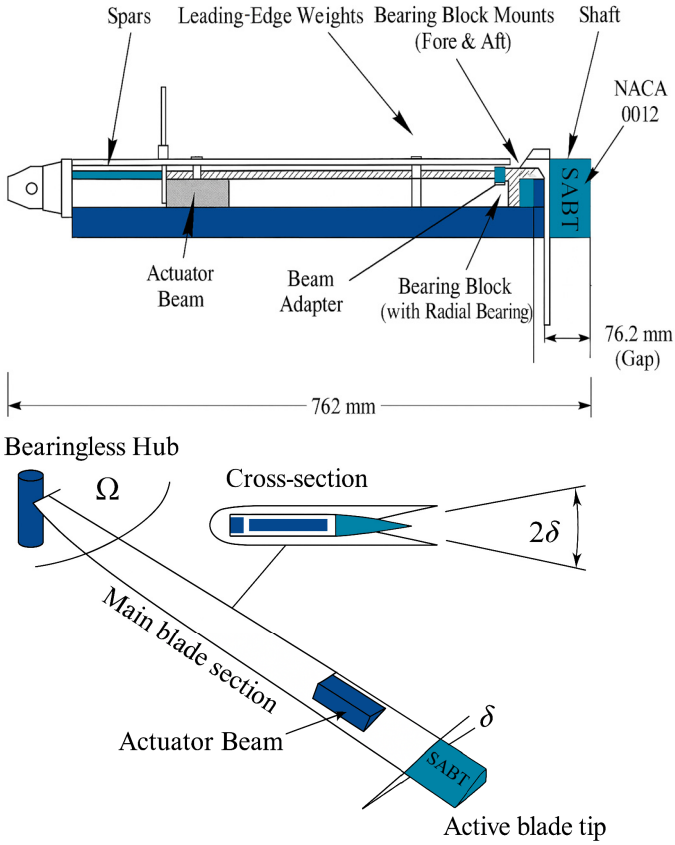

Figure 21. Schematic representation of the smart active blade tip (SABT) and its integrated actuation mechanism [108].

2.3.2. Quasi-Static Actuation (Variable-Twist Rotor Designs)

The literature suggests that variable-twist rotors (quasi-static twist variation; less than 1/rev) have received less attention than the active-twist rotor investigations [2]. The fundamental problem is that these systems require a large amplitude, up to 30 degrees in some circumstances. It is important to note that these technologies must not only provide substantial twist variation but also retain blade stiffness to endure applied inertial

or dynamic stresses [2]. Beginning in the late 1980s and continuing into the early 1990s, NASA collaborated with the US Army to create extension–twist-linked composite blades enabling quasi-static modification of blade twist for tilt-rotor applications [112,113]. The key advantage was the elimination of an actuation device, which minimises manufacturing and operational complexity.

Nampy and Smith [114] and Kosmatka and Lake [115] have examined centrifugally driven variable-twist rotors. However, most manned aircraft currently have a fixed rotor speed configuration. The exceptions include tilt-rotor aircraft and Karem Aircraft's optimal speed rotor (OSR) design. The latter is presently included in the A-160 Hummingbird [116] in development with Boeing. As a result, such a centrifugally driven system would be unsuitable for retrofitting into other platforms. This pattern may alter in the future as the rotorcraft community's interest in variable-rotor speed concepts grows [117–123]. Active device systems have also been studied. Two shape memory alloy (SMA) tubes were employed in the ONR-funded reconfigurable rotor blade (RRB) programme for tilt-rotor blade applications to elastically twist the blade as the torque tube rotated rigidly [124–127]. The blade/actuator system was wind-tunnel-tested on a 1/8th scale, three-bladed model in the late 2000s. This is the only actuated variable-twist rotor wind-tunnel test of its type to date. Other approaches based on SMA actuation have also been studied [128–130]. Warp–twist coupling of open-section beams and warping of the blade skin were two alternatives for quasi-statically altering blade twist [81,131–133].

2.4. Variable Span Rotary Morphing

Because of its potential to increase aircraft performance, variable span was the subject of early research. Linden et al. [134] offered an overview of variable-span rotor technology studied prior to the 1960s. Young et al. of HaigK Helicopters developed a variable-diameter rotor (VDR) system for traditional edgewise rotors in the early 1960s [134]. The technology, which was extensively hover tested, included telescoping blades whose motion was controlled by a cable/strap arrangement. Full-power tests of the project's most recent iteration, the VDR-4 test article, were conducted in the early 1970s. This prototype design included a locking mechanism to keep the blades in place during testing, as well as a unique mechanical approach for moving the telescoping portions. Following the testing of the VDR-4 prototype, the project was terminated, and no further work was done until the mid-2000s, when Fenny [135] at Bell Helicopters introduced a compound differential rotary mechanism for the cable system, which allowed for increased system reliability, a major problem with the original VDR project mechanism. In the Telescoping Rotor AirCraft (TRAC) project, Sikorsky studied variable span, employing a jackscrew system to operate telescoping blade sections [136].

In contrast to the Bell proposal, this design intended for an inboard torque tube through which an aerodynamic blade portion might move. The design allowed the jackscrew to be controlled by the main rotor power supply. A scaled replica of this design was extensively wind-tunnel-tested and shown to increase performance [137–140]. In the early 1990s, this concept was updated for a tilt-rotor aircraft layout and termed the variable-diameter tilt-rotor (VDTR) project [141,142]. A scaled prototype was subjected to extensive wind-tunnel and hover testing as part of this effort. The incorporation of a second motor housed in the rotor hub to activate the jackscrew mechanism was the main distinction for the scale rotor testing of this project. Bell Helicopters worked on variable-rotor systems again in the late 1990s as part of the Army's variable-geometry advanced rotor technology (VGART) programme. As this was a closed-door cooperation, no thorough description of the actuation mechanism is accessible.

Simultaneously, The Boeing Company worked on the construction of a variable-geometry rotor (VGR) employing a jackscrew mechanism in combination with a hydro-pneumatic accumulator in the late 1990s [143,144]. A mechanism was also incorporated in the proposal to automatically modify the blade's built-in twist when the span was changed. This was accomplished by including helically curved grooves on the main span of the blade into which the blade section's connect points would slide, resulting in a rotational and spanwise motion of the section. Prabhakar, Steiner, and Gandhi have recently collaborated on the creation of a passive, centrifugally actuated variable-span rotor system [145,146]. The authors imagined a system in which the rotor speed was varied to regulate the blade spanwise placement. Mistry [147] in 2012 investigated the effects of varying span on a UH-60A-type aircraft at various gross weights and altitudes. The investigation revealed that variable span in the range of +17% to −16% of baseline radius might lower the helicopter's power need by up to 20% for high-altitude and high-gross-weight situations.

Wang et al. [148] investigated a Variable-Diameter Tiltrotor (VDTR) concept as part of NASA's Short-Haul Civil Tiltrotor (SHCT) programme, aimed at enhancing both hover and cruise performance for large civil tilt rotors. The concept featured telescoping blades that extended to 100% span in hover and retracted to approximately 67% in cruise, reducing disc loading during hover and improving aeroelastic stability in forward flight, all while maintaining constant rotor RPM. The actuation system employed a motor-driven jackscrew housed within a torque tube to translate axial motion and adjust blade span, with centrifugal forces carried by tension straps that enabled the blade to operate primarily in compression (Figure 22).

The design was validated through finite element modelling using UMARC/S and supported by wind-tunnel and hover stand testing. The study demonstrated several advantages, including improved hover efficiency, enhanced cruise stability, reduced rotor outwash, and increased autorotation capability. However, the system introduced mechanical complexity, added structural mass, and potential reliability concerns due to in-flight telescoping under high centrifugal loads. Overall, the VDTR provided a promising morphing solution for reconciling the divergent aerodynamic requirements of hover and cruise in tilt-rotor aircraft.

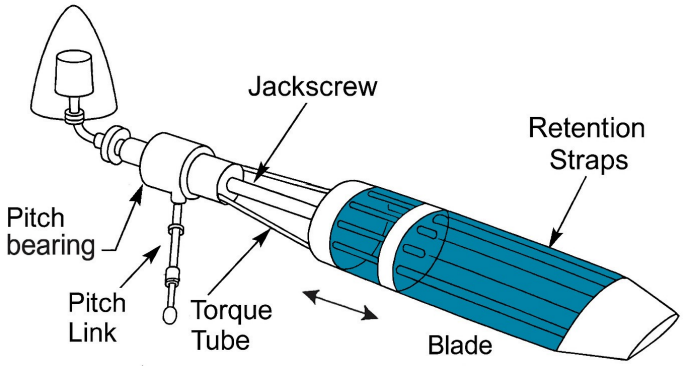

Figure 22. Schematic representation of the VDTR variable-span tilt rotor [148].

Vocke et al. [149] developed a span-extending rotor blade tip system under DARPA's Mission Adaptive Rotor programme, enabling a 100% increase in blade tip span while maintaining constant chord, effectively doubling the active airfoil area. The actuation system itself was not part of the study; instead, the focus was on structural design (Figure 23). The design used a titanium honeycomb-like morphing core with zero Poisson's ratio and a polyurethane-based elastomer-matrix composite (EMC) skin. The system relied on centrifugal force for extension, requiring minimal actuation effort, and was intended for quasi-static reconfiguration rather than high-frequency control. Advantages included aerodynamic

continuity, low added weight, and passive force-assisted deployment. Testing confirmed structural integrity under 100% strain and 300+ cycles, with good agreement between experimental and FEM results. Disadvantages included lack of dynamic response capability, unproven flightworthiness of cast titanium parts, and sensitivity to skin–core bonding quality. The concept demonstrated strong potential for passive morphing to improve rotor efficiency and mission flexibility.

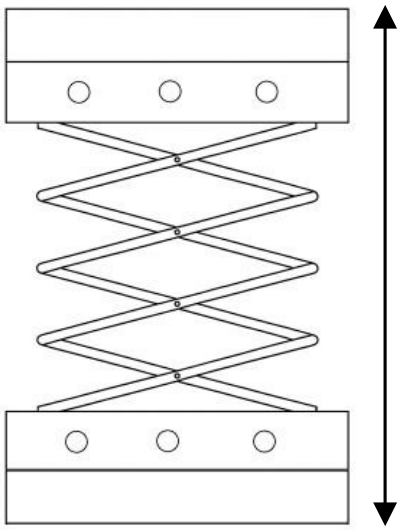

Figure 23. Schematic representation of the span-extending rotor blade tip system under DARPA [149].

2.5. Variable-Chord Rotary Morphing

Variable-chord systems have the ability to increase aircraft and rotorcraft performance significantly and gained some momentum in the early 2000s [150–157]. The Japan Aerospace Exploration Agency's (JAXA) active tab mechanism project focused on the development and testing of a high-frequency (N − 1, N, N + 1/rev) actuated rotor tab for noise reduction. The programme included a wind-tunnel test on a model scale. A motor situated within the hub drove the tab. There was a relatively large noise reduction capability for each frequency from 2 to 5/rev if 1.5 degree blade tip deflection is assumed [2].

Another investigation by O. Léon et al. [150] demonstrated an efficiency increase of 16.7% in power required at sea-level conditions for a rotor blade when a 30% chord extension increase was applied. The lift coefficient optimisation increased the maximum gross weight capability by 6.7% at low altitude and 10% at high altitude. The study investigated a Static Extended Trailing Edge (SETE) to enhance helicopter rotor performance by increasing the chord of the rotor blade. The SETE mechanism used a motor-driven morphing X-truss to extend a thin plate through a trailing-edge slit, achieving a 30% increase in chord length when fully deployed (Figure 24). The mechanism consisted of two rails attached to the rear spar and the SETE plate, driven by a stepper motor connected to threaded blocks and an all-thread rod. The prototype, based on a BO-105 blade with a 10.75-inch chord, housed the actuation mechanism within these dimensions. In the extended configuration, the mechanism spanned from 30% to 60% chord length, occupying 15.3 inches of the 20.5-inch spanwise length. In its retracted state, it had a chordwise dimension of 2.25 inches, achieving a 28% extension when deployed. The SETE offered additional significant advantages, such as reducing power requirements by 450 HP, increasing maximum speed by 26 knots and raising maximum altitude by 3000 feet. Challenges included the need for precise control of the actuation mechanism and potential reliability concerns due to system complexity. Despite these issues, the SETE mechanism demonstrated considerable potential for enhancing lift, reducing drag, and expanding the rotorcraft flight envelope [150].

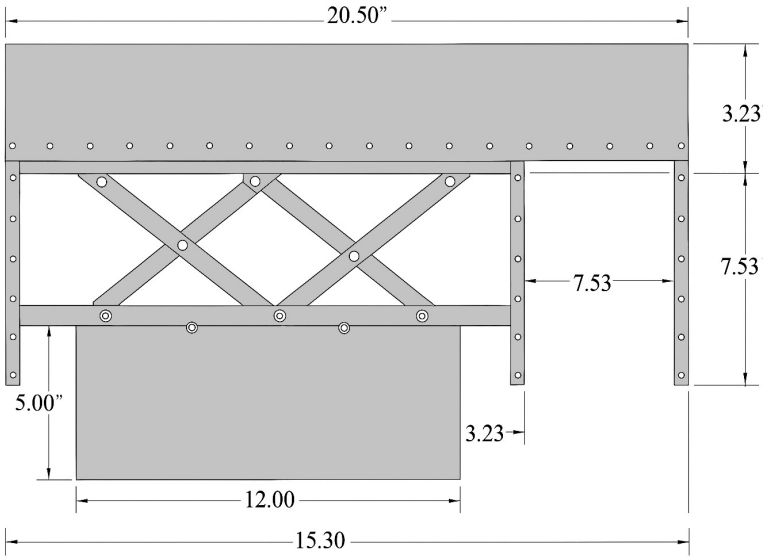

Figure 24. Actuation mechanism and dimensional schematic representation of the chord-extendable Static Extended Trailing Edge (SETE) [150].

Khoshlahjeh and Gandhi looked at the advantages of a quasi-static variable chord. This prompted numerous Penn State University researchers to create several variable-chord rotor systems for quasi-static actuation employing a variety of actuation techniques [2]. Passive, centrifugally actuated discrete stiff plates [151], compliant cellular structures [152], electric and pneumatic actuators to drive an X-truss mechanism [150,153,154], and SMA-based amplification mechanisms [155,156] are examples of these investigations.

Khoshlahjeh et al. [153] investigated the use of a 20% chord extension over a 20% blade span region (from 63% to 83% radius) via a trailing-edge plate (TEP) deployed through a slit in the blade, to alleviate stall and expand the flight envelope of a UH-60A helicopter (Figure 25). The TEP was deployed at a 2° downward angle and actuated via a motor-driven morphing truss. CFD-based aerodynamic data for the modified airfoil were coupled with structural modelling in RCAS to simulate performance across speed, altitude, and weight variations. TEP extension reduced rotor power by up to 18% in stall-dominant conditions and increased max gross weight by up to 1500 lb, max altitude by 1800 ft, and cruise speed by 18 kt (from 115 kt to 133 kt). At 115 kt, power was reduced by nearly 12%, and the minimum cruise power was reduced by 4.3%. Compared to a fixed chord increase, the TEP offered similar benefits at high loads and altitude without the 4% power penalty at low weight and sea level, since it could be retracted when not needed. Advantages included low actuation force, reconfigurability, and improved performance near flight boundaries. Disadvantages involved increased pitch link loads at higher deployment angles, aerodynamic penalties from elastic twist at the blade tip, and structural integration complexity [153].

A novel extendable chord system for helicopter blades was developed and tested by Hayden [154]. This system employed a morphing truss actuation mechanism to achieve significant chord extension. The design utilised an inline X-truss structure, which was preferred over other truss designs due to its ability to translate spanwise movements into chordwise extension efficiently. This was a four-step translation: First was the Truss Structure: the inline X-truss was designed to deform in a controlled manner. When the truss was compressed or expanded spanwise (along the length of the blade), its geometry caused it to extend or retract chordwise (across the width of the blade). Second was the Actuation: a 1271 brushed DC motor was connected to a threaded rod. When the motor turned the rod, it moved the truss structure in a spanwise direction. Third was the Mechanical Linkage: the

mechanical linkage of the X-truss was configured so that spanwise movement of the truss caused the elements of the truss to change angle relative to each other. This change in angle forced the trailing edge of the blade to extend or retract chordwise. The final step in this translation was the Resulting Extension: as the motor actuated the truss, the truss elements moved, translating the spanwise compression or expansion into a chordwise extension (Figure 26). This system was capable of extending the blade chord by approximately 8.1%, achieving 1.3 inches of extension from a 16-inch chord. The actuation mechanism was primarily electromechanical, involving a geared DC motor connected to a threaded rod, which in turn moved the truss structure. The motor used was a 1271 brushed DC motor, which allowed for precise control of the chord extension. The entire mechanism was designed to fit within the blade's limited space, with the truss occupying the trailing-edge area while avoiding interference with the main spar. One of the key advantages of this system was its ability to maintain blade stability by positioning the heavy actuator along the spar, thus minimising shifts in the blade's centre of gravity. Additionally, the mechanism included features to accommodate blade twist, such as rotational elements on the linkage and plate assembly. However, the system faced challenges, particularly in managing the high actuation forces required under centrifugal loads. The prototype demonstrated successful operation up to a rotational speed of 385 RPM, corresponding to a centrifugal loading of approximately 209.5 g. Despite this, the electromechanical actuator showed a decrease in efficiency in a rotating environment, requiring higher currents than its rated capacity, which suggested the need for further future optimisation. While the prototype showed promise in extending the blade chord and improving aerodynamic performance, future iterations would need to address the high actuation forces and enhance the actuator's efficiency under full-scale centrifugal loads. The study provided a valuable foundation for further development of extendable chord systems in rotorcraft, highlighting both the potential benefits and the technical challenges involved.

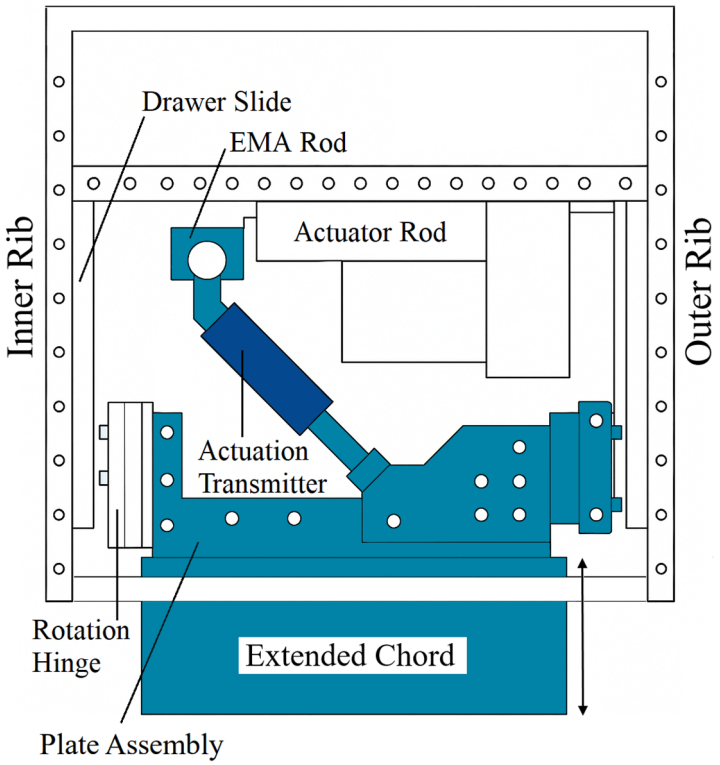

Figure 25. Actuation mechanism and schematic representation of electromechanically actuated chord system in the extended configuration [153].

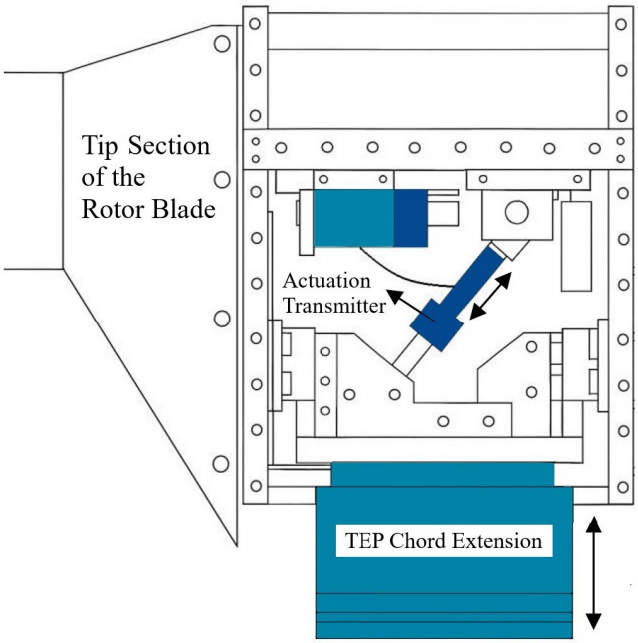

Figure 26. Actuation mechanism and schematic representation of the trailing-edge plate (TEP) chord extension mechanism [154].

A study by Barbarino et al. [155] investigated a bistable von Mises truss (VMT) actuated by shape memory alloys (SMAs) for morphing applications. The VMT-SMA system used resistively heated SMA wires to induce snap-through motion, achieving two-way actuation by positioning the wires symmetrically around the truss's unstable equilibrium. The experimental setup featured a VMT prototype with pin joints at the ends of rigid links, allowing horizontal sliding. SMA wires were connected to the VMT vertex for Joule heating, with convective cooling for reverse phase transformation. Two electrical circuits, controlled by an external switch and a Tektronix PWS4000 DC power supply, provided heating. Measurements were taken using a linear potentiometer and thermocouples linked to an NI DAQ 6212 system. The system's key advantage was achieving large displacements with short SMA wires by amplifying recoverable strain through the bistable mechanism, eliminating the need for a locking mechanism. However, it required precise control of SMA wire pre-strain and management of complex thermal and stress behaviour. The study showed that the VMT-SMA system effectively achieved significant morphing, with experimental results closely matching numerical predictions.

2.6. Variable-Camber Rotary Morphing

Active flap systems are often designed to generate an effective change in the rotor camber; however, due to the discretised nature of these systems, bigger chord flaps can result in increases in rotor profile power. An alternative is to directly vary the camber of blade sections to generate the necessary changes in the blade section's aerodynamic properties. These devices confront the added issue of creating a smooth aerodynamic surface. DLR suggested (but did not build) an idea employing MFCs to generate camber of rotor blade sections [157]. Pennsylvania State University researchers collaborated on the creation of an active camber system based on a compliant truss assembly [158,159]. Gandhi et al. [159] developed and optimised a deformable rotor airfoil capable of high-frequency camber variation for helicopter vibration reduction, offering a low-drag alternative to traditional trailing-edge flaps. The design incorporated four compliant mechanisms embedded chordwise aft of a rigid D-spar, actuated by five pairs of piezoelectric stack actuators (PZT-5H) using the d33 effect.

These actuators expanded and contracted the upper and lower skins, enabling smooth camber deformation without external surfaces or mechanical linkages (Figure 27). Shape optimisation was carried out using sequential linear programming, targeting either maximum trailing-edge tip deflection (TD) or the best ratio of actuation-induced deflection to deformation under aerodynamic loads. The TD-optimised configuration achieved a 6.0 mm tip deflection, equivalent to a 4.6° trailing-edge flap, while the ratio-optimised variant achieved 3.7 mm (2.84° equivalent) with greater stiffness and load resistance. A benchtop prototype based on the TD design demonstrated a 3.65 mm static tip deflection and a natural frequency of 38.75 Hz, closely aligning with analytical predictions. Compared to a 15% chord flap, the conformable airfoil achieved a 17–22% lift increase with 50–75% less drag penalty. Key advantages included embedded actuation with aerodynamic cleanliness, effective stroke amplification through compliant geometry, and suitability for high-frequency operation. Limitations included lower lift gain per degree of deflection relative to flaps, sensitivity to material and geometric constraints, and increased fabrication complexity due to the internal compliant structure.

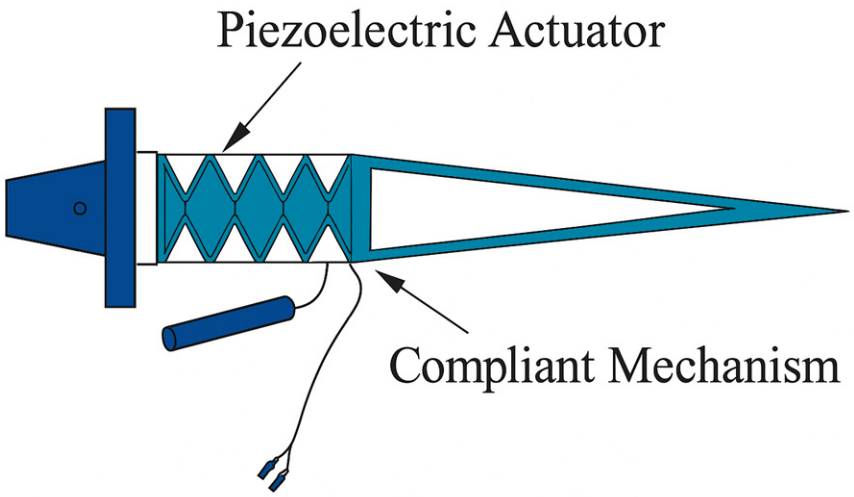

Figure 27. Schematic representation of the piezoelectric actuator and compliant mechanism [159].

Kammegne et al. [160] presented the design, modelling, and experimental validation of a new electrically actuated rotary morphing system for an ATR-42 airfoil aimed at improving aerodynamic efficiency through active camber morphing. The actuation mechanism employed two DC motors connected to eccentric shafts, placed at 30% and 50% chord locations, to deform a composite flexible upper skin (Figure 28). A position controller based on proportional-derivative control and an inner-loop current controller were implemented to precisely track desired morphing profiles.

Wind-tunnel tests validated the controller's real-time performance, showing good agreement with simulations and achieving stable actuation within ~1 s. Aerodynamically, the optimised morphing shapes resulted in transition point delays of 2% to 18% of the chord and drag reductions between 3% and 10.5%, depending on flow conditions. Compared to prior SMA-based systems, this rotary approach eliminated high power demands and slow thermal response. However, two main disadvantages were noted: (1) space constraints required complex mechanical linkages (eccentric shafts) for motion transmission, and (2) although more responsive than SMA, electric rotary actuators still imposed integration challenges in wing structures due to actuator bulk and installation limitations. Overall, the work demonstrated a promising and practical electric actuation system for morphing applications, balancing control precision with aerodynamic performance gains.

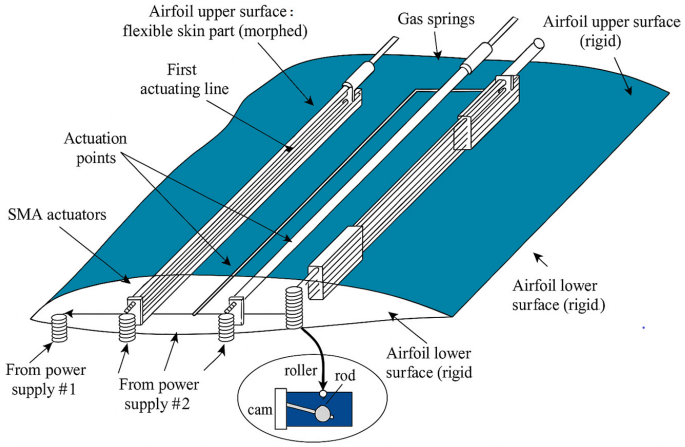

Figure 28. Schematic representation of the morphing wing model in CRIAQ 7.1 research project, its actuation mechanism and compliant variable-camber structure [160].

2.7. Variable-Nose-Droop Rotary Morphing

Nose-droop devices can efficiently mitigate concerns associated with blade section dynamic stall [161]. Rotor blades often have a D-spar or C-spar at the leading edge, which contributes the majority of the blade rigidity. Because they are in the same position as the important blade structure, nose-droop systems present a substantial design issue. Shaner and Chopra collaborated on the design of a piezo-stack actuator feasible for a leading-edge nose-droop system [162]. Despite some design improvements, the actuator did not perform to expectations when benchtop testing. Martin et al. [161] evaluated a Variable-Droop Leading-Edge (VDLE) concept for dynamic stall control on a VR-12 airfoil under compressible flow conditions representative of retreating blade stall. The design used a 25% chord droop section hinged at the quarter-chord, actuated via external linkages to produce either fixed or variable droop during pitch oscillations (Figure 29). In the variable configuration, the droop remained fixed in space while the main airfoil oscillated, altering the effective leading-edge shape through the cycle. Wind-tunnel tests (Mach 0.2–0.45; reduced frequency up to 0.1) and CFD showed drag reductions of up to 63%, peak moment reductions of 31–37%, and complete elimination of negative pitch damping, with lift penalties limited to ~8%. The VDLE outperformed fixed droop by avoiding low-angle drag and moment penalties, reducing $\alpha = 0$ drag by a factor of three. Advantages included effective stall mitigation across Mach regimes and minimal mechanical complexity for 2D implementation. Limitations included modest lift loss and the challenge of integrating a variable mechanism into full-scale rotor blades. The results demonstrated VDLE's potential for rotor stall alleviation and aeroelastic stability improvement.

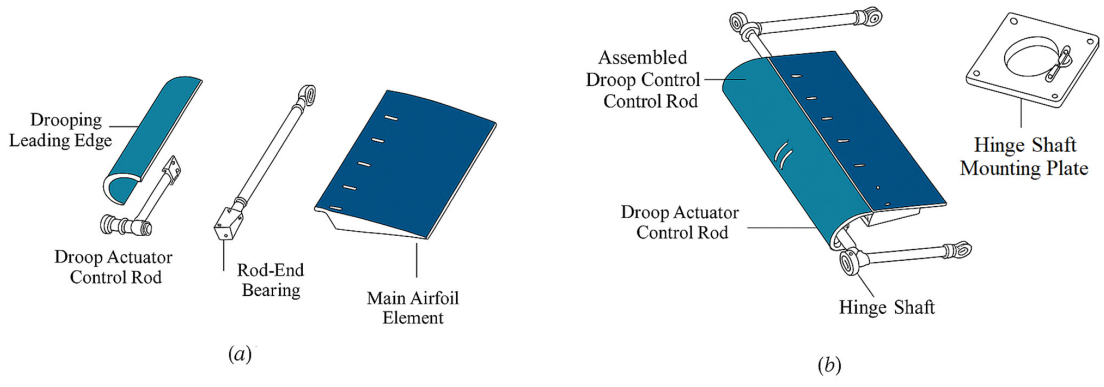

Figure 29. (**a**) VDLE airfoil model with nose-droop leading edge detached. (**b**) VDLE airfoil with nose-droop leading edge assembled [161].

Shaner and Chopra [162] designed and tested a piezo-stack-actuated leading-edge flap system for helicopter rotor applications, targeting stall delay and vibration/noise reduction. The system used six LVPZT piezo-stacks (10 × 10 × 18 mm; 144 layers each) arranged to actuate a 25% chord leading-edge flap via a single amplification lever in a 12-inch chord NACA 0012 section. The target was a 5° flap deflection, corresponding to approximately 10 mm tip travel, under aerodynamic hinge moments of ~41.3 mN for a 1-foot span at a 10° angle of attack (Mach 0.42; 90% span). An amplification ratio of ~7:1 and application point 14 mm from the hinge were determined via optimisation. Initial static tests showed a maximum flap deflection of ~1°, only 20% of the intended output, with stroke beginning to plateau above 120 V. Frequency response remained flat across 0–10 Hz. Advantages included compact integration ahead of the quarter chord, high force output, and minimal drag impact. However, actuator output fell short due to stroke losses from wire slack, geometric misalignment in force transmission, and excessive hinge stiffness. Future improvements were proposed, including rigid linkage replacement, flexure bearings, and increasing actuator span density (from 1 to 1.33 per foot) to meet required deflection. The study established baseline feasibility but highlighted the need for significant mechanical refinement. Fink et al. [163] at Diversified Technologies, in collaboration with the Aeromechanics Division of the Aeroflightdynamics Directorate (AMRDEC), developed the leading-edge electromagnetic airfoil (LEEMA) actuator for a variable-nose-droop rotor system. The system design was optimised to ensure a smooth actuation of the nose droop through a linear electromagnetic actuator located at the front of the blade section. A benchtop prototype of this actuator system was constructed and tested to demonstrate its effectiveness in achieving the desired nose droop.

FlexSys, in partnership with AMRDEC, created a conformable leading-edge compliant structure using optimisation techniques [92]. This technology was created to translate the rotating motion of a motor into the effective rotation of the blade's leading edge. The reduced number of moving components makes this design more practical, although it is not as sturdy as the typical spar structure. Other concerns such as anti-ice and erosion were not addressed. To demonstrate the system's actuation properties, a benchtop prototype of the idea was developed and tested. This investigation presented a novel approach to rotor blade design by implementing a variable-geometry leading edge using compliant systems. The study successfully developed a leading edge that morphed to an aerodynamically optimised 10-degree cambered profile, improving performance in the blade-retreated position once per revolution. This adaptation aimed to delay blade stall, thereby enhancing forward speed, manoeuvrability, and payload capacity.

Actuation System and Mechanism: The actuation system employed compliant mechanisms, which were single-piece, flexible structures without joints, integrated with actuators. The mechanism included a driving link that rotated to achieve the desired cambered shape.

The system reduced torsional stiffness and minimised high-stress concentrations by distributing flexion across the structure rather than localising it in hinges. The compliant leading edge could achieve a +/−10-degree deflection, operating at 6 Hz, driven by a 34-pound linear electromagnetic actuator located at the rotor base. This setup ensured low actuation force and power requirements, estimated at 885 Watts for a 7-foot span flap. Materials and Fabrication: The prototype was fabricated from titanium alloys, specifically Ti-10V-2Fe3Al, chosen for its superior static and fatigue strength. The leading-edge structure underwent a series of optimisations to reduce stress concentrations and improve shape matching. The final design included 25 machined titanium ribs and a polycarbonate skin bonded using epoxy adhesive and vacuum bagging techniques.

Setup and Layout: The compliant structure was integrated into a 3-foot span, 18-inch chord model with a 1-foot adaptive leading-edge flap. The D-spar was moved rearward

to accommodate the compliant structure and actuator hardware. The actuation system converted linear spanwise motion into rotary motion to drive the flap, ensuring precise control over the adaptive surface. The adaptive leading-edge design offered significant aerodynamic benefits, including a higher maximum lift coefficient and the elimination of the dynamic stall vortex. The technology demonstrated a 35% increase in retreating blade lift without stall, improving overall rotorcraft performance.

The unitised construction of compliant mechanisms simplified manufacturing and provided a smooth aerodynamic contour, free of the discontinuities associated with traditional joints. On the contrary, disadvantages included the need for further structural optimisation to reduce stress levels and the complexity of integrating the system into a full-scale rotorcraft. The benchtop prototype (Figure 30) highlighted issues with cam-wedge system backlash, indicating the need for design improvements to achieve precise flap positioning. Additionally, packaging constraints and high centrifugal forces necessitated careful actuator placement and system architecture design. Further testing, including static and dynamic wind-tunnel tests and full-scale implementation, was recommended to validate and mature the technology for practical use in rotorcraft.

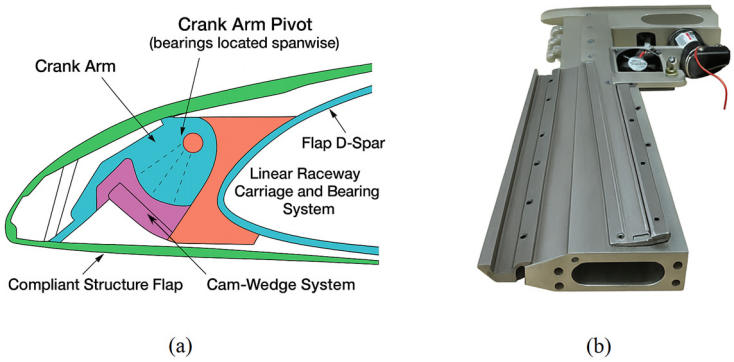

Figure 30. (**a**) CAD model of nose-droop leading-edge flap cam-wedge system and D-spar. (**b**) The D-spar, crank arm and cam-wedge linear transmission system and the compliant structure [92].

2.8. Variable-Speed Technologies

Traditionally, rotary-wing aircraft are designed with an optimal rotor speed dependant on the operating flight regime (hover, forward flight, etc.). With the launch of the A160 Hummingbird unmanned aerial vehicle and its optimal speed rotor technology [116], the field of variable-speed (variable RPM) rotors has lately acquired traction. Pennsylvania State University researchers investigated the performance benefits solely with rotor RPM change across the complete flight envelope of a UH-60A type aircraft model [92,117,124,164]. This study demonstrated the feasibility of achieving a maximum power reduction of up to 14% for defined instances by employing only a restricted rotor RPM variation. Mistry [147] improved on this work by combining 11% variation in rotor speed with +17% to 16% variation in baseline blade spread over a variety of gross weights and altitudes. Bowen-Davies and Chopra [120] investigated the performance advantages and vibratory features of a variable RPM rotor system on a comparable kind of aircraft. Berry and Chopra [121] conducted a model-size wind-tunnel experiment to understand the behaviour of a variable RPM system at the same time. Furthermore, Datta, Yeo, and Norman investigated the consequences of a slower rotor arrangement at high advance ratios [122].

At NASA Ames' 40 × 80 wind tunnel, a slowed rotor experiment was carried out on a full-scale UH-60A rotor system. The study presented a comprehensive investigation of a full-scale slowed UH-60A rotor tested at the National Full-Scale Aerodynamics Complex wind tunnel. This research explored the aeromechanics of a rotor operating at high advance ratios (up to 1.0) and reduced revolutions per minute (rpm). The study provided an

extensive set of measurements, including performance, blade loads, hub loads, and pressures/airloads, revealing unique aeromechanical phenomena. The experiment involved the UH-60A rotor mounted on the NFAC Large Rotor Test Apparatus (LRTA). The rotor was tested at 65% and 40% of its nominal rpm, with maximum forward speeds up to 182 knots. Special considerations were made for the slowed rotor test, including modifications to the main rotor dynamic flap and droop stop mechanisms to allow for adequate flapping at reduced rpm. The actuation system, part of the test setup, was designed to handle these changes effectively. The test plan included parametric sweeps with tip Mach number as the primary variable, adjusting shaft angles and tunnel speeds to achieve the desired advance ratios. The rotor blades were instrumented with 160 pressure transducers, 26 strain-gauge bridges for structural loads, and multiple devices for blade motion and hub measurements. Data were acquired at 2048 samples per revolution for blade pressures and 256 samples per revolution for motions and loads. The experimental setup allowed for detailed measurements of performance metrics, structural loads, and pressure distributions under various operating conditions. The performance data revealed significant phenomena unique to high advance ratios, including reverse-chord dynamic stall, retreating side impulse in torsion load, and large inboard–outboard elastic twist differential. At high advance ratios, the rotor demonstrated diminishing forces but dramatic increases in blade loads, along with benign levels of vibratory hub loads. The study showed a decrease in thrust sensitivity to collective at high advance ratios, with thrust reversal occurring around $\mu = 0.9$–1.0. The efficiency was higher at a positive shaft angle but decreased sharply at high advance ratios due to increased drag.

3. Critical Analysis of Existing Systems

This chapter presents a critical synthesis of the actuation systems and morphing concepts reviewed in Section 2, prioritising technical viability and conceptual novelty. Rather than treating morphing approaches in isolation, the analysis consolidates results across actuation categories to identify which techniques have demonstrated credible performance under representative rotary-wing conditions and which remain constrained by actuation authority, bandwidth, structural compatibility, or integration complexity.

A comparative assessment highlights the fundamental trade-offs between high-bandwidth, low-authority approaches (such as piezoelectric trailing-edge flaps and active twist) well-suited to vibration and noise mitigation, and high-authority, quasi-static morphing concepts including variable span, chord, and camber, which offer greater aerodynamic potential but incur significant penalties in mass, reliability, and system integration. Few concepts demonstrate credible multi-objective capability when realistic rotor-system constraints are applied.

Fixed-wing morphing studies are examined selectively as a reference baseline, focusing on actuation architectures with plausible rotary-wing relevance. While informative at the mechanism level, many fixed-wing solutions fail to translate to rotating blades due to centrifugal loading, fatigue, bandwidth, stiffness, and hub–blade integration constraints. An Actuation Concept-Transfer Feasibility (ACTF) study is therefore used to identify actuation principles with genuine transfer potential from fixed-wing to rotary-wing platforms.

Finally, the reviewed technologies are assessed in terms of implementation maturity and technology readiness. Numerical and computational investigations, experimental fidelity, and system-level integration are synthesised into a unified Technology Readiness Level (TRL) framework, organised into four categories and rated 1 to 9 (from proof-of-concept to flight-representative validation). This assessment underscores the persistent gap between aerodynamic promise and operational feasibility and provides a clear basis for prioritising future research.

3.1. Camber, Chord and Spanwise "Location" of Rotor Blade Actuation System

The rotary morphing actuation literature presents many studies regarding the optimised location for the rotor blade's actuation system (i.e., spanwise or chordwise as a percentage of the rotor blade length or radius using trailing-edge flap and piezo-stack actuator). Ref. [26] suggests that an integral flap spanning from 74% to 92% radius contributed significantly to reducing noise and vibrations. Using active camber and active-twist methods, a 2021 investigation [165] using preCICE (LGPLv3) looked at dynamically modifying the associated blade planform. By simulating a modified, isolated BO105 rotor, the capability of the designed CFD/CSD connection was confirmed. With a linear transition towards the inboard and outboard passive sections of the rotor blade, the active section was integrated between r = 0.25R and r = 0.95R. Following a non-harmonic schedule, the active region was dynamically transformed from 75%C to the blade's trailing edge.

A study [166] in agreement with another investigation in 2018 [165] suggests that camber twist increased the lift-to-drag ratio (aerodynamic efficiency) by 20% when compared to active trailing-edge flaps. The best optimised location for the actuation mechanism in forward flight conditions was achieved by a 0.2R morphed camber section located at 0.5–0.7R. Previously, it was reported that M. Mistry et al. [132] suggested an active rotor blade twist of 12 to 32% of the outboard section (rotor tip) for optimum performance, since rotor blades produce the majority of the lift at the tip of the blade (flange tips that produce "Vlasov bimoments"). This study investigated the twisting of an I-beam spar through the application of differential axial loads (Vlasov bimoments). This research was particularly relevant for developing variable-twist helicopter rotor blades, where the outboard 12–32% of the blade could undergo large quasi-static twist variations for optimal performance under diverse operating conditions. The study utilised Vlasov beam theory and finite element models to analyse the influence of geometric parameters on the I-beam's twisting behaviour.

The actuation system involved applying differential axial forces to the I-beam flange tips to generate Vlasov bimoments. This method exploited the inherent torsional softness of open-section beams like the I-beam, which only warped at the flanges, while the web remained unaffected. This configuration allowed the I-beam to exhibit reduced torsional stiffness, similar to a free–free beam, thereby requiring less input energy to achieve the desired twist. The BO-105 rotor blade's dimensions and a NACA 0012 airfoil shape served as the basis for the design study. The design space variables considered included web height, flange width, beam span, and wall thickness, with aluminium 2024-T3 as the reference material for its mechanical properties. The research setup included finite element models built using ANSYS Academic Research software (v. 11.0). The I-beam was clamped at the root by its web, leaving the flanges free to warp. The applied axial forces (bimoments) were varied across different locations (root, tip, and both) to study the resultant twist distribution. The study found that the tip twist of the I-beam increased with larger flange widths, despite the corresponding increase in torsional stiffness. The beam span had negligible effect on tip twist when bimoments were applied, contrasting with the linear relationship observed in torque actuation. The twist distribution was more uniform with larger flanges or shorter spans, and the maximum bending stiffness was achieved with an optimal web height of 1.075 inches. This investigation demonstrated that using Vlasov bimoments for twist control in I-beam spars was effective, allowing for significant twist variations with relatively modest actuation force and power requirements. This method was advantageous for applications requiring large quasi-static twist changes, such as transitioning between hover and forward flight in helicopters or between rotor and propeller modes in tilt rotors. However, challenges included local deformations at the flange tips, such as out-of-plane warping and in-plane chordwise bending, which were not captured by Classical Vlasov

theory but were predicted by finite element models. These deformations could impact the overall structural integrity and performance of the rotor blade. Additionally, the need for precise application and control of axial forces presented a technical challenge in practical implementations. Overall, the study successfully investigated the twisting behaviour of an I-beam spar under Vlasov bimoment actuation, providing valuable insights into its potential application in variable-twist rotor blades. The findings indicated that differential axial forces could achieve significant twist variations, with design optimisation required to balance bending and torsional stiffness. Further research and development are needed to address the local deformation issues and to refine the actuation mechanism for practical rotorcraft applications.

3.2. Main Challenges for Rotary Actuation Systems

The structural, mechanical, and aerodynamic complexity and interdisciplinary character of rotorcraft provide more opportunity for the use of smart-structure technologies than any other system, with the potential for significant gains in system effectiveness. Helicopters experience more severe vibration and fatigue loads than fixed-wing aircraft and therefore are more susceptible to aeromechanical instability, excessive noise levels, poor flying stability characteristics, and poor aerodynamic performance. The main rotor is the root cause of all these issues because it operates in an unstable and complex aerodynamic environment that causes stalled and reversed flow on the retreating side of the disc, transonic flow on the advancing blade tips, highly yawed flow on the front and back part of the disc, and blade–vortex interactions in specific flight conditions. In order to increase the performance and effectiveness of rotor systems, a substantial amount of research is now being undertaken in this area. As presented in the literature, various different types of smart-rotor actuation concepts are being developed, amongst which are: active blade tips with custom smart actuators, programmable camber/twist blades with incorporated piezoelectric elements, and leading- and trailing-edge flaps with smart material actuators.

Structural and Mechanical Complexity: The main rotor blade of a helicopter operates under extremely high centrifugal forces, dynamic pressures, and frictional moments, especially at high rotating speeds. These conditions pose substantial challenges to the structural integrity and mechanical performance of morphing actuation systems. Actuators must be robust enough to withstand these forces without compromising their functionality or the structural integrity of the rotor blade. Additionally, the materials used must be lightweight yet strong, as adding significant weight to the rotor blades could negatively impact the helicopter's performance and efficiency.

Aerodynamic Complexity: The aerodynamic environment of a helicopter rotor is highly complex, involving a variety of flow conditions that change rapidly during flight. The actuation systems must be able to respond quickly and accurately to these changing conditions to effectively modify the blade shape and improve aerodynamic performance. This requires precise control mechanisms and real-time feedback systems, which add to the complexity of the design and implementation of smart-rotor technologies.

Interdisciplinary Challenges: The development of effective rotary morphing actuation systems requires a multidisciplinary approach, involving expertise in materials science, aerodynamics, structural mechanics, and control systems. Coordination among these disciplines is crucial to design actuators that can operate effectively in the challenging rotor environment. For instance, materials scientists must develop piezoelectric or magnetostrictive materials that can withstand high stress and fatigue while providing the necessary actuation forces. Aerodynamicists must ensure that the morphing shapes improve the aerodynamic performance of the rotor blades. Structural engineers need to integrate these actuators into the rotor blade without compromising its strength or durability. Control

engineers must develop algorithms that can accurately and efficiently control the actuators in real time.

Performance Degradation: The performance of morphing actuation systems often deteriorates rapidly under the harsh conditions experienced by helicopter rotors. Actuators for flap actuation, including piezobimorphs, piezo-stacks, and composite linked systems driven by piezoelectricity and magnetostrictive force, are particularly susceptible to performance degradation. High centrifugal forces can cause fatigue and failure in the materials used for actuators. Dynamic pressures and frictional moments can lead to wear and tear, reducing the effectiveness of the actuators over time. Ensuring the longevity and reliability of these systems in such a demanding environment is a significant challenge.

Integration and Control: Integrating smart actuators into existing rotor blade designs is a complex task that involves significant modifications to the blade structure. This integration must be carried out in a way that does not negatively impact the aerodynamic performance or structural integrity of the blade. Additionally, the control systems required to manage these actuators need to be highly sophisticated yet compliant, capable of real-time adjustments based on changing flight conditions. This requires advanced sensors, fast processing units, and reliable algorithms, all of which add to the complexity and cost of developing smart-rotor systems.

3.3. Actuation Synthesis

Across all trailing-edge actuation morphing implementations, the literature consistently shows that piezoelectric stack-driven flaps remain the most mature and experimentally verified high-bandwidth actuation approach for rotary systems. A summary of 'types and purpose' of rotary morphing investigations is provided in Table 1, with 'actuation-focused' mechanisms, performance, advantages, and limitations detailed in Table 2. In Table 2, PZT-based mechanisms, including benders, tapered bimorphs, C-block stacks, L–L amplifiers, and X-frame architectures, routinely achieve 3–7° harmonic deflection, maintain sufficient bandwidth for 3–6/rev control, and have demonstrated meaningful vibration and BVI noise suppression under centrifugal loads approaching 600–700 g. These systems benefit from compact in-blade integration, high force density, and favourable dynamic behaviour but remain constrained by high-voltage operation, hysteresis and creep, bond-line sensitivity, and fatigue concerns, all of which complicate long-term durability and certification.

Magnetostrictive and electromagnetic actuators provide attractive force output and, in some cases, large achievable flap authority, but they continue to lag behind piezoelectric solutions in authority-to-weight ratio, integration feasibility, and dynamic efficiency. Magnetostrictive systems have demonstrated substantial vibration reduction, yet their high mass, frictional losses, and thermal sensitivity restrict practical implementation. Electromagnetic actuators deliver near-constant force across stroke but suffer from significant weight penalties, magnetic stiffness effects, and control hysteresis, limiting their suitability for multi-harmonic control.

Pneumatic muscle (PAM) systems offer the largest stroke capability of all TE flap actuators (with deflections approaching ±40° demonstrated on scaled rotor systems) but this comes at the expense of bulky pneumatic infrastructure, limited bandwidth, and durability challenges under cyclic loading. SMA-driven devices provide quasi-static authority suitable for trim control, yet thermal response time and fatigue behaviour prevent their use in high-frequency HHC applications.

Leading-edge morphing remains aerodynamically attractive, particularly for dynamic-stall suppression where studies have reported drag reductions exceeding 50–60%. However, LE concepts face substantial barriers in structural integration, as compliant skins, flexible

cores, and embedded actuators must withstand high centrifugal stresses, pressure gradients, and repeated dynamic loading while preserving a smooth aerodynamic contour. As a result, LE morphing remains considerably less mature than trailing-edge actuation for rotorcraft.

Gurney flaps and serrated leading edges offer passive lift augmentation and noise reduction benefits; nonetheless, these gains are offset by increased drag, pitching-moment penalties, and sensitivity to operating conditions, limiting their operational utility without adaptive scheduling or hybrid actuation. Collectively, the evidence shows that trailing-edge piezoelectric actuation is the only morphing approach to have demonstrated repeatable, high-bandwidth performance under realistic rotor dynamic environments. All alternative technologies (magnetostrictive, electromagnetic, pneumatic, SMA-based, and compliant leading-edge mechanisms) remain promising but face unresolved challenges in mass, bandwidth, structural integration, fatigue behaviour, and in-flight durability. As a result, trailing-edge flaps represent the current state of the art, while other morphing concepts remain aerodynamically compelling but technologically immature.

Across both active- and variable-twist implementations, the literature consistently identifies twist-based morphing as aerodynamically efficient yet mechanically restrictive for rotorcraft load control. High-frequency active-twist systems, predominantly enabled by piezoelectric actuation, exhibit reliable but inherently limited authority, with achievable tip twist amplitudes generally confined to approximately 2°. Although modest, this level of dynamic twist has proven adequate for higher harmonic vibration and noise mitigation, particularly at N and N $\pm$ 1/rev excitation frequencies. Early demonstrations [84] using directionally attached piezoelectrics established the feasibility of inducing shear-driven twist through surface-mounted actuators, while subsequent developments [7–87] in active fibre composites and macro-fibre composites improved strain transfer efficiency, electrical performance, and operational robustness, enabling comparable authority at reduced power levels and with lower sensitivity to operating conditions.

Notwithstanding these advances, active-twist concepts remain fundamentally authority-limited, as piezoelectric actuators contribute minimally to the blade's primary load-bearing structure. Efforts to increase twist authority through internal actuation architectures (such as bending–torsion-coupled beams and active blade tip concepts) have achieved increased twist amplitudes, in some cases exceeding $\pm 2^\circ$, but only at the expense of substantial mass growth. Reported mass penalties approaching 50% significantly exacerbate centrifugal loads, alter modal characteristics, and restrict allowable rotor speed, thereby limiting scalability. Quasi-static variable-twist systems provide substantially greater geometric authority, with achievable twist magnitudes exceeding 20–30°, but are inherently confined to low-frequency or trim applications. Passive extension–twist-coupled composite blades reduce system complexity by eliminating active actuators yet lack adaptability and are unsuitable for most fixed-speed rotor systems. Shape memory alloy-driven quasi-static twist concepts further demonstrate technical feasibility, particularly for tilt-rotor platforms, but remain constrained by thermal response time, cooling demands, and fatigue behaviour. Overall, while twist morphing remains an aerodynamically attractive solution for vibration-focused objectives, no existing actuation architecture simultaneously delivers high authority, low mass penalty, high bandwidth, and long-term durability, placing twist-based morphing at an intermediate level of technological maturity.

Variable-span morphing is among the most aerodynamically impactful rotorcraft morphing strategies, providing direct leverage over disc loading, induced power, and authoritative capability. Reported span variations in the literature range from approximately -16% to increases approaching 100% of the baseline radius, with associated power reductions of up to ~20% under high-altitude and high-gross-weight conditions. Actuation solutions are predominantly mechanical, relying on telescoping blade architectures driven

by jackscrews, cable systems, or compound transmission mechanisms integrated within torque tubes. Early variable-diameter rotor concepts established hover feasibility but suffered from reliability and controllability limitations inherent to cable-driven actuation. Subsequent systems, including TRAC and VDTR, adopted motor-driven jackscrews with improved load paths, locking features, and redundancy, enabling successful wind-tunnel and hover demonstrations.

More recent passive and semi-passive approaches (such as centrifugally assisted span extension and zero-Poisson ratio honeycomb cores) seek to reduce actuation power and improve structural continuity by exploiting centrifugal forces to drive deployment. While these concepts enable large quasi-static geometric changes with minimal active input, they transfer the primary technical risk from actuation to materials and structural durability. Their performance remains highly dependent on bond integrity, skin–core compatibility, and fatigue resistance, none of which have been demonstrated at flight-representative scale. Across all variable-span implementations, mechanical complexity, mass growth, and long-term reliability under sustained centrifugal loading remain the dominant constraints. Consequently, despite clear aerodynamic benefits, variable-span morphing remains at a low-to-mid Technology Readiness Level, with practical applicability largely restricted to tilt-rotor and variable-speed rotor configurations rather than conventional fixed-speed helicopters.

Variable-chord morphing has been shown to deliver some of the largest aerodynamic performance gains reported for rotary-wing morphing concepts, with multiple studies indicating power reductions of approximately 15–20%, cruise speed increases exceeding 25 knots, and significant expansion of the operational envelope. Actuation approaches are predominantly electromechanical, most commonly employing motor-driven X-truss mechanisms, threaded rod systems, or deployable trailing-edge plates actuated through chordwise slots. Among these, X-truss architectures represent the most developed class, effectively translating spanwise actuation into chordwise extension while maintaining acceptable aerodynamic continuity. These systems offer relatively low actuation force requirements, precise positional control, and configuration flexibility, enabling chord augmentation to be applied selectively and thereby avoiding performance penalties under low-thrust or sea-level conditions.

Shape memory alloy-based bistable truss mechanisms further extend achievable chord change by providing large strokes from compact actuators, but their applicability is limited by thermal management requirements and slow response times, confining their use to quasi-static operation. Notwithstanding their aerodynamic effectiveness, variable-chord concepts introduce significant structural and integration challenges. Increases in chordwise bending moments, elevated pitch-link loads, and heightened sensitivity to elastic twist (particularly near the blade tip) are consistently identified in the literature. Experimental validation has largely been restricted to sub-scale testing, with pronounced reductions in actuator efficiency observed under centrifugal loading. As a result, although variable-chord morphing is aerodynamically well characterised and offers compelling performance potential, its overall technological maturity remains limited by mechanical complexity, packaging constraints, and unresolved long-term durability concerns.

Variable-camber morphing occupies an intermediate position between discrete trailing-edge flaps and large-scale chord morphing, offering smoother aerodynamic modification with reduced drag penalties. Actuation strategies in this category are dominated by piezoelectric stack-driven compliant mechanisms and, in some fixed-wing-derived concepts, electric rotary actuators coupled to eccentric shafts. Compliant camber systems actuated by piezoelectric stacks demonstrate effective stroke amplification and smooth surface deformation, achieving camber changes equivalent to approximately 3–5° trailing-edge flap

deflection while incurring 50–75% lower drag penalties than conventional flaps. These systems benefit from embedded actuation, high-frequency capability, and aerodynamic cleanliness, making them attractive for vibration and noise applications.

However, variable-camber systems consistently exhibit lower lift authority per unit deflection compared to discrete flaps and are highly sensitive to material selection, bonding quality, and geometric tolerances. Electric motor-driven camber concepts offer improved controllability and eliminate thermal constraints associated with SMA actuation yet introduce integration challenges that are particularly restrictive within slender rotor blades. As with many compliant morphing architectures, the dominant barriers to maturity are structural stiffness under centrifugal loading and fatigue durability of flexible skins. As a result, variable-camber morphing remains aerodynamically efficient but structurally constrained, positioning it at a lower TRL than trailing-edge flap systems despite promising fixed-wing precedents.

Leading-edge nose-droop morphing is among the most aerodynamically effective morphing strategies for rotorcraft, particularly for mitigating dynamic stall on the retreating blade. Multiple studies report drag reductions exceeding 60%, elimination of negative pitch damping, and substantial improvements in lift behaviour across a range of Mach numbers. Actuation approaches span piezoelectric stack-driven flaps, electromagnetic linear actuators, and compliant cam-wedge mechanisms. Piezo-stack-driven nose-droop systems offer high force density and compact integration but consistently fall short of required stroke due to mechanical losses, hinge stiffness, and force-transmission inefficiencies. Electromagnetic and compliant cam-wedge systems provide improved stroke capability and smoother kinematics, achieving leading-edge deflections on the order of $\pm 10^{\circ}$ at low frequencies, but incur significant mass and integration penalties.

Compliant leading-edge architectures represent a promising shift away from discrete hinges, distributing deformation to reduce stress concentrations and preserve aerodynamic smoothness. These systems demonstrate substantial lift enhancement and stall suppression but remain challenged by erosion resistance, anti-icing integration, packaging constraints, and fatigue under centrifugal loading. Consequently, despite strong aerodynamic justification, nose-droop morphing remains at an early experimental TRL, with actuation feasibility demonstrated but full-scale structural integration unresolved.

Variable rotor speed represents a system-level morphing strategy that fundamentally alters the aerodynamic and structural environment of the rotor rather than directly modifying blade geometry. Studies consistently demonstrate that modest reductions in rotor RPM can yield power savings on the order of 10–14%, with further benefits achieved when combined with span or twist morphing. From an actuation perspective, variable-speed morphing transfers complexity away from the blade and into the drivetrain, requiring variable-speed transmissions, adaptive engine control, and modified hub mechanisms. Full-scale slowed-rotor experiments have demonstrated feasibility at advance ratios approaching unity but also revealed new aeroelastic phenomena, including reverse-chord dynamic stall and large torsional load excursions. While variable-speed operation enables or enhances several passive morphing concepts by modifying centrifugal stiffening and dynamic pressure, its adoption is limited by system-level integration challenges rather than aerodynamic effectiveness. Consequently, variable rotor speed is best viewed as an enabling technology whose maturity is dictated by drivetrain and control architecture readiness, positioning it as a complementary rather than standalone morphing solution.

3.3.1. Gaps in Aerodynamic and Full-Scale Investigations of Rotary-Wing Morphing Concepts

As demonstrated in previous sections, rotary morphing actuation as a technology faces numerous challenges in that the methodology, means, variation, experimental studies,

wind-tunnel tests, small-scale and-large scale demonstrators and full-scale studies are incomparable to those of non-rotary investigations (see Figures 31–33). Servo flaps, which were originally utilised in the Kaman K-125, which had its first flight on 15 January 1947, and more recently in the K-Max, are the only morphing actuation technology to date to have made it to a production helicopter. The active twist of rotor blades can be produced using a variety of cutting-edge techniques.

However, none of the programmes mentioned have been created for full-scale active-twist rotor systems, with the exception of the active fibre composite (AFC) actuator design. Despite the substantial amount of work that has been done in this field, there is still a significant need for creative solutions for full-scale active-twist rotor designs. Having said that, the designs as they are now, as previously indicated, are developed enough to be employed for UAVs. IBC is being researched in a number of projects involving full-scale helicopters and may be the one closest to production. Numerous authors have looked into and tested the advantages of increased harmonic control.

The usage of on-blade morphing elements, which are typically located more outboard and primarily effect blade twist, is not excluded when IBC technology is used as the principal control of the blade root actuation. A more complex and evenly distributed approximation of the ideal profile section orientation could be achieved by using a co-ordinated mix of higher harmonic blade root and active flap motions. One of the oldest technologies to be studied is variable span, but it is also one of the most challenging to put into practice, and there has not been any success yet (for the main rotor). Its application on full-scale helicopters has been hampered by complexity, actuation needs, and safety issues, and there is no known ongoing research in this area [2]. As previously alluded to, for a transformative technology to make a significant impact within the aerospace and aviation industry, it must successfully navigate through the following critical phases: (1) a quantitative, computational examination or preliminary prototype development; (2) experiments conducted using scaled wind-tunnel testing; (3) comprehensive wind-tunnel testing at full scale; (4) demonstrator level; and (5) actual production/or fabrication. The end target of all new or proposed actuation or morphing technologies is, without doubt, fabrication. This can be substantiated by examining Figure 32, which illustrates a noticeable trend that with developmental progression, there is a decrease in the quantity of research, focus, analysis, allocation of funds, full-scale wind-tunnel testing, and eventual production related to rotary actuation morphing technology readiness. Intriguingly, this observed trend seems to be a consistent pattern for all actuation methodologies and techniques discussed in this study.

Figure 32 also illustrates that despite numerous methodologies and studies associated with active flap actuation, none have reached the stage of fabrication or application in a rotorcraft or helicopter. Additionally, only a mere handful have managed to progress to the whirl or demonstrator stage. Despite numerous methodologies and studies connected with this type of actuation, none have advanced to the stages of fabrication or implementation in a rotorcraft or helicopter, nor have they been subjected to full-scale wind-tunnel testing. A distinct issue, specifically for rotary morphing actuation, emerges from this lack of completion of the full developmental sequences (as previously discussed, i.e., from quantitative and numerical analysis to fabrication). This problem has been a consistent observation throughout the course of this review.

A comprehensive study spanning the entire development process is crucial as results from isolated stages can potentially misdirect conclusions. For instance, certain investigations [26] have suggested several advantageous locations along the span of a rotor blade (e.g., 0.5–0.7R and 74% to 92% radius) as being optimal for improving the blade's performance. Nevertheless, a thorough investigation at full scale or during the fabrication phase might unveil that these proposed positions can impose significant centripetal and

aerodynamic loads on the system, possibly triggering a structural failure or reducing the material's life expectancy. Hence, particularly in the context of a rotary actuation system, relying exclusively on numerical or computational investigations may not sufficiently delineate the most favourable scenario when contrasted with the baseline design. This problem is further exacerbated by the fact that (as highlighted in the introductory segment of this review paper) the experimental (particularly at full-scale) and fabrication phases of the morphing actuation evolution have not adequately matured. Moreover, they have not kept pace with the intricacy and diversity of the conceptual designs for morphing actuation. This holds particularly true in the context of rotary morphing actuation (Figure 25 and Table 1). Furthermore, considerable potential exists for innovation and novel designs from three different perspectives: (1) optimising the use of more chord length in the actuation system design, as previous studies have only utilised a fraction of the chord (i.e., for actuation methodology (twist, etc) and for embedding the actuator); (2) optimising a greater portion of the span length with an innovative actuation methodology which has not been practiced or investigated in the previous literature; (3) investigating a novel actuation system design using a full-scale rotor blade which implements points (1) and (2). The literature revealed that morphing rotorcraft research has looked towards expanding the flight envelope and reducing power to increase helicopter effectiveness and performance and reduce noise and vibration.

While the majority of the prior research demonstrates positive performance increases, there are still drawbacks, hence the additional following remarks are made: (1) Noise and vibration research of rotorcraft, albeit important, has had much more attention than helicopter/rotor blade aerodynamic performance, thus the data/research on aerodynamic aerodynamics has been somewhat limited (Table 1; although some investigations have explored contact load (C_L) and contact duration (C_D) separately, there is a notable lack of studies that examine C_L/C_D as a primary focus). (2) The morphing skin and actuation system remain a challenge. In the case of a variable rotor span, the actuation required is in the same direction as the large centrifugal force. Therefore, a reliable system with span flexibility becomes costly in terms of weight penalty, complexity, and maintenance. Similar challenges exist for variable rotor twist morphing and camber morphing skin/actuation systems. Since a variable rotor twist morphing system dynamically adjusts the twist of the rotor blade to optimise aerodynamic performance during flight, the materials used for variable rotor twist morphing must allow for significant deformation while maintaining structural integrity. Traditional materials often cannot provide this balance, necessitating the development of advanced composites or smart materials like shape memory alloys (SMAs).

In the case of camber rotary morphing, which adjusts the curvature of the rotor blade airfoil to optimise aerodynamic efficiency, the skin must be exceptionally flexible to accommodate significant shape changes while being robust enough to withstand substantial aerodynamic loads. This balance is challenging to achieve, and current materials often fall short, leading to the exploration of advanced composites and smart materials that can provide the necessary flexibility and strength. The actuation mechanisms for camber morphing are typically complex, involving multiple actuators and precise control systems to achieve the desired curvature adjustments. Additionally, actuators generate heat during operation, which must be efficiently dissipated to prevent overheating and ensure reliable performance. This requires advanced thermal management solutions to maintain the system's integrity and functionality over extended periods. (3) Most rotary morphing research has been numerical, computational or on scaled models with limited wind-tunnel testing. The literature suggests that rigorous research on full-scale morphing platforms is yet to fully mature. The rotary morphing methodologies (which are easier to implement), for example the trailing-edge flaps, have proven to be less effective than

other morphing solutions/methodologies (i.e., rotor twist morphing or camber morphing) yet easier to implement. Additionally, the effect of trailing-edge flaps (TEFs) has not been extensively studied in low-speed environments, and therefore, the current available information remains limited.

To transform rotary morphing technologies, significant advancements in actuation technologies are imperative. Developing more powerful and efficient actuators is crucial, as they must overcome the substantial centrifugal and aerodynamic forces experienced by rotor blades. These forces are particularly challenging at high rotational speeds and high advance ratios, where the actuators need to deliver precise and reliable performance without failure. Longer stroke actuators are also essential to achieve greater deformation capabilities, allowing for more significant adjustments in blade shape and improving aerodynamic efficiency across different flight regimes.

Lightweight materials and compact actuator designs are vital to mitigate weight penalties and facilitate integration into existing rotorcraft. Advanced composites, such as carbon fibre-reinforced polymers and lightweight alloys, offer the necessary strength-to-weight ratios. These materials must be engineered to endure the stresses and strains of morphing operations without compromising the structural integrity of the rotor blades. Enhanced durability and reliability are paramount, given the harsh operational conditions of rotorcraft.

Actuators and morphing systems must withstand high-frequency vibrations, temperature extremes, and repeated mechanical stresses. This requires the use of materials with excellent fatigue resistance and the development of robust mechanical designs that can endure prolonged use. Sophisticated control algorithms are essential to manage the complex dynamics of morphing actuators in real time. These algorithms must process sensor data swiftly and adjust actuator positions accurately to maintain optimal aerodynamic performance. Integration with the aircraft's existing avionics and flight control systems adds another layer of complexity, necessitating seamless coordination between various subsystems to ensure safety and efficiency. Effective thermal management is critical to prevent overheating of actuators, especially those based on smart materials like shape memory alloys and piezoelectrics, which generate significant heat during operation. Advanced cooling solutions, such as heat sinks, active cooling systems, and thermally conductive materials, are needed to dissipate heat efficiently and maintain the system's operational integrity. This, as alluded to earlier, requires an increased investigation into rotary morphing platforms in the coming years so they can become as diversified as the fixed-wing counterparts.

The higher diversification in actuation methodology for fixed-wing systems is primarily a consequence of fewer structural constraints and more forgiving dynamic conditions compared to their rotary-wing counterparts. In particular, traditional motor-cam systems have proven useful in fixed-wing applications where discrete hinge-line deflection or linear extension mechanisms are required such as in telescoping wings or deployable leading-edge devices [49,50]. These solutions, though mechanically intensive, offer reliable control authority and have been flight-tested in multiple adaptive wing demonstrators [2,167]. Magnetostrictive and electromagnetic actuators, on the other hand, provide compact, high-bandwidth options well-suited to localised control of aerodynamic surfaces. Their integration with unsymmetric composite laminates, as demonstrated in Schultz's pioneering work on snap-through behaviour [50,51], enables bistable morphing mechanisms that minimise energy usage during steady-state conditions [2,167]. These bistable systems can be toggled between aerodynamic states using short-duration control pulses, thereby reducing the continuous power requirements often associated with morphing actuation [52,53].

Hydraulic actuation, while less common due to complexity and weight penalties, has nonetheless been successfully employed in certain high-lift or high-load morphing scenarios [54]. The high force output of hydraulic systems makes them particularly useful for large-surface morphing or where structural resistance is significant, though their applicability is largely confined to larger, slower fixed-wing platforms [2,167]. Despite these advantages, hydraulic systems exhibit poor compatibility with rotorcraft environments due to the challenges of fluid routing through rotating assemblies and the unacceptable mass penalties they impose under high centrifugal loads [2]. Of particular interest is the emergence of hybrid actuation systems, which combine the fast response and surface-level control of piezoelectric actuators with structural features like compliant skins or bistable elements. Notably, efforts from DLR and related European programmes have demonstrated the value of these systems in dynamically altering wing camber and flow control characteristics under both open- and closed-loop regimes [55,56]. These designs emphasise the synergistic potential of actuator material co-design, leveraging the strengths of each component while mitigating their individual limitations [2,167].

Such approaches are further refined in the form of distributed smart-skin concepts, combining embedded sensors and actuation to achieve fine-grained shape control with minimal aerodynamic penalty [2]. Pneumatic actuators and compliant mechanisms represent an innovative and lightweight approach to fixed-wing morphing. Studies involving lattice-based cellular structures actuated via internal pressurisation [60], as well as bistable morphing wing sections with embedded pneumatic logic [61], show great promise for next-generation UAV platforms. These systems offer smooth, continuous shape change without relying on traditional joints or high-density power supplies, an attribute particularly valuable in applications where stealth, reliability, and adaptability are paramount [167]. However, as highlighted in recent evaluations, the power needed by pneumatic systems to overcome the stiffness of high-strength compliant materials may negate their theoretical efficiency, especially under significant aerodynamic loads. This limits their scalability for larger aircraft or highly loaded surfaces [2,62]. The literature reveals a robust fixed-wing interest in variable-camber and twist morphing using shape memory alloys (SMAs), as evidenced by a multitude of SMA torsion tube- and wire-based systems validated through wind-tunnel and benchtop testing [51–54,167]. These systems often exploit SMA's high energy density and structural integration potential, though their inherent slow thermomechanical response has led to auxiliary implementations such as active cooling and pre-stressed elastic skins to improve dynamic performance [2,167]. In rotary-wing applications, SMA use is far more limited. The dynamic and vibratory loads on helicopter rotor blades impose severe constraints on allowable actuation delay, leading to only isolated demonstrations of SMA blade twist or chord morphing, mostly in laboratory testbeds or reduced-scale UAV prototypes [2,54,167]. Piezoelectric actuators, particularly Lead Zirconate Titanate (PZT) stacks and bimorphs, continue to dominate high-frequency morphing applications in both fixed and rotary systems. In fixed-wing contexts, their integration into trailing-edge camber surfaces and smart skins enables precise roll control and flutter suppression [55,56,167]. In rotorcraft, PZT-driven flaps and twist actuators offer unparalleled vibration suppression potential, with reductions exceeding 80% demonstrated in NASA wind-tunnel tests [2,167]. However, limitations including low stroke, fragility under strain, and complex integration hinder broader deployment, especially where large deflection is needed. These constraints have pushed innovation toward composite-coupled actuators and embedded strain amplification techniques [2,57–60]. Compliant morphing technologies have emerged as a transformational alternative for both aircraft types. These systems eliminate hinges and joints by using monolithic elastic structures that deform under load, offering zero backlash and low maintenance [2,62]. Their suitability for embedded sensing and actuation makes

them ideal for seamless morphing control surfaces. In fixed-wing systems, compliant trailing edges have achieved up to 35° of control deflection without mechanical joints [2,62]. In rotorcraft, however, the challenge lies in achieving the necessary fatigue resistance and dynamic stiffness while maintaining structural compliance, a balance not yet fully resolved [2,167]. Collectively, these actuation strategies illustrate a rich and evolving landscape of morphing technologies in fixed-wing aircraft. In contrast to the piezo-dominated and dynamically constrained domain of rotary-wing morphing, the fixed-wing environment has fostered a broader experimental space, permitting the maturation of novel hybrid, bistable, and distributed actuation concepts [167]. Recent trends emphasise the transition toward fully embedded "morphing subsystems" combining actuation, control, and sensory feedback into cohesive, lightweight modules, particularly for fixed-wing UAVs [2,59–61]. In contrast, rotary-wing advancements remain narrowly focused on vibration reduction, noise control, and flight stability, reflecting the intrinsic demands of their operational environment [2,167]. This breadth not only reflects the relative ease of integration in fixed-wing platforms but also highlights the growing potential for transferring these technologies, as they evolve, into the more demanding realm of rotary-wing flight.

Table 1. Rotary morphing investigations (type and purpose).

Author & Year	Type of Investigation	Purpose of Investigation	Rotor Type	Vibration Reduction	Controller Response Time	Noise Reduction	Performance
Martin & Hall (1969) [168]	Experimental	P	tilt rotor	•	•	•	disc loading, rotor tip speed, drag
Fradenburgh (1973) [137]	Wind tunnel	P	helicopter	↓	•	•	drag at high advance ratios
Keys et al. (1987) [77]	Wind tunnel	P (-ve twist)	single blade	•	•	•	↓ hover power: −2.4%; ↑ FM: +2.4%; ↑ load: +5%; ↑ download: +6%; ↑ fwd power: +5%; ↓ L/De: −11%
Spangler & Hall (1990) [169]	Wind tunnel	C & P	CH-47D (scaled)	Potential IBC/HHC capability	3 Rev.	•	↑10–20% C_L and bandwidth ↑30%
Studebaker & Matuska (1993) [142]	Experimental	P	tilt rotor	•	•	•	↑ hover and cruise
Fenn et al. (1993) [170]	Theoretical & Design Study	VR	UH-60A	↓ >90% (predicted)	Moderate	•	actuation weights 1% of total gross weight and only uses 0.7% of cruise power
Barrett et al. (1996) [171]	Experimental	C	small UAV	•	•	•	•
Brender et al. (1997) [172]	Experimental	P	tilt rotor	•	•	•	disc loading
Wang et al. (1999) [148]	Numerical	P	tilt rotor	•	•	•	disc loading
Lee (1999) [22]	Wind tunnel	C	•	•	•	•	•
Barrett (2002) [173]	Experimental	P & C	enhanced co-axial rotor	•	Moderate (servo-based)	•	safe transition between modes
Bernhard & Chopra (2002) [108]	Experimental	P	single blade	Demonstrated at 1–3/rev	3 Rev.	•	up to ±2.2° twist; 1.9° at 3/rev; 10% thrust variation at 150 V RMS
Martin et al. (2003) [161]	Wind tunnel	P	airfoil	31–37% peak moment reduction			drag ↓ 63%, lift ↓ ~8%, drag @ α = 0
Nissly et al. (2005) [159]	Experimental	VR	airfoil		Freq. 38.75	•	↑ 17–22% lift, ↓ 50–75% drag
Dietrich et al. (2006) [4]	Experimental	VR	4-bladed	↓ >80% (at 2/rev, 40% amplitude)	3-5 Rev.	•	•
Kim et al. (2007) [70]	Computational & Experimental	VR	single blade	•	•	•	actuation auth. ↑2.1–3.5X
Kota et al. (2008) [93]	Computational & Experimental	P	single blade	•	6 Hz	•	↑ 35% in $C_{L\text{-}Max}$
Mistry et al. (2008) [80]	Numerical	P	single blade	•	•	•	↑ 1.5% FoM
Léon et al. (2009) [150]	Experimental	P	generic rotor	•	Low freq. (Q-S)	•	0.03–0.14% strain, ↓ required power 450 HP, ↑ 6.7% MTOW
Gagliardi et al. (2009) [69]	Computational	P	4-bladed	↑ 37.3% to 126%	2 Rev.	•	↑ 2.4% FoM

Table 1. *Cont.*

Author & Year	Type of Investigation	Purpose of Investigation	Rotor Type	Vibration Reduction	Controller Response Time	Noise Reduction	Performance
Barbarino et al. (2010) [174]	Experimental	P	full-scale rotor blade	•	Low freq. (Q-S)	•	30% chord extension; 39.7% strain; 610 N force; 86:1 efficiency
Khoshlahje et al. (2010) [175]	Numerical	P	single blade	•	•	•	↑ 18% power
Kammegne et al. (2015) [160]	Computational & Experimental	P	airfoil	•	~1 s	•	↓ 3–10.5% drag
Takeda et al. (2015) [81]	Computational	P	HOITS	•	•	•	↑ +1.5% FoM
Chia et al. (2017) [71]	Computational	NR & VR	4-bladed	↑ 47.1% near-field ↑ 14% far-field.	•	↓ in-plane noise 6 dB	out-of-plane noise ↑ (up to 18 dB)
Feinerman et al. (2017) [72]	Experimental	NR	single blade	•	•	3 dB	•
Xiong et al. (2020) [176]	Computational & Experimental	NR	KDE & APC	•		KDE: ↓ 2.1 dB (hover), ↓ 1.1 dB (forward flight) APC: ↓ 4.0 dB (hover), ↓ 1.3 dB (forward flight), ↓ 6 dB (experiment)	thrust ↑ up to 5.1% (KDE), ↑ 3.9% (APC)
Koning et al. (2024) [177]	Experimental (Wind Tunnel)	NR & P	4-bladed	•	•	↓ qualitative only, BVI lower in spectrograms; no dB value reported	Cl ↑ 11.8%, Cd ↓15.6%, thrust/power ↑ 9.7% (calculated from tables)

Guide: VR: vibration reduction, NR: noise reduction, P: performance, C: control, Rev: revolutions, ↑: increase, ↓: decrease, •: not explicitly addressed.

3.3.2. Technology Readiness Level for Rotary-Wing vs. Fixed-Wing Morphing Actuation Systems

An assessment of Technology Readiness Level (TRL) across rotary-wing morphing actuation systems reveals a highly non-uniform maturity landscape, with readiness strongly governed by both the intended morphing function and the associated actuation architecture. As synthesised from the reviewed literature (active-flap vs. variable-twist actuation) and reflected in the TRL distributions shown in (Figures 31–33), only a small subset of concepts has progressed beyond laboratory-scale validation, while the majority remain confined to analytical studies, bench experiments, and isolated component demonstrations. Among the reviewed technologies, trailing-edge flap actuation (particularly systems driven by piezoelectric stack actuators) exhibits the highest overall maturity. PZT-based trailing-edge flaps have advanced from early proof-of-concept testing (TRL 3–4) to repeated validation under representative centrifugal loading in whirl-tower, wind-tunnel, and scaled-rotor environments (TRL 5–6). Reported results consistently demonstrate stable multi-harmonic authority, bandwidth compatible with 3–6/rev control, and verified reductions in vibration and noise, placing these systems near the upper bound of TRL 6. Nevertheless, no trailing-edge flap system has yet achieved sustained flight demonstration (particularly mass production and implementation) or certification-level integration, with unresolved issues related to durability, high-voltage power electronics, long-term fatigue, and redundancy preventing progression beyond this level.

Active-twist morphing occupies a similar but slightly lower readiness regime. Surface-mounted piezoelectric approaches, including DAP, AFC, and MFC configurations, as well as internally embedded bending–torsion coupling concepts, have repeatedly demonstrated twist amplitudes on the order of 1–2.5° under rotating conditions, sufficient for higher-harmonic vibration control. These systems have achieved small-scale and Mach-scaled rotor testing, situating them predominantly within TRL 4–6. However, substantial blade mass penalties, actuator degradation under centrifugal loading, wiring complexity, and limited repairability have constrained advancement toward full-scale demonstrators. Quasi-static twist concepts based on centrifugal coupling or SMA actuation remain largely at TRL 3–4, with only limited wind-tunnel validation reported.

Variable-span morphing displays a bifurcated maturity profile. Mechanically actuated telescoping systems, including VDR, TRAC, and VDTR architectures, have reached extensive wind-tunnel and hover testing and, in some historical cases, approached demonstrator-level maturity (TRL 5–6). While these systems offer clear aerodynamic benefits, they remain burdened by mechanical complexity, mass growth, and reliability concerns under sustained centrifugal loading. In contrast, passive and semi-passive span-extension concepts (such as zero-Poisson ratio morphing tips) remain at TRL 3–4, having demonstrated promising structural behaviour but lacking flight-representative validation or integrated actuation strategies. Variable-chord morphing is aerodynamically attractive but technologically immature. Motor-driven X-truss mechanisms and deployable trailing-edge plates have demonstrated substantial performance gains in numerical studies and bench or low-speed rotating tests, placing them primarily within TRL 3–5. SMA-based bistable chord-extension concepts offer mechanically efficient stroke amplification but remain constrained by thermal response time, fatigue uncertainty, and control complexity. To date, no variable-chord system has demonstrated sustained operation under full centrifugal rotor environments, limiting readiness progression. Variable-camber morphing remains predominantly within TRL 2–4. Piezoelectrically actuated compliant camber concepts provide smooth aerodynamic shaping with reduced drag penalties relative to discrete flaps but suffer from limited authority and increased fabrication complexity. Electrically driven camber mechanisms offer improved control responsiveness yet face packaging and integration constraints

incompatible with current rotor blade architectures. Consequently, camber morphing has not progressed beyond bench-scale or fixed-wing wind-tunnel demonstrations for rotary-wing application.

Leading-edge and nose-droop morphing systems consistently occupy the lowest readiness levels among aerodynamically aggressive concepts. While two-dimensional studies report significant reductions in dynamic stall loads and drag, associated actuation mechanisms (whether piezoelectric, electromagnetic, or compliant) remain largely at TRL 2–4. Integration of actuators within the highly loaded leading-edge region continues to present fundamental challenges related to structural integrity, erosion resistance, and anti-icing compatibility. Finally, variable rotor speed should be regarded as a system-level enabler rather than a morphing actuation technology in isolation. Variable-RPM concepts have reached TRL 5–6 in both scaled and full-scale wind-tunnel testing and demonstrate measurable performance benefits; however, their readiness is intrinsically tied to transmission architecture and aircraft-level redesign, limiting applicability as a retrofit solution. Overall, the TRL assessment confirms that piezoelectric trailing-edge flap actuation represents the most mature and experimentally substantiated morphing actuation approach for rotary-wing systems. All other morphing categories, while often aerodynamically compelling, remain constrained by unresolved challenges in actuation authority, structural integration, fatigue durability, and certification viability. This disparity underscores a persistent gap between demonstrated aerodynamic potential and flight-ready implementation and highlights the need for future research to prioritise durability, power electronics integration, and maintainability alongside aerodynamic performance.

In contrast to rotary-wing morphing, fixed-wing morphing actuation systems have benefited from sustained investigation over multiple decades, resulting in a markedly higher and more uniform level of technological maturity (Figure 33). The fixed-wing literature [2,32,167,178] and Table A1 documents a clear progression from analytical and numerical studies through wind-tunnel validation to full-scale flight demonstrators and, in selected cases, operational deployment. This progression is reflected in the corresponding TRL distribution (Figure 33), where several actuation-driven morphing categories now reside within TRL 6–9, supported by validated structural integration, repeatable actuation performance, and demonstrated aerodynamic benefit under representative loading conditions. Planform-level morphing represents the most mature class within fixed-wing applications. Technologies such as folding wingtips, variable sweep, multi-segment wings, and polymorphic planforms have advanced to TRL 7–9 through full-scale demonstrators and flight-validated architectures. These systems typically employ robust electromechanical or hydraulic actuation integrated at the wing root or hinge line, enabling large geometric changes without disrupting primary load paths. Their high readiness is attributable to well-defined kinematics, predictable structural response, and manageable certification pathways, as actuation is largely decoupled from local aeroelastic sensitivities. Consequently, planform morphing is among the few morphing categories to approach operational viability.

Adaptive trailing-edge and leading-edge morphing systems also exhibit comparatively high readiness, generally spanning TRL 6–8. Compliant trailing-edge devices, adaptive leading-edge droop mechanisms, and continuous-camber concepts have been validated through extensive wind-tunnel campaigns and large-scale demonstrators. Actuation strategies in this category range from distributed electromechanical drives to geared motor systems and smart-material-assisted compliant mechanisms. These systems demonstrate repeatable aerodynamic improvements, including drag reduction and lift increase while maintaining acceptable surface continuity and structural durability. The absence of sustained centrifugal loading permits fixed-wing implementations to prioritise geometric fidelity and actuation precision over extreme force density, accelerating technology matura-

tion. Variable-camber and -thickness morphing concepts occupy an intermediate-to-high readiness regime, typically within TRL 5–7, depending on actuation architecture and structural complexity. Compliant mechanisms actuated by piezoelectric devices, electric motors, or hybrid schemes have demonstrated reliable shape control and measurable aerodynamic benefit, particularly in drag reduction and boundary layer management. Although mechanically more complex than discrete control surfaces, these systems benefit from relaxed packaging constraints, lower fatigue demand, and improved accessibility for inspection and maintenance. As a result, several variable-camber architectures have progressed beyond laboratory validation into large-scale demonstrators, indicating credible certification pathways.

Smart-material-based morphing systems in fixed-wing applications span a broader TRL range, from TRL 3–7, reflecting variability in actuation concept and integration strategy. Piezoelectric fibre composites, macro-fibre composites, and shape memory alloy-based systems have been extensively investigated for camber control, trailing-edge morphing, and local surface deformation. While many efforts remain at the sub-component level, multiple fixed-wing demonstrators have successfully integrated smart materials into compliant structures, achieving repeatable morphing with acceptable authority and bandwidth. The primary barriers to uniform advancement lie in actuator fatigue life, power electronics integration, and long-term reliability, rather than in fundamental actuation capability.

Overall, the fixed-wing morphing literature presents a mature and stratified TRL landscape, with several morphing actuation categories having progressed beyond experimental novelty to demonstrator-level readiness. This advancement has been enabled by comparatively benign structural environments, lower actuation bandwidth requirements, and the ability to segregate morphing mechanisms from primary load-bearing elements. Consequently, fixed-wing morphing provides not only validated aerodynamic concepts but also concrete precedents in actuator integration, redundancy management, and durability design that inform the broader development of morphing technologies across aerospace applications.

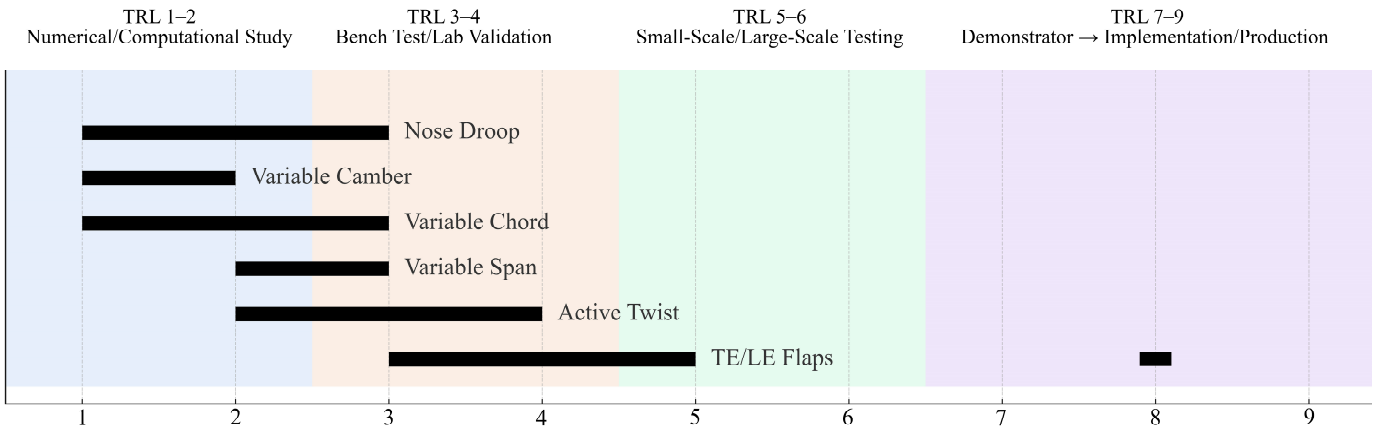

Figure 31. The Technology Readiness Level (TRL) for rotary-wing morphing actuation.

Table 2. Actuation-focused comparison of rotary-wing morphing concepts, mechanisms, performance, advantages and limitations.

Actuation Type	Key Studies	Platform	Performance/Output	Advantages	Limitations
Piezo-bender/piezo-stack TE flaps (incl. L–L amplifiers, X-frame, C-block stacks)	Lee & Chopra [20–22]; Hall & Prechtl [23–25]; Clement et al. [33]	Bench + spin + wind tunnel/scaled rotor	C-block: ≥8° pp (0–40 Hz), 11.6–13.6° pp @ 40 Hz, extrapolated ≈20° pp at 340 V; validated under rotor-relevant dynamics	High bandwidth; compact integration; high force density	High voltage; hysteresis/creep; bond-line sensitivity (≈40% variation noted); fatigue/long-life certification risk

Table 2. *Cont.*

Actuation Type	Key Studies	Platform	Performance/Output	Advantages	Limitations
ADASYS flap optimisation (geometry/placement)	Dietrich et al. [4]	Numerical (design optimisation)	$\Delta CL \lesssim 0.3$ for ~+5° TE flap; at Mach 0.33 ΔCL ~0.2, at Mach 0.74 ΔCL ~0.3	Identifies "minimum chord" designs that still deliver most controllability	Aero-performance implications secondary (study emphasis is loads/noise/vibration)
Resonant PZT TE flap (tuned system)	Kim, Wang & Smith [70]	Rotor vibration-control concept	Up to 4.5° flap deflection; 2.1–3.5× authority increase vs. non-resonant; resonance at 4/rev (26.6 Hz)	Authority boost without scaling actuator size	Resonant fatigue/heating concerns; narrowband sensitivity (needs robust control)
Closed-loop TE flap noise control (HHC framework)	Chia et al. [71]	Numerical framework (aeroelastic–acoustic)	Up to 6 dB in-plane noise reduction (left-boom feedback) but out-of-plane noise up to +18 dB; vertical hub shear +14% (far-field) and +47.1% (left-boom)	Demonstrates controllability and sensor-placement sensitivity	Explicit noise–load trade-offs; saturation/tuning complexity
Passive/deployable TE flaps for hover performance	Gagliardi & Barakos [69]	BE + RANS CFD	Best case: inboard slotted flap (32% chord, 10°) → FoM +4.7%; configuration matched "+6° twist" equivalence; further case reported +6.5% performance gain with trim reduction ~1°	Shows flap scheduling can recover hover performance without committing to high twist	Wake interaction + structural complexity; sensitive to spanwise placement/operating point
Magnetostrictive TE actuation (Terfenol-D families)	Fenn et al. [47]; Bothwell/Chandra/Chopra [63]	Bench- + concept-level rotor integration	Reported: ~90% vibration reduction (system-level concept) but with major installed mass	Attractive force characteristics; demonstrated vibration benefit	Authority-to-weight weak vs. piezo; mass + integration burden (e.g., many actuators, linkages)
Electromagnetic TE actuator	Duvernier et al. [64]	Bench	Near-constant force across stroke; mass penalty highlighted	Good controllability in principle	Weight, hysteresis/friction, and magnetic stiffness effects reduce feasibility
PAM-based TE flap	Woods et al. [65]	Wind tunnel/scaled rotor	Very large authority (reported up to ±40° on scaled tests)	Highest stroke of all approaches	Pneumatic infrastructure; bandwidth/response; durability under cyclic loading
Gurney flaps (active/passive concepts)	Concilio et al. [2]; Woodgate et al. [68]	CFD + concept studies	~7.4% thrust increase in selected configurations but ~20% average nose-down pitching-moment increase noted	Large lift augmentation with small device	Drag + pitching-moment penalties; scheduling complexity for rotor azimuth variation
LE serrations (passive)	Feinerman et al. [72]	Hover/BVI experiment	Up to 3 dB peak-to-peak BVI noise reduction (primary direction)	Passive, low integration complexity	Directional/encounter sensitivity; possible aero penalties/non-optimal response
Quasi-static twist (retwist for performance)	Keys, Tarzanin & McHugh [77]	Mach-scaled rotor test	Twist 11.5° → 17.3° → FoM +2.4% hover but 4/rev hub loads +37.3% to +126%; torsion +6% to +11%	Demonstrates measurable performance benefit	Potentially unacceptable vibration penalties; not "free" aeromechanically
Surface-mounted piezo: DAP (directionally attached)	Barrett [83] & Chopra [87]	Bench/concept lineage	"First-generation" active twist (modest twist authority)	Integrable approach; enabled later architectures	Limited strain authority; early maturity
AFC/IDEPFC/MFC-class fibre composites	NASA/Army/MIT ATR; Boeing AMR; DLR; etc. [87–108,179]	Wind-tunnel + hover tests	Tip twist up to ~1.5°; reported relative insensitivity vs. flight state in cited work	Better d33 utilisation; improved authority vs. DAP	High voltage (often hundreds of V); durability/fatigue and repairability concerns
Internal active twist (bend–torsion beam concepts)	Bernhard & Chopra (SABT lineage) [108,109]	Hover/Mach-scale	Reported tip twist up to ±2.2° (hover); control authority reported as >10% at 3/rev in described case	Clean aerodynamic integration (no external flap)	Large mass penalty (example text cites ~48% blade mass increase); piezo degradation risks

Table 2. *Cont.*

Actuation Type	Key Studies	Platform	Performance/Output	Advantages	Limitations
TWISCA/cut-section twist concepts	AT1 vs. AT2 [98], ONERA [111];	Experimental comparisons	Reported better twist performance per active area (low-voltage concept cited)	Potentially lower drive voltage than some MFC systems	Failure safety + maintainability/repairability flagged as major barriers
Quasi-static variable twist by centrifugal/coupling	NASA/Army composite coupling [112,113]; centrifugal concepts [114,115]	Concept + limited demonstrations	Large twist targets (up to ~30° cited as requirement class)	Avoids large on-blade high-frequency actuators	Strongly coupled to RPM architecture; limited retrofit feasibility
Telescoping blades (VDR/TRAC/VDTR line)	VDR (HaigK); TRAC (Sikorsky); VDTR; Wang et al. [148]	Hover stand + wind tunnel + analysis	Example stated: telescoping to 100% span hover and ~67% cruise (VDTR class)	Reconciles hover vs. cruise requirements	Mechanical complexity; mass and reliability under centrifugal loads
Passive span-extending morphing tip	Vocke et al. [149]	Structural test /concept	"100% increase" span extension (tip concept class)	Low actuation energy (centrifugal assisted)	Quasi-static; flightworthiness/bonding/skin durability remain limiting
Static Extended Trailing Edge (SETE)	Léon et al. [150]	Analysis + prototype description	30% chord extension → 16.7% power reduction (sea-level class); +6.7% to +10% GW capability (low/high altitude noted in text)	Very large aero benefit	Mechanism complexity; packaging; reliability/certification burden
Deployable trailing-edge plate (TEP) via morphing truss	Khoshlahjeh et al. [153]	CFD + RCAS	20% chord over 63–83%R; power ↓ up to 18%; cruise speed ↑ 18 kt; altitude ↑ 1800 ft (as described)	Retractable: avoids "always-on" penalty	Pitch-link load growth; aeroelastic twist interactions; integration complexity
X-truss electromechanical chord extension	Hayden [154]	Bench/rotating prototype	~8.1% chord extension (1.3 in of 16 in chord); demonstrated operation to ~209.5 g (385 rpm class)	Compact TE packaging; controllable	Efficiency/current draw issues under rotation; scaling risk
SMA bistable truss (VMT)	Barbarino et al. [156]	Bench	Snap-through with short SMA wires (amplified stroke)	Lock-free bistability	Thermal lag; fatigue; control complexity; integration into rotor TE remains immature
Hub-driven high-frequency tab concepts	JAXA active tab programme [2]	Model-scale wind tunnel (noted in text)	Noise reduction potential (described as multi-harmonic)	Moves actuation off-blade	Adds hub complexity; authority limits; transmission requirements
Conformable camber (compliant mechanisms + PZT stacks)	Gandhi et al. [158]	Bench prototype	TD-optimised: 6.0 mm (≈4.6° flap equiv); tested: 3.65 mm static; natural freq 38.75 Hz; lift +17–22% with 50–75% less drag penalty vs. 15% flap (as reported)	Aerodynamically clean; lower drag penalty than discrete flap	Fabrication complexity; lower lift per "equiv. deflection"; stiffness trade-offs
Electrically actuated camber (motor + eccentric shafts)	Kammegne et al. [160]	Wind tunnel + control validation	Transition delay 2–18% chord; drag ↓ 3–10.5%; stable actuation ~1 s	Avoids SMA thermal limits; controllable shapes	Actuator bulk; linkage complexity; packaging limits
VDLE (variable drooped LE)	Martin et al. [161]		Drag ↓ up to 63%; peak moment ↓ 31–37%; negative pitch damping eliminated; lift penalty ~8%	Strong dynamic-stall mitigation with fewer low-AoA penalties	Full-scale integration in D-spar region is difficult; mechanism packaging in rotor blade remains a key barrier
Piezo-stack nose droop	Shaner & Chopra [162]		Achieved ~1° vs. 5° target (as described)	Compact; high force potential	Stroke losses, hinge stiffness, alignment issues dominate; needs major mechanical refinement
Electromagnetic droop (LEEMA)	Fink et al. [163]	Bench prototype demonstration (as described)		Smooth actuation feasibility	Mass/packaging remain key concerns

Table 2. *Cont.*

Actuation Type	Key Studies	Platform	Performance/Output	Advantages	Limitations
Variable RPM envelope studies (UH-60A-type models)	[92,116–119,164]		Power reduction up to ~14% (described)	Benefits increase when combined with span/twist morphing; shifts complexity to drivetrain/controls	
Compliant morphing LE (FlexSys /AMRDEC class)	FlexSys/AMRDEC [180]		±10° at 6 Hz (described); 35% retreating-blade lift increase without stall; power ~885 W for 7 ft span flap (described)	Jointless smooth surface; high aerodynamic benefit	Stress/structural optimisation needed; backlash issues noted; full-scale integration not yet mature
Slowed-rotor experiment (NFAC 40 × 80, UH-60A)	[122,123]	Full-scale	Tested at 65% and 40% nominal RPM; advance ratio up to ~1.0; max forward speed reported up to 182 kt	Revealed new aeroelastic phenomena (reverse-chord dynamic stall and large torsional excursions); feasibility demonstrated but system-level integration dominates maturity	

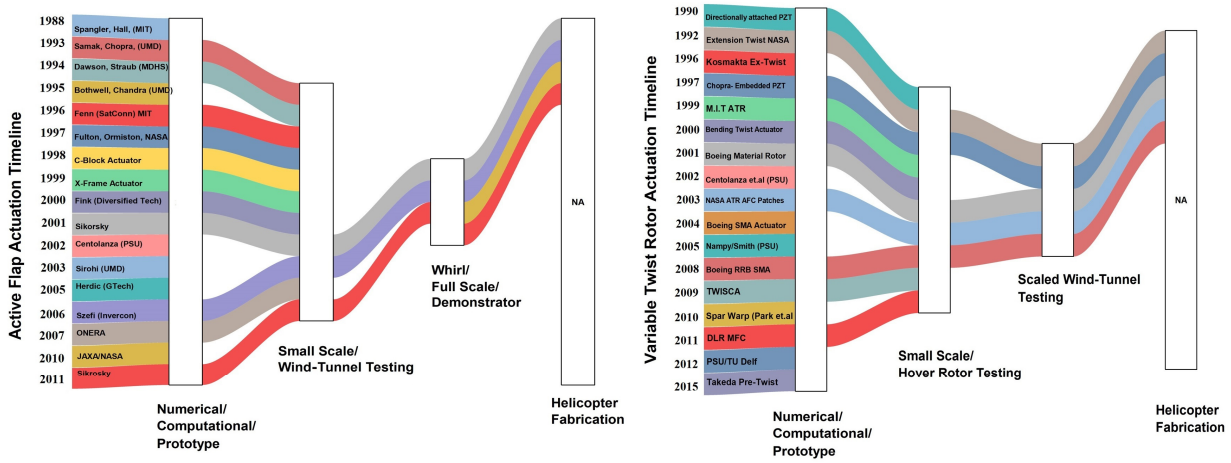

Figure 32. Active flap actuation timeline: decline in research, testing and no fabrication (**left**). Variable-twist rotor actuation timeline: decline in research, testing and no fabrication (**right**).

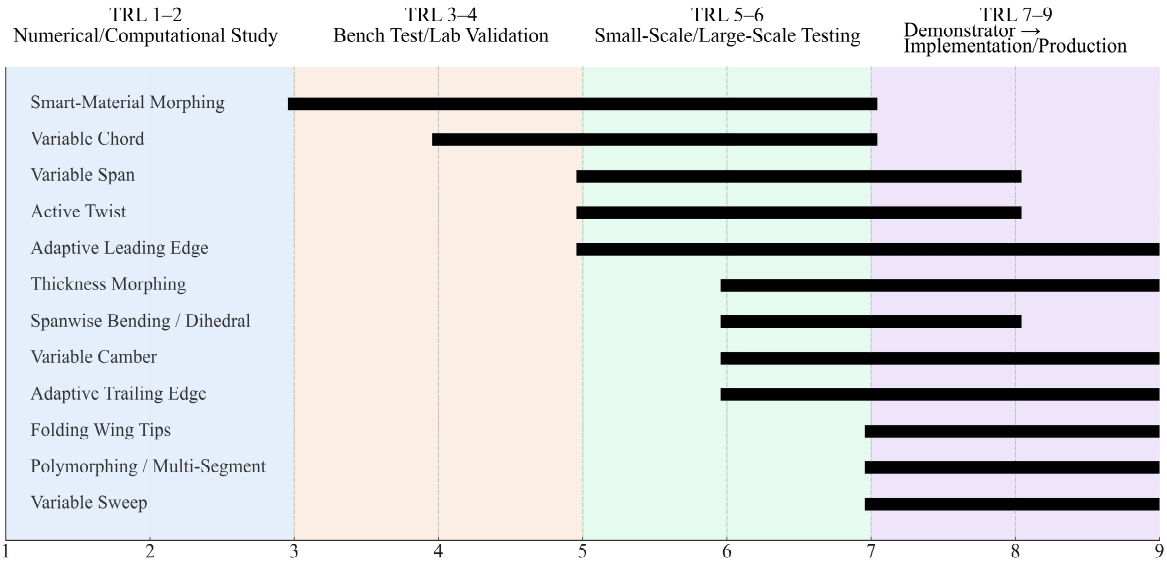

Figure 33. The Technology Readiness Level (TRL) for fixed-wing morphing actuation systems.

3.3.3. Actuation Concept-Transfer Feasibility (ACTF) Study of Mature Fixed-Wing Morphing Systems to Rotary-Wing Platforms

The evolution of morphing-wing technologies over the past two decades has been predominantly shaped by fixed-wing research, where large lifting surfaces, benign dynamic environments, and comparatively relaxed structural constraints have enabled the maturation of several advanced actuation concepts. A key example of this is the study conducted by Crawley and de Luis (1987) [181], who explored piezoelectric actuators in intelligent structures, focusing on static and dynamic coupling with substructures. They presented analytic models, validated with aluminium, glass/epoxy, and graphite/epoxy beams using surface-mounted or embedded actuators. Their findings showed good correlation between predicted and experimental results for modal damping and forced response, with constant damping ratios for the materials tested. The study demonstrated that piezoelectric actuators could control deformation while being compact and lightweight, without significantly affecting mass or dynamics, which also offered a promising solution for vibration damping and dynamic control, but challenges in material selection and scale remained.

Crawley's work highlights the significance of this article's Actuation Concept-Transfer Feasibility (ACTF) study; although his research was not specifically applied to rotorcraft, the groundwork he established in integrating piezoelectric materials has had a lasting impact, influencing subsequent studies by Spangler, Hall, Chen, Chopra, and others. This set the stage for the application of piezoelectric actuators in rotor control and vibration damping, which are now being explored for real-time active control in rotary systems. As a result, we turn our attention to the ACTF study (categorised in Table 3), evaluating recent actuation technologies that have the potential to enhance and be implemented into rotary-wing platforms.

In this feasibility study, the fixed-wing morphing and actuation architectures are examined through the lens of rotary-wing operational requirements: extreme centrifugal loads, multi-axis vibratory forcing, high-frequency dynamic bandwidth, and slender structural envelopes. Clear patterns emerge in terms of which technologies are realistically transferable, which require substantial adaptation, and which are fundamentally incompatible. The resulting feasibility map reveals three categories, transferable technologies, partially transferable technologies, and non-transferable technologies, each defined by structural scalability, achievable bandwidth, fatigue behaviour, and integration viability.

(a). Fully Transferable Technologies

Several actuation systems originally developed for fixed-wing morphing have demonstrated strong potential (or direct experimental success) when applied to rotorcraft blade morphing. Foremost among these are piezoelectric actuation technologies (PZT stacks, MFC patches, and bimorph benders), which offer the high bandwidth, compact form factor, and structural compatibility required for trailing-edge flap modulation and active-twist control. Fixed-wing studies established their efficiency in camber modulation and smart-skin architectures, while rotary-wing investigations have already implemented them in testbed systems such as servo-actuated piezo flaps, segmented flexure-driven trailing edges, and piezoelectric torsion actuators. This makes piezoelectric-based systems not merely transferable but transition-ready for full-scale rotor applications, with the major limitations being voltage requirements and dielectric fatigue under cyclic loads rather than any fundamental incompatibility.

Shape memory alloy (SMA) actuation also occupies a high-feasibility category, particularly SMA torque tubes, SMA flexural ribs, and compact torsion actuators. Although SMA actuators are thermally bandwidth-limited, fixed-wing research has already demonstrated their significant torque density and structural integration benefits. Rotary-wing environments impose stricter thermal response and cooling requirements but do not in-

validate SMA morphing mechanisms; thus, SMA systems are considered conditionally transferable, best suited for low-rate morphing tasks such as adaptive twist biassing and slow camber reconfiguration.

Similarly, compliant and bistable mechanisms (including flexure-driven morphing devices, cambered trailing-edge architectures, and bistable snap-through elements) exhibit high promise for transfer due to their lightweight nature and lack of multi-link mechanical assemblies. These systems reduce part count, eliminate hinges, and avoid the use of heavy actuation hardware, thereby aligning well with rotorcraft's mass and fatigue constraints. Fixed-wing research shows that such systems can maintain significant deformation authority while resisting compressive and shear loads; translating these into rotor blades primarily requires validating their endurance under vibratory load spectra and large cyclic stress reversals.

Finally, smart skins incorporating embedded piezoelectric elements represent a conceptually elegant solution for rotorcraft: continuous, surface-integrated actuation without discrete movable surfaces. Fixed-wing work on compliant skins provides an essential knowledge base for producing smooth, load-bearing, morphable surfaces. Their transferability is high, but their integration in rotary systems hinges on developing robust bonding methods, skin lay-ups, and patch architectures that survive centrifugal stiffening and rotating-frame fatigue.

(b). Partially Transferable/High-Risk Technologies

Some fixed-wing morphing systems present partial feasibility but require major adaptation before becoming viable in the rotary domain. Pneumatic morphing structures, such as pressurised elastomeric honeycombs or inflatable sections, function effectively in fixed-wing applications due to their ability to generate smooth, continuous deformation. However, under rotor conditions (where centrifugal loads exceed several hundred g at the blade tip), the internal pressurisation needed to sustain deformation becomes impractical. These systems may still find use in hub-mounted morphing devices or slow-rotating UAV rotors but are not yet suitable for high-speed rotors.

Magnetostrictive actuators, while powerful and capable of driving bistable mechanisms in fixed-wing contexts, face challenges in rotary blades: added mass, coil heating, and power-conditioning requirements. Their theoretical feasibility is not excluded, but they remain unvalidated in dynamic rotating environments.

Traditional servo-based mechanisms (cams, geared motors, and screw-driven actuators) fall into this mid-feasibility category. Fixed-wing morphing demonstrations often rely on robust mechanical linkages to generate large camber or chord changes. Such systems, however, do not readily scale into rotating frames, where mechanical routing, high-frequency vibration, and mass penalties render conventional servo linkages unsuitable. Only servo architectures that operate at the hub or use very short internal linkages may be considered for future scaling.

(c). Non-Transferable Technologies

A wide range of morphing geometries well-explored in fixed-wing platforms do not transfer at all to rotorcraft blades due to fundamental physical and structural incompatibilities. Most prominently, variable-span, variable-sweep, and large-scale planform morphing mechanisms are incompatible with rotorcraft operation. The centrifugal stiffening of rotor blades makes span extension mechanically impossible and sweep and dihedral changes structurally unfeasible. These morphing classes are irrevocably grounded in the fixed-wing domain and do not possess plausible adaptation pathways for rotorcraft.

Likewise, thickness morphing systems, such as elastomeric bumping and SMA-induced thickness variation, cannot be integrated into the extremely thin and structurally

efficient cross-sections of rotor blades. These concepts rely on internal volume, bending flexibility, and structural redundancy that rotor blades cannot physically accommodate.

Finally, multi-segment polymorphing architectures (including scissor mechanisms, sliding ribs, segmented wingboxes, and HECS-type modular morphing structures) are fundamentally incompatible with rotor load cycles. The complex interactions of joints, bearings, and sliding elements cannot withstand the high-frequency load reversals and combined bending–torsion loads experienced along the blade span. Thus, these systems are categorically non-transferable.

In summary, the transferability of fixed-wing morphing technologies into the rotary-wing domain is governed not by the raw morphing capability of each system but by its scalability under centrifugal loading, bandwidth under vibratory forcing, mass efficiency, and structural compatibility with slender, rotating blades. The technologies with the highest feasibility (piezoelectric actuation, SMA torsion mechanisms, compliant/bistable architectures, and smart skins) share key attributes: minimal moving parts, compact integration, and the ability to withstand or avoid high dynamic loads. Conversely, technologies rooted in large geometric changes, heavy mechanical assemblies, or volumetric deformation mechanisms are fundamentally incompatible.

Table 3. Expanded transferability matrix (fixed → rotary actuation systems).

	Actuation Specifics	**Transferability**	**Why/Why Not**	**Evidence**
Piezo-electric				
	Piezoelectric Servo Flaps [9,10,24]	High	Proven for HHC, BVI noise reduction	Rotary: ADASTYS, Hall & Precht, CH-47D scale tests
	Piezo Bimorphs [13]	Moderate–High	Good flap authority but limited stroke; fatigue minor issue	Fixed: LE/TE flexure actuation; Rotary: several 0.125R–0.2R flap demos
	PZT Stack Actuators [30]	High	High bandwidth, high force, compact; ideal for TE flaps	Fixed: TE camber actuation; Rotary: Hall & Precht, APC-850 servo flaps
	Macro-Fibre Composite (MFC) [52,108,111,159]	High	High strain, surface-conforming, lightweight	Fixed: FishBAC/MFC skins; Rotary: MFC twist prototypes
	Surface-Embedded Piezo Patches [86]	Moderate–High	Scalable and low-mass for dynamic control; voltage limits	Fixed: Aeroelastic control; Rotary: concept studies + limited tests
SMA				
	SMA Flexure Mechanisms [10,13]	Moderate	Good for LE morphing; thermal lag limits high-freq control	Fixed: LE droop demos; Rotary: feasible only for slow morphing
	SMA Wires [33]	Moderate	High force, slow response; thermal issues at rpm	Fixed: LE morphing; Rotary: limited twist demos
	SMA Bistable Structures [51,52,156,167]	Moderate	High energy efficiency; snap-through may fatigue under rpm	Fixed: bistable camber; Rotary: no demos yet
	SMA Torque Tubes [64,182]	Moderate–High	Good torsion, compact; heating/cooling challenge	Fixed: Ajaj et al. torque work; Rotary: twist actuation prototypes
Compliant & Flexural Architectures				
	Bistable Composite Surfaces [50,51]	Moderate	Lightweight but bistability may cause dynamic instability	Fixed: Schultz et al.; Rotary: no high-rpm data
	Compliant LE Skins [93,162,163]	Moderate	Good morphing but high suction peaks under rpm	Fixed: LE adaptive structures; Rotary: structural risk at high Mach tip
	Compliant TE (FishBAC) [182,183]	High	Smooth continuous camber, low mass	Fixed: FishBAC proven; Rotary: high potential but needs fatigue proofing
	Corrugated/Zigzag Skins [184]	Low–Moderate	Flexible but structurally weak under centrifugal force	Fixed: Zigzag wingbox; Rotary: insufficient stiffness

Table 3. *Cont.*

	Actuation Specifics	Transferability	Why/Why Not	Evidence
Magnetic/Electromagnetic Actuation				
	Magnetostrictive (Terfenol-D) [47,64]	Low–Moderate	Good force; very heavy; heating at rpm	Fixed: limited camber work; Rotary: untested
	Electromagnetic Linear Actuators [164]	Low	Too heavy + wiring complexity in rotating frame	Fixed: some prototypes; Rotary: impractical
	Magnetic Torque Rods (Magnetorquers) [167]	Low	Weak torsion under centrifugal stiffening (mainly used in satellites)	Only conceptual evidence
Piezo-electric				
	Piezoelectric Servo Flaps [9,10,24]	High	Proven for HHC, BVI noise reduction	Rotary: ADASTYS, Hall & Precht, CH-47D scale tests
	Piezo Bimorphs [13]	Moderate–High	Good flap authority but limited stroke; fatigue minor issue	Fixed: LE/TE flexure actuation; Rotary: several 0.125R–0.2R flap demos
	PZT Stack Actuators [30]	High	High bandwidth, high force, compact; ideal for TE flaps	Fixed: TE camber actuation; Rotary: Hall & Precht, APC-850 servo flaps
	Macro-Fibre Composite (MFC) [52,108,111,159]	High	High strain, surface-conforming, lightweight	Fixed: FishBAC/MFC skins; Rotary: MFC twist prototypes
	Surface-Embedded Piezo Patches [86]	Moderate–High	Scalable and low-mass for dynamic control; voltage limits	Fixed: Aeroelastic control; Rotary: concept studies + limited tests
SMA				
	SMA Flexure Mechanisms [10,13]	Moderate	Good for LE morphing; thermal lag limits high-freq control	Fixed: LE droop demos; Rotary: feasible only for slow morphing
	SMA Wires [33]	Moderate	High force, slow response; thermal issues at rpm	Fixed: LE morphing; Rotary: limited twist demos
	SMA Bistable Structures [51,52,156,167]	Moderate	High energy efficiency; snap-through may fatigue under rpm	Fixed: bistable camber; Rotary: no demos yet
	SMA Torque Tubes [64,182]	Moderate–High	Good torsion, compact; heating/cooling challenge	Fixed: Ajaj et al. torque work; Rotary: twist actuation prototypes
Compliant & Flexural Architectures				
	Bistable Composite Surfaces [50,51]	Moderate	Lightweight but bistability may cause dynamic instability	Fixed: Schultz et al.; Rotary: no high-rpm data
	Compliant LE Skins [93,162,163]	Moderate	Good morphing but high suction peaks under rpm	Fixed: LE adaptive structures; Rotary: structural risk at high Mach tip
	Compliant TE (FishBAC) [182,183]	High	Smooth continuous camber, low mass	Fixed: FishBAC proven; Rotary: high potential but needs fatigue proofing
	Corrugated/Zigzag Skins [184]	Low–Moderate	Flexible but structurally weak under centrifugal force	Fixed: Zigzag wingbox; Rotary: insufficient stiffness
Magnetic/Electromagnetic Actuation				
	Magnetostrictive (Terfenol-D) [47,64]	Low–Moderate	Good force; very heavy; heating at rpm	Fixed: limited camber work; Rotary: untested
	Electromagnetic Linear Actuators [164]	Low	Too heavy + wiring complexity in rotating frame	Fixed: some prototypes; Rotary: impractical
	Magnetic Torque Rods (Magnetorquers) [167]	Low	Weak torsion under centrifugal stiffening (mainly used in satellites)	Only conceptual evidence
Pneumatic/Hydraulic/Fluidic Systems				
	Hydraulic Micro-Actuators [53]	Low–Moderate	High authority, too heavy unless near hub	Fixed: control surfaces; Rotary: mass penalty
	Fluidic Flexible Matrix Composites (F2MC) [114]	Low	Pressure-dependent response incompatible with rpm	Fixed: twist & bend; Rotary: no viable path
	Pneumatic Elastomeric Honeycombs [149]	None–Low	Pressurisation fails under 300–600 g centrifugal loads	Fixed: camber/thickness morphing; Rotary: impossible at tip loads

Table 3. *Cont.*

	Actuation Specifics	Transferability	Why/Why Not	Evidence
Deployable Structures				
	Origami/Folding Structures [185–188]	None	Joints and folds fail under cyclic rpm loads	Fixed: deployables; Rotary: impossible
	Scissor/Lattice Deployables [189]	None	Cannot withstand centrifugal stiffness demands	Fixed: polymorphing wings; Rotary: nonviable
	Multi-Segment Wingboxes [190,191]	None	Too many moving parts; vibration-induced failure	Fixed: HECS-type wings; Rotary: structurally impossible
Aeroelastic Morphing				
	Passive Twist (bend–twist coupling) [178]	High	Already used in rotor blades; natural transfer	Fixed: aeroelastic tailoring; Rotary: standard practice
	Aeroelastic Camber Morphing [178]	Moderate	Needs compliant skins; risks LE/TE divergence	Fixed: passive cambering; Rotary: partially feasible
	Flutter-Induced Morphing [178]	Moderate	High risk; nonlinear behaviour	Fixed: academic; Rotary: hazardous but theoretically usable
	Post-Buckling Morphing [178]	Low	Uncontrolled under rpm; dangerous	Fixed: safe on static wings; Rotary: catastrophic risk
	Passive Twist (bend–twist coupling) [178]	High	Already used in rotor blades; natural transfer	Fixed: aeroelastic tailoring; Rotary: standard practice
	Aeroelastic Camber Morphing [178]	Moderate	Needs compliant skins; risks LE/TE divergence	Fixed: passive cambering; Rotary: partially feasible
Macro-mechanical Actuator				
	Servo-Driven Flaps [9,10,23,24]	Moderate–High	Proven using specialised linkages; mass penalty	Fixed: ubiquitous; Rotary: used in slow-rotor UAVs
	Tendon/Cable Systems [192]	Moderate	Lightweight; routing complexity in rotating frame	Fixed: compliant TE; Rotary: possible but delicate
	Rack-and-Pinion Systems [193]	Low–Moderate	Hard to embed in slender blade	Fixed: span morphing; Rotary: geometric incompatibility
	Linear Screw Actuators [194]	Low	Heavy, slow, friction-sensitive	Fixed: chord morphing; Rotary: impractical
Unique Fixed-Wing only (Non-transferable)				
	Variable Span [134–149]	None	Centrifugal stiffening prevents telescoping	Fixed: telescopic wings; Rotary: impossible
	Thickness Morphing [178]	None	No internal volume in rotor airfoils	Fixed: pneumatic skins; Rotary: incompatible
	Variable Sweep [195,196]	None	Cannot pivot under 400 g loads	Fixed: mission adaptive wings; Rotary: nonviable
High-TRL Rotary-Specific				
	High-Bandwidth TE Flaps [20,30]	High	Already used in fixed-wing gust control	Rotary → Fixed proven
	Active Twist (distributed) [7,74,75,83,85–87,92,94–102,105,107,108,110,111,133]	Moderate	Fixed wings do not need high-frequency twist	Rotary: lab demos
	Smart Spars [197]	Moderate	Possible but limited payload	Rotary: concept-level

This ACTF and transmissibility analysis underscores that future advances in rotorcraft morphing will not necessarily arise from the invention of entirely new actuation technologies; instead, the most rapid progress will occur by strategically translating, miniaturising, and dynamically hardening the fixed-wing morphing systems that already exhibit strong structural and functional alignment with rotary-wing constraints.

4. Conclusions

Rotary morphing actuation systems present a range of complex challenges that differ significantly from those encountered in non-rotary systems. One of the main challenges is the highly dynamic and complex aerodynamic environment of rotorcraft, which places

unique demands on both the structural and mechanical components of morphing systems. The rotary-wing environment involves rapidly changing flow conditions, high centrifugal forces, and significant vibration loads, all of which complicate the design and integration of actuation mechanisms. Actuators in rotary systems must not only withstand these harsh conditions but also operate efficiently without compromising the structural integrity or aerodynamic performance of the rotor blades.

A key takeaway from this study is that no single actuation system can universally address all morphing requirements. Each system must be evaluated against the specific challenges it will face in a given application. For example, while trailing-edge flaps have been widely studied and demonstrated to reduce noise and vibration, their integration into full-scale rotorcraft has been limited due to the complexity and weight of the systems required. Active-twist systems offer promising performance enhancements, yet they too have struggled to progress beyond laboratory and small-scale testing.

The review also reveals that a significant portion of research on rotary systems has not advanced beyond preliminary stages, such as computational modelling or limited wind-tunnel tests. Only a few studies have moved on to more extensive testing or the construction of prototypes, with merely one rudimentary model being tested on an actual helicopter. This gap in research and development suggests that many promising technologies are not being fully realised, pointing to a critical need for more comprehensive studies that include full-scale testing and prototype fabrication.

Furthermore, an evident gap exists in the focus and distribution of investigative efforts across different performance objectives. While noise and vibration reduction have received considerable attention, investigations centred on enhancing aerodynamic efficiency (C_L/C_D) have been markedly scarce. This underrepresentation indicates an important area for future research. To address this imbalance, future design efforts should prioritise in-depth aerodynamic studies of rotary morphing systems, employing advanced and innovative approaches that extend beyond conventional morphing techniques. Such work is essential for optimising aerodynamic performance, which remains a relatively unexplored dimension in the current literature.

In addition to these observations, the comparative Technology Readiness Level (TRL) assessment presented in this review highlights a pronounced maturity gap between fixed-wing and rotary-wing morphing actuation systems. While several fixed-wing morphing technologies have progressed to high TRL states through full-scale testing and, in some cases, flight demonstration, the majority of rotary-wing morphing actuation concepts remain constrained to low-to-mid TRLs. This disparity underscores the limited progression of rotary morphing systems through later development stages, particularly full-scale validation and operational demonstration, and reinforces the need for structured TRL-driven development strategies tailored specifically to the rotorcraft environment.

The Actuation Concept-Transfer Feasibility (ACTF) analysis further indicates that, although many fixed-wing morphing actuation technologies demonstrate sufficient authority and maturity, direct transfer to rotary-wing platforms is rarely straightforward. Centrifugal loading, bandwidth requirements, aeroelastic coupling, and stringent reliability constraints introduce fundamental challenges that must be addressed through targeted redesign rather than direct adoption. Nevertheless, the analysis identifies select actuation architectures (particularly high-force-density piezoelectric and electromechanical systems) as promising candidates for transfer, provided that their integration is re-optimised for rotating structures and validated under representative centrifugal and vibratory conditions.

Overall, the findings of this review indicate that future progress in rotary morphing actuation will depend not only on the development of novel actuation mechanisms but also on systematic and coordinated efforts to advance promising concepts through higher

Technology Readiness Level (TRL) stages. In this context, clear opportunities are identified for the development of rotary morphing actuation systems employing larger chord sections (i.e., full-chord twist morphing), extended spanwise actuation regions, and innovative actuation architectures that can be rigorously matured through all stages of the development lifecycle. This progression must encompass coordinated numerical investigations, computational fluid dynamics (CFD) simulations, small-scale experimental validation, full-scale demonstrator testing, and ultimately fabrication for practical implementation. Such structured, TRL-driven development pathways are essential for explicitly addressing scalability, durability, and integration challenges, while also enabling informed technology-transfer strategies. By aligning morphing actuation research with these comprehensive frameworks, the rotorcraft community can more effectively bridge the gap between conceptual innovation and operational implementation, thereby advancing rotary morphing technologies beyond their current limitations and closer to deployment within the aerospace industry.

Author Contributions: Conceptualization, A.G.; methodology, M.B.; software, M.B.; validation, A.G. and M.B.; formal analysis, M.B.; investigation, M.B.; resources, M.B.; data curation, M.B.; writing—original draft preparation, M.B.; writing—review and editing, A.G.; visualization, M.B.; supervision, A.G.; project administration, M.B.; funding acquisition, not applicable. All authors have read and agreed to the published version of the manuscript.

Funding: This investigation was conducted as part of the doctoral research of the corresponding author, and therefore, there are no external or internal sources of funding to declare.

Data Availability Statement: The data underlying the findings of this study are available from the corresponding author upon reasonable request.

Conflicts of Interest: The authors declare no conflicts of interest.

Declarations: Figures 1, 4–17 and 21–33 are original illustrations generated digitally based on conceptual information available from their respective sources [2,10,13,20,23,30,31,33,47,63,65,69–72,92,108,149–151,154,155,160–162]. These illustrations are not redistributions of published figures. Figures 18–20 are investigations conducted by DLR and are licenced under CC BY 3.0, ref. [98] along with the copyright permissions granted by the authors of the ERF2014 Proceedings for open redistribution. These figures are part of the ERF2014 Proceedings, which are freely available in an online repository. The authors have confirmed permission for publication and distribution, as stated in the copyright statement [95].

Abbreviations

ACTF	Actuation Concept-Transfer Feasibility
ADASYS	ADAptive Dynamic SYStems
AFC	Active Fibre Composite
AMR	Advanced Material Rotor
AMRDEC	Aviation & Missile Research, Development, & Engineering Center
APC	Automatic Pitch Control
ATR	Active-Twist Rotor
ATB	Active-Twist Blade
AVINOR	Rotorcraft Analysis Code
BCDI	Blade-Controlled Disturbance Interaction
BVI	Blade–Vortex Interaction
CFD	Computational Fluid Dynamics
CFD/CSD	CFD & Computational Structural Dynamics Coupling Investigation
DAP	Directionally Attached Piezoelectric
DSP	Digital Signal Processor
EMC	Elastomer-Matrix Composite

FEM	Finite Element Method
FoM	Figure of Merit, $C_{TH}^{\frac{3}{2}}/C_{PH}\sqrt{2}$
HELINOIR	Rotorcraft Acoustic Code
HHC	Higher Harmonic Control
HOTIS	Hover Tip Vortex Structure Test
IBC	Individual Blade Control
IDEPFC	Interdigitated Electrode–Piezo Fibre Composite
JAXA	Japan Aerospace Exploration Agency
Ksi	Kilo-pounds per square inch
LEEMA	Leading-Edge Electromagnetic Airfoil
LRTA	Large Rotor Test Apparatus
LVPZT	Low-Voltage Lead Zirconate Titanate
MFC	Macro-Fibre Composite
MTOW	Maximum Take-Off Weight
NACA	National Advisory Committee for Aeronautics
NFAC	National Full-Scale Aerodynamics Complex
NIDAQ	National Instruments Data Acquisition System
ONERA	Rotorcraft CFD tool
OSR	Optimal Speed Rotor
PAM	Pneumatic Artificial Muscle
PZT	Lead Zirconate Titanate (chemistry notation)
RANS	Reynolds-Averaged Navier–Stokes
RCAS	Rotorcraft Comprehensive Analysis System
RMS	Root Mean Square (effective/equivalent DC voltage)
RPM	Rotations Per Minute
RRB	Reconfigurable Rotor Blade
SABT	Smart Active Blade Tip
SETE	Static Extended Trailing Edge
SHCT	Short-Haul Civil Tiltrotor
SMA	Shape Memory Alloy
SMART	Smart-Material-Actuated Rotor Technology
TEF	Trailing-Edge Flap
TEP	Trailing-Edge Plate
TD	Tip Deflection
TRAC	Telescoping Rotor AirCraft
TRL	Technology Readiness Level
TWISCA	TWIstable Section Closed by Actuation
UAV	Unmanned Aerial Vehicle
UMARC	FEM-Based Helicopter Simulation Code
VDLE	Variable-Droop Leading Edge
VDR	Variable-Diameter Rotor
VDTR	Variable-Diameter Tilt Rotor
VGART	Variable-Geometry Advanced Rotor Technology
VMT	Von Mises Truss
Vrms	Volts Root-Mean-Square

Nomenclature and Greek Symbols

C_D	drag coefficient
C_L	lift coefficient
C_L/C_D	aerodynamic efficiency
$C_{L\text{-}Max}$	maximum lift coefficient
C_M	moment coefficient
C_P	power coefficient
C_T	thrust coefficient
C_T/σ	blade loading

c	blade chord, m
D	drag force, N
L	lift force, N
L/D	aerodynamic efficiency
M	Mach number
r/R	the ratio of spanwise blade position to total rotor length
σ	solidity ratio, $\sigma = N_b c_{ref}/\pi R$
μορφη′	morphing

https://doi.org/10.3390/aerospace13030297

Appendix A

Table A1. Actuation-focused comparison of fixed-wing morphing concepts, mechanisms, performance, advantages and limitations.

Actuation Mechanism	Key Investigation	Investigation Type	Performance Output	Actuation Advantages	Actuation Limitations
Span					
Rack-and-pinion (Servo-driven telescoping wing)	Arrison et al. (2003) [198]	Design, fabrication, CFD (VLM), flight testing (RC demonstrator)	• Span increase: +36% (54 → 74 in) • Wing area increase: +15% • Predicted range increase: +19% (up to +57% if mass-normalised) • Lift-to-drag ratio increase (extended): L/D ≈ 53.6 vs. 34.1 baseline	• High force authority suitable for large geometric change • Fast response, reversible, and repeatable • Mature, low-risk electromechanical technology • Easily integrated with conventional control systems	• Increased mass and volume penalty (gears, racks, servos) • Mechanical complexity and wear points • Requires continuous power for motion
Pneumatic inflatable telescopic spar—Span/aspect-ratio morphing	Blondeau et al. (2003) [199]	Structural design, analytical modelling, wind-tunnel experimental validation	• Aspect ratio change: +114% (7″ → 15″ span) • Supported wing loading: up to 30–32 lb/ft^2 (≈2× typical UAV loading) • Smooth deployment/retraction at 50–70 psi • Measured L/D (fully deployed): ≈9–10 • L/D penalty vs. rigid wing at max span: ≈−25%	Very low mass compared with lead-screw or motorised telescoping systems • High force-to-weight ratio via pressure actuation • Minimal moving mechanical parts → reduced wear • Intrinsically compliant, enabling load accommodation • Compact stowage capability	• Requires onboard pneumatic system (pressure source, valves, seals) • Leakage and seal integrity are critical reliability drivers • Pressure-regulated actuation complicates precise positioning
Obliquing, symmetric & asymmetric span extensions (electromechanical)	Sullivan and Watkins (2003) [200]	Numerical and prototype	• Aspect ratio change: 3.3 → 4.7 (~30%) • An increase in take-off ground roll (100% increase)		

Table A1. *Cont.*

Actuation Mechanism	Key Investigation	Investigation Type	Performance Output	Actuation Advantages	Actuation Limitations
Hybrid pneumatic-electromechanical system enabling multi-DOF planform morphing (span, sweep, twist, tail extension)	Neal et al. (2004) [201]	Full-scale wind-tunnel demonstrator; analytical modelling; control-system integration	• 7-DOF morphing capability (span, sweep, twist ×2 wings, tail extension) • Span increase: +38–44% (17″ → 24.5″ per wing) • Aspect-ratio change: +131% (AR 1.4 → 3.24) • Sweep variation: 0–40° • Twist authority: ±20° per wing • Demonstrated drag minimisation across wide C_L range via configuration switching • Stroke: 8 in (span), 6 in (tail) • Position accuracy: ±0.05 in • Max extension rate: 8 in/s • Output torque: ≈106 in-lb at 70 psi • Linear spanwise twist distribution achieved • Sweep rate: 30°/s • Position accuracy: ±0.3° • Load-holding under aerodynamic forces	• Hybrid approach assigns actuators by load requirement • Pneumatics used where large stroke/low mass is critical • Electromechanical sweep actuators provide load-holding capability • Very high force-to-weight ratio for large strokes • Lighter than hydraulic or screw-drive alternatives • Simple on–off solenoid control with PWM pressure modulation • Intrinsic compliance reduces peak load transmission	• Requires compressed air system (mass + complexity) • Bandwidth limited vs. electromechanical actuators • Position precision inferior without pressure regulators • Pneumatic dynamics complicate closed-loop flight control • Higher mass than pneumatic alternatives • Electrical power demand (24 V, 2.5 A) • Twist authority increases with span → nonlinear control coupling
Hybrid pneumatic-electromechanical actuation enabling large- and small-scale morphing (span, sweep, twist, tail translation, tail incidence)	Neal et al. (2006) [202]	Wind-tunnel experimental testbed; structural design; actuation integration; strength analysis	• 8 DOF morphing capability • Span extension under load (loiter ↔ dash) • Sweep variation combined with span contraction • Independent wing twist replaces conventional elevons • Demonstrated morphing under ≥4W design load • Twist torque: ≈113 in-lbs at 80 psi • Achieved smooth ±20° twist under aerodynamic load • Deformation reduced from ~1.5 in → 0.02 by using internal inserts • Tail contraction: 6 in • Lateral extension: 4 in (≈3 s)	• One of the most complete multi-DOF morphing wind-tunnel platforms to date • Enables study of both planform morphing and control morphing • Supports symmetric and asymmetric morphing for manoeuvring research • Exceptional force-to-weight ratio for large strokes • Lower mass than screw or hydraulic alternatives • Proportional flow valves enable trajectory and rate control	• Highly nonlinear dynamics • Requires sophisticated closed-loop control • External air supply required for wind-tunnel operation • PID control insufficient for precise multi-DOF coordination • Higher mass and power demand than pneumatics • Requires precise timing coordination with other DOFs • Failure of timing synchronisation risks mechanical interference

Table A1. *Cont.*

Actuation Mechanism	Key Investigation	Investigation Type	Performance Output	Actuation Advantages	Actuation Limitations
Telescopic variable-span morphing wing (span/aspect-ratio DOF)	Bae et al., 2005 [203]	Aerodynamic analysis (DHM panel code), structural FE modelling (MSC/NASTRAN), static aeroelastic analysis	• Span increase: up to +50% • Aspect ratio increase: 5.0 → 8.18 • Wing area increase: +38% • Induced drag reduction: ≈25% • Predicted range increase: ≈30% • Lift at M = 0.7 (50% span): ≈1.6× baseline • Wingtip deflection at 50% span: ≈230 mm (~15% span) • Natural frequencies reduced by 29–50% • Divergence dynamic pressure (50% span): ≈30 kPa • Total drag reduction: ≈25% • Range increase: ≈30%	• Strong induced-drag reduction due to higher AR • Lower required AOA for same lift • Spanwise lift redistribution reduces local loading • Allows isolation of aerodynamic and aeroelastic effects • Generalizable to multiple actuator technologies (servo, pneumatic, SMA-hybrid) • Clear load-path representation for span morphing • Identifies dominant bending (not torsion) effects	• Wing-root bending moment (WRBM) increases ≈50% at full span • Large static deformations at extended span • Requires substantially increased bending stiffness • No actuator mass, power, or bandwidth considered • No assessment of actuator force required to overcome WRBM • Control authority and rate constraints ignored • Wingtip deformation exceeds acceptable limits (>10% span)
Electromechanical DC motor + reduction gear + lead-screw linkage (span/aspect-ratio morphing DOF)	Heryawan et al. 2005 [204]	Structural design, fabrication, wind-tunnel experimental validation (Re ≈ 30,000)	• Aspect ratio change: 4.7 → 8.5 • Span change achieved in ≈2 s • Lift increase during expansion: >3× (measured) • Total drag reduction: >10% • L/D increase: ≈7–13× depending on AOA • Camber-induced lift increase: ≈16% (expanded state) • Voltage input: ≈200 Vpp	• Very fast response • No mechanical linkages required • Smooth camber change without discrete flaps • Speed controllable via voltage and lead-screw pitch • Mature, low-risk technology for MAV scale • Minimal number of moving parts • Lightweight composite rods and plastic hinges • Low-cost fabrication	• Limited force authority → unsuitable for high-load wings • Mechanical friction in screw and linkages • Efficiency loss due to gear reduction • Scalability restricted to small UAV/MAV regimes • No load-holding lock under aerodynamic loads • Wear and backlash at joints • Sensitivity to manufacturing tolerances • Long-term durability not assessed • High-voltage requirement • Limited stroke and force authority • Only effective at low Reynolds number

Table A1. *Cont.*

Actuation Mechanism	Key Investigation	Investigation Type	Performance Output	Actuation Advantages	Actuation Limitations
Electromechanical screw-driven telescopic ribs + telescopic spars—Span, chord, thickness (airfoil shape) morphing DOFs	Vale et al. 2006 [205]	Multidisciplinary design optimisation (MDO); aero-structural FEM coupling; mission-level performance assessment	• Span variation: 2.4 → 3.4 m (≈+42%) • Chord variation: 0.22 → 0.33 m (≈+50%) • Airfoil thickness variation: 14 → 25.2 mm • Wing drag reduction (ideal morphing): ≈50% at 30 m/s, ≈60–70% at ≥40 m/s • Power required at cruise: ≈−20% • Predicted range increase: ≈10%, endurance ≈ 13% • Drag reduction (ideal morphing): up to 69% at 50 m/s • Drag reduction (deformed wing): ≈21% at 30 m/s, ≈45% at 50 m/s	• High force and load-holding capability (screw mechanisms) • Precise, deterministic displacement control • Capable of supporting simultaneous multi-DOF morphing • Compatible with large structural loads (no reliance on smart materials) • Enables coordinated planform + airfoil optimisation • Actuation geometry directly tied to MDO results • High axial load capability • Compatible with large AR changes • Allows discrete airfoil shape control • Enables coupling of chord and thickness variation	• High mechanical complexity (multiple screws per rib) • Increased mass and packaging volume • Linear displacement–nonlinear aerodynamic response mismatch • Requires many actuators • Actuation power and synchronisation demands not flight-validated • Span extension increases skin tension requirements • Structural stiffness must increase with span • Section straightening between ribs • Loss of effective wing area under load • Aeroelastic deformation degrades low-speed performance
Electromechanical screw-driven rib expansion + telescopic spar actuation (span and chord morphing DOFs)	Gamboa et al. 2007 [206]	Aerodynamic optimisation (XFOIL + lifting-line), coupled aero-structural FEM, prototype design and partial testing	• Span variation: 2.4 → 3.4 m (+42%) • Chord variation: 0.22 → 0.33 m (+50%) • Optimised drag reduction: 52–70% (ideal geometry, ≥30 m/s) • Deformed-wing drag reduction: 22–35% (realistic geometry) • Stall speed increase (deformed wing): 12 → 15.5 m/s • Ideal vs. deformed: ≈30–40% drag benefit loss • Skin stretch capability: ≈50%	• Very high force and load-holding capability • Deterministic, repeatable displacement via screw actuation • Independent rib actuation allows tailored planform shaping • Suitable for load-bearing primary morphing DOFs • High geometric fidelity vs. single-actuator systems • Greater planform freedom • Actuation sized using FEM-derived skin deformation loads • Explicit link between optimisation and mechanism geometry	• Extremely high torque demand (up to ≈5.5 Nm per actuation nut) • Requires multiple motors (≈12 for chord actuation) • High mass and packaging complexity • Synchronisation of many actuators nontrivial • Straightening between ribs → wing area loss • Local curvature discontinuities cause parasite drag • Aeroelastic deformation reduces optimised benefit • Actuator proliferation increases weight • Control coordination complexity

Table A1. *Cont.*

Actuation Mechanism	Key Investigation	Investigation Type	Performance Output	Actuation Advantages	Actuation Limitations
Tendon (cable)-actuated cellular mechanism using parallelogram linkage cells—Span reduction & sweep increase DOFs	Bharti et al. 2007 [192]	Kinematic design, structural sizing, analytical load modelling, prototype fabrication and bench testing	• Target morphing: 61% span reduction, 43.3° backward sweep • Achieved morphing (prototype): 55% span reduction, 44° sweep • Required actuation force: ≈2.2 lb • Morphing time: ≈9 s • Bending moment (10 lb aircraft): ≈65.3 lb·in • Establishes feasibility envelope: ≤360 lb aircraft for wing weight fraction <0.1	• Actuator can be placed remotely (motor not embedded in wing) • Very low in-wing mass penalty • Distributed actuation naturally compatible with cellular structures • High mechanical advantage via linkage geometry • High torque at very low speed • Friction clutch provides overload protection	• Cable elasticity and stretch reduce positioning accuracy • Wear, abrasion, and fatigue of tendons • Requires precise spooling and end-stop control • Very slow morphing response • Precise stopping required to avoid cable damage • Skin effects not modelled • Aerodynamic performance not experimentally validated
Folding-wing morphing architecture with seamless skins—Span, wing area, effective sweep DOFs	Bye et al. 2007 [207]	Mission-driven system design; CFD; MDO; full-scale subcomponent testing; large-scale half-span wind-tunnel testing (NASA TDT)	• Wing area increase: ≈2.8× • Span increase: ≈1.7× • Effective sweep change: ≈30° • Validated morphing under realistic flight loads up to Mach 0.9 • Mission radius improvement vs. best conventional vehicle: ≈22% • Elastic strain capability: 50–150% (SMP up to ≈200%) • Maintained integrity during folding to 130°	• Enables radically different loiter, cruise, and dash configurations in a single vehicle • Distributed loads (vs. point loads in swing-wing aircraft) • Seamless outer mould line reduces gap/interference drag • Extremely high force density • Compact packaging within ≈4.5 in wing depth	• Extreme geometric changes require extensive aero-structural integration • Performance highly sensitive to folded-state profile drag • Complex vehicle-level integration and validation effort • Thermal activation → slow response • Complex thermal management required • Ultimately judged too high risk for TDT model
Out-of-plane folding wing using electromechanical drivetrains—Span, wing area, effective sweep DOFs	Ivanco et al. 2007 (DARPA MAS Phase II) [208]	Large-scale semi-span wind-tunnel testing (NASA TDT); aeroelastic validation; system-level demonstration	• Wing fold range: 0° → 130° • Wing area change: ≈2.8× • Span change: ≈1.7× • Sweep change (½-chord): ≈30° • Successful morphing under ≈1 g aerodynamic load	• First validated demonstration of radical morphing under realistic loads • Smooth, repeatable morphing without binding • Demonstrated multi-configuration stability (Mach 0.2–0.9) • Mature, reliable technology • Precise position control with feedback	• High geometric and control complexity • Large mass and size required for representative actuation • Performance sensitive to folded-state drag • Motor current feedback issues during unfolding under assisting aerodynamic loads • Requires re-zeroing for long-duration operation

Table A1. *Cont.*

Actuation Mechanism	Key Investigation	Investigation Type	Performance Output	Actuation Advantages	Actuation Limitations
Coordinated electromechanical rotary actuation with hinge-line brakes—Primary wing-fold DOF (span, wing area, effective sweep)	Love et al., 2007 (DARPA MAS) [209]	Large semi-span wind-tunnel testing (NASA TDT); ground vibration tests; FEM–CFD correlation	• Wing fold range: 0° → 130° • Morphing under 1g steady flight equivalent (Mach 0.3–0.9, q up to 200 psf) • Smooth, repeatable actuation over 19 active morphs • Measured hinge moments correlate with prediction within ≈3–7%	• Mature, flight-qualified rotary actuators (Curtiss-Wright class) • High load-holding capability via hinge-line brakes • Precise positional control with encoder + hinge-angle feedback • Robust under aerodynamic loads with conservative torque margin	• Conservative torque sizing increases mass and power demand • Drivetrain efficiency uncertainty complicates accurate sizing • Brake wear and slippage require monitoring over long cycles • Thermal activation → slow response • Certification and schedule risk prevented use for primary fold DOF • Thermal management complexity
Computer-controlled linear actuators driving mechanised four-bar linkage—Wing sweep & in-plane shear (wing area) DOFs	Andersen et al., 2007 (DARPA N-MAS) [190]	Full-scale half-span wind-tunnel testing (NASA TDT); subscale UAV flight testing; FEM-based aeroelastic analysis	• Two primary morphing DOFs: sweep + shear angle • Five discrete in-flight configurations: high-lift, climb, loiter, cruise/dash, high-speed manoeuvre • Successful morphing across entire TDT envelope (Mach 0.2–0.9, air & R134a) • No flutter encountered within test matrix	• High force authority suitable for load-bearing morphing • Precise, deterministic positioning via linear actuators • Compatible with classical control and certification pathways	• Actuators introduce in-plane compliance • Low effective stiffness in morphing DOFs • Increased susceptibility to in-plane dynamic modes • Actuator stiffness must be explicitly modelled for aeroelastic clearance
Electromechanical rack-and-pinion linear actuator + servo-driven bell-crank—Span (telescopic), gull, and inverted-gull DOFs	Supekar, 2007 [193]	Structural design; FEM (ANSYS); AVL aerodynamics; low-speed wind-tunnel testing	• Span change: 40 in → 60 in (AR ≈ 4.45 → 8) • Out-of-plane morphing: ±30° gull/inverted-gull • Lowest natural frequency: ≈47.6 Hz (extended) • Wing loading reduced from ≈20 → 13.3 oz/ft^2 (extended)	• Simple, low-cost, commercially available servos • Independent control of span and out-of-plane morphing • Deterministic kinematics suitable for quasi-static morphing	• Limited torque margin restricts dynamic morphing • Rack-and-pinion introduces backlash and friction • Insufficient authority for rapid or in-flight load-changing morphs • Actuator stiffness contributes to increased root bending

Table A1. *Cont.*

Actuation Mechanism	Key Investigation	Investigation Type	Performance Output	Actuation Advantages	Actuation Limitations
Shape Memory Polymer (SMP) composite hinge actuator—Wing sweep angle and planform area reduction DOFs	Yu et al., 2007 [210]	Material characterisation (DMA); analytical modelling (ADAMS); prototype fabrication; experimental validation	• Sweep angle change: ≈5–30° depending on initial twist angle • Planform area reduction: ≈6–16% • Actuation temperature: >Tg ≈ 64 °C • Morphing magnitude increases with initial twist angle and temperature	• Very high recoverable strain compared with SMA • Lightweight, compact, and hinge-integrated actuation • Large angular deformation achievable without complex mechanisms • Good repeatability over multiple thermal cycles • Actuator doubles as structural joint • Simple linkage-based wing architecture	• Thermally driven → very slow response (minutes) • Requires external heating and cooling • Actuation authority strongly temperature-dependent • Unsuitable for rapid or continuous in-flight morphing • Requires careful thermal management
Electromechanical screw-driven telescopic ribs + telescopic spars—Span, chord, airfoil thickness/camber DOFs	Gamboa et al., 2009 [194]	Multidisciplinary design optimisation (SQP); coupled aero-structural FEM; mission-level UAV performance analysis	• Span variation: 2.4 → 3.4 m (+42%) • Chord variation: 0.22 → 0.33 m (+50%) • Thickness variation: 14 → 25.2 mm • Optimised morphing drag reduction: ≈52% at 30 m/s, ≈70% at 50 m/s • Deformed morphing drag reduction: ≈27% at 30 m/s, ≈40% at 40 m/s • Maximum speed increase: ≈3% • Endurance increase (ideal morphing): ≈5.8% • Deformed morphing reduces range/endurance	• Very high load-carrying capability (screw actuation) • Precise, deterministic displacement control • Enables simultaneous multi-DOF morphing using conventional materials • Allows local airfoil thickness control • Compatible with optimisation-defined shapes	• Linear screw kinematics poorly approximate nonlinear optimised shapes • High actuator count required to improve geometric fidelity • Flexible skin negates majority of optimised benefit • Stall speed increase: ≈+16–17% • Straight-line deformation between ribs • Large deviation from optimised airfoil shapes • Dominant source of drag penalty

Table A1. *Cont.*

Actuation Mechanism	Key Investigation	Investigation Type	Performance Output	Actuation Advantages	Actuation Limitations
Distributed linear pneumatic actuators embedded in scissor (four-bar) cellular mechanism—In-plane shear/wing area/ sweep-related DOF	O'Grady, 2010 [211]	Experimental testing (single-cell & three-cell); multibody dynamics (ADAMS); FEM (NASTRAN); SQP optimisation	• Morphing defined by internal cell angle: $\theta_i = 105^\circ \rightarrow \theta f = 150^\circ$ • Three-cell system represents section of N-MAS wing • Two-actuator configuration reduces work input vs. single or three actuators • Total work reduction of ≈5–15% via optimal actuator placement • Flexible link thickness cases: 0.5″, 0.125″, 0.1″ • Increased flexibility shifts optimal actuator orientation • Spring constants: ≈1.45–1.60 lb/in • Captures skin-induced resistance to morphing	• Distributed actuation reduces peak force per actuator • Pneumatic actuators provide high force at low mass • Actuator placement/ orientation strongly tunable for efficiency • Captures strain-energy losses explicitly • Demonstrates coupling between stiffness and actuation efficiency • Confirms benefits of distributed actuation experimentally • Demonstrates scalability trends from single- to multi-cell	• Pneumatic actuation has low bandwidth and poor position precision • Requires external air supply (non-flight-practical without redesign) • Flexible link induces vibration and numerical instability • Requires artificial damping for model convergence • Increased joint count raises friction and uncertainty • Control complexity increases with actuator number
Chord					
Shape Memory Polymer (SMP) skin with internal sliding/telescoping ribs—Chord morphing DOF (primary)	Perkins et al., 2004 (CRG Phase I) [212]	Conceptual design; material development; subcomponent fabrication and testing. Material & structural feasibility study (sub-scale prototypes)	• Target lift increase: ≈80% via chord expansion • SMP strain capability demonstrated: up to ≈125–200% (bench tests) • Morphing requirement: <1 s (design goal) (not achieved) • DMF supports ≈400% compression (bench-scale) • SMP heated above Tg at ≈40 W input	• SMP provides large recoverable strain with low mass • Actuator and skin functions integrated • No discrete hinges or gaps in outer mould line • Simple, compact internal heating solution • Activation integrated within skin • Extremely large strain at low mass • Skin acts as actuator + aerodynamic surface • Eliminates hinges and gaps	• Thermally activated → slow and energy intensive • Actuation force strongly temperature-dependent • Non-uniform heating causes local surface defects • Power and voltage requirements nontrivial • Thermal lag limits response speed • High power & temperature control needed • Actuation force/device not yet defined
Out-of-plane morphing: Twist					

Table A1. *Cont.*

Actuation Mechanism	Key Investigation	Investigation Type	Performance Output	Actuation Advantages	Actuation Limitations
Hydraulically actuated leading- and trailing-edge control surfaces on a flexible wing—Aeroelastic twist & camber control (roll, load, and mode control DOF)	Miller (1988), Active Flexible Wing (AFW) Technology [213]	Large-scale wind-tunnel experimental validation with active control	• Roll rate up to ≈66–100°/s at M ≈ 1.2, q up to 2150 psf • Trailing-edge actuator power reduced ~65–75% vs. stiff wing • Estimated 15–30% TOGW reduction for equivalent performance	• Much lower actuator hinge moments and power due to small deflections (<5°) • Uses wing flexibility to enhance control effectiveness • Proven at transonic conditions in wind tunnel	• Relies on hydraulic actuators → high system complexity & weight • Requires precise sensing and control law tuning • Not a true shape-morphing skin (still discrete surfaces)
Aerodynamic control surfaces + adaptive stiffness attachments (active aeroelasticity, not geometric morphing)—Wing twist, roll effectiveness, load redistribution DOFs	Kuzmina et al. (2002), ICAS Congress [214]	Analytical + wind-tunnel + flight-test review (Russia & Europe, incl. 3AS project)	• Roll effectiveness increases with dynamic pressure using fore-ailerons • Aileron reversal mitigated without structural stiffening • Flutter boundaries increased via outboard/LE control surfaces • Fin efficiency >1.0 achievable with adaptive stiffness attachments	• Exploits natural structural flexibility → reduced actuator force & power • No large shape-change mechanisms required • Weight savings vs. stiff-wing solutions • Compatible with conventional actuators	• Not true morphing of outer mould line • Strong dependence on aeroelastic modelling accuracy • Control-law complexity critical • Benefits diminish at low dynamic pressure
Electromechanically actuated movable & rotating wing spars—Aeroelastic twist control DOF (via shear-centre and torsional stiffness shift)	Amprikidis & Cooper (2003), AIAA 2003-1799/EU 3AS [197]	Analytical aeroelastic modelling + bench tests + low-speed wind-tunnel tests	• Wingtip twist variation ≈2–2.5× between stiff and flexible spar settings • At 30 m/s: ≈2.2° (flexible) vs. 0.9° (stiff) • Flutter & divergence speeds tunable via spar position/orientation	• Very low actuation energy (uses aerodynamic loads to twist wing) • Actuation changes internal structure, not outer mould line • Avoids large hinge moments and high-power actuators • Compatible with conventional electric motors	• Not true geometric morphing (planform unchanged) • Twist authority limited (few degrees) • Strong coupling between stiffness and aeroelastic stability • Requires accurate aeroelastic modelling for safe operation
Hydraulically actuated Variable Stiffness Spar (VSS)—Aeroelastic twist & stiffness tuning DOF (via spar rotation vertical↔horizontal)	Florence et al. (2004) [215]	Large-scale wind-tunnel experiment (NASA TDT) with aeroelastic measurements	• Wing torsional stiffness varied ≈2–3× via spar rotation • Achieved significant change in twist response and load distribution under aerodynamic loading • Demonstrated real-time stiffness modulation at transonic conditions	• Very low actuation displacement and power (rotates spar, not wing shape) • Uses aerodynamic loads to generate twist → high efficiency • Actuators remain internal and load-path efficient • Demonstrated in a realistic wind-tunnel environment	• Not true geometric morphing (outer mould line unchanged) • Twist authority limited to a few degrees • Requires complex hydraulic system and control integration • Strong coupling with aeroelastic stability margins

Table A1. *Cont.*

Actuation Mechanism	Key Investigation	Investigation Type	Performance Output	Actuation Advantages	Actuation Limitations
Distributed anisotropic piezoelectric actuators (AFC/SCFC) embedded in wing skin—Wing warping (torsion & shear) for roll control DOF	Sahoo & Cesnik (2002) [216]	Coupled aeroservoelastic modelling + optimisation (UCAV case study)	• Roll rate with AFC: ≈13°/s at M = 0.85 • Optimised SCFC case: >90°/s roll rate • Required ≈3–4× increase in actuator authority vs. AFC • Active skin thickness ≈1.3 mm per side	• No discrete control surfaces → drag reduction • High-bandwidth actuation (piezoelectric) • Distributed actuation reduces hinge moments • Enables seamless wing warping	• Current AFC authority insufficient • Requires advanced SCFC technology (not mature) • High voltage (~1000 V) required • Strong coupling with flutter & structural constraints
Shape memory alloy (NiTi) torque tube + SMA wire-actuated hingeless trailing-edge surfaces + TERFENOL-D linear actuators—Wing twist, camber, and control-surface contouring DOFs	Martin et al. (1998),” Smart Materials and Structures—Smart Wing Phase I” [217]	Large-scale wind-tunnel experiments (16% scale, NASA LaRC TDT) + system integration study	• Up to 5° wing twist via SMA torque tube • ≈8–12% increase in lift & rolling moment vs. conventional surfaces • Combined effects ≈15–17% improvement • Transonic cruise studies predict ≈5% fuel savings	• High-force-density smart actuators enable hingeless, smooth OML • Reduced hinge moments and drag vs. conventional flaps/ailerons • Demonstrated aero benefits in wind tunnel (subsonic & transonic concepts)	• SMA bandwidth limited (few Hz) → unsuitable for fast manoeuvres • Thermal management and fatigue life unresolved • High system complexity and integration effort • Actuation authority and rates still below operational needs
Servo-driven torque tubes—Wing-warping (spanwise twist) DOF, 3 independent actuation sections	Gatto (2023) [218]	Wind-tunnel experiments + CFD/AVL/FEA + closed-loop control implementation	• Maximum wingtip twist ≈ ±22° • Aileron deflection of 3.5–8.2° • C_L/C_D improvement up to 72% (real-time morphing) • Demonstrated closed-loop lift-distribution control	• High authority morphing using low-power rotary servos • Continuous, gapless aerodynamic surface (no ailerons) • Distributed actuation increases redundancy and control richness	• Added mass and packaging constraints inside UAV fuselage
Shape memory alloy (SMA) face sheets on a bio-inspired “vertebrate” cellular metal core—Fully reversible bending/curvature morphing DOF (airfoil camber & twist)	Elzey et al. (2003) [219]	Analytical modelling + prototype morphing airfoil panel demonstration	• Recoverable SMA strain: ≈5–8% • Achievable curvature: $\kappa_0 \approx 2\varepsilon/H$ • Actuation moment limited by SMA yielding (~550 MPa) • Core relative density ≈0.23	• High actuation authority with low mass • Fully reversible without bias springs • Core offers minimal bending resistance, improving efficiency • Enables continuous, hingeless OML	• Thermal SMA actuation → very low bandwidth • Requires careful temperature sequencing to avoid core buckling • Power-intensive heating and cooling • No aerodynamic load testing reported
Dihedral/Gull					

Table A1. *Cont.*

Actuation Mechanism	Key Investigation	Investigation Type	Performance Output	Actuation Advantages	Actuation Limitations
Servo-driven linear lead-screw actuator + jointed spar linkage—Variable gull-wing dihedral (±40° inboard/outboard) DOF; wingtip twist via rotary servo	Abdulrahim & Lind (2004) [220]	Flight testing of small UAV + system identification of dynamics	• Wingspan change: 20–26 in; area 77.7–101.4 in^2 • Gull-wing angle: −40° to +40° • Glide ratio: ≈11 (0°) → ≈1–2 (+30°) • Positive gull-wing improves stall recovery & Dutch-roll damping; roll control maintained via twist	• Very simple, lightweight actuation using commercial servos • Quasi-static morphing holds shape with no power • Large dihedral change achieved without high actuator loads • Flight-validated impact on handling qualities	• Very slow morphing rate (lead-screw) → quasi-static only • Limited structural stiffness → small-UAV scale only • Morphing reduces roll control effectiveness at large angles • Not suitable for high-speed or high-load aircraft
Independently servo-actuated articulated split wingtips (fore & aft)—Wingtip dihedral morphing for roll, pitch & yaw control DOFs	Bourdin, Gatto & Friswell (2007) [186]	VLM analysis + wind-tunnel experiments (Re ≈ 3.2 × 10^5)	• Wingtip dihedral range: ±75° • Generates coupled roll, yaw & pitch moments without elevons • Roll effectiveness increases with lift coefficient • ≈10% L/D improvement for down-deflected fore wingtip cases	• Very large control authority from small actuators • Eliminates conventional control surfaces (smooth OML) • Over-actuated system enables drag-optimised control allocation • Effective at low–moderate speeds	• Not continuous shape morphing (discrete hinges) • High dihedral angles increase structural & hinge loads • Control effectiveness reduced at low lift coefficients • Integration complexity for full-scale aircraft
High-torque servo-actuated articulated winglets (belt-drive, ±75° dihedral)—Wingtip dihedral morphing for load redistribution, roll & gust alleviation DOFs	Gatto, Bourdin & Friswell (2010) [221]	Wind-tunnel experimental study with dense surface-pressure measurements	• Winglet dihedral range: ±75° • Significant upper-surface C_P redistribution extending 4–5 spanwise stations inboard • C_P change up to ≈±11% locally near wing/winglet junction • Strong influence at mid-chord; effect increases with AoA	• Very large aerodynamic authority from small servo motion • Low actuation power and simple electromechanical system • Enables gust-load alleviation without morphing main wing • Demonstrated experimentally with high-fidelity pressure data	• Discrete hinge → not continuous morphing • High dihedral angles introduce flow disorder and local separation • Effectiveness degrades at higher AoA (α ≈ 12°) • Structural and hinge loads grow rapidly at large deflections
Thermopolymer actuator driving helical spline (primary wing fold) + electromechanical fallback; seamless elastomeric/SMP skins—Large out-of-plane wing folding DOFs (span, wing area, effective sweep)	Bye & McClure (2007) [207]	System-level design + full-scale subcomponent tests + large half-span TDT wind-tunnel validation	• Wing area change ≈ 2.8× • Span change ≈ 1.7× • Effective sweep change ≈ 30° • Fold rotation ≈ 130° • ≈22% mission radius increase vs. best conventional aircraft	• Very-high-force-density thermopolymer actuation suitable for extreme load-bearing morphing • Actuators packaged within ≈4.5 in wing depth • Distributed folding loads vs. point-loaded swing wings • Demonstrated under realistic flight loads in TDT	• Thermal actuation → low bandwidth & high risk • Helical spline galling/tolerance sensitivity • Smart actuators not flight-ready → electromechanical fallback required • High system integration complexity
Camber					

Table A1. *Cont.*

Actuation Mechanism	Key Investigation	Investigation Type	Performance Output	Actuation Advantages	Actuation Limitations
Servo-actuated torque rods (24-in MAV) and Kevlar-thread pulling mechanism (12-in MAV)—Wing twist + twist/span coupling for roll-control DOF	Garcia et al. (2003) [222]	Flight testing of two MAVs with system identification	• Roll rates up to ≈150–200°/s (24-in MAV) with near-pure roll (minimal yaw) • Morphing roll authority greater than rudder-based control • Linear models show morphing behaves like effective ailerons	• Very high control authority from extremely simple, lightweight actuation • Uses existing wing flexibility → low actuator force & power • Flight-validated effectiveness for roll control • Enables control where ailerons are infeasible	• Not continuous shape morphing (localised twist/curl) • Authority depends on membrane flexibility → limited scalability • Single-wing morphing introduces drag-induced yaw delay • Applicable mainly to low-speed MAV regime
Micro-servo-actuated compliant camber mechanism (pulling inflexion point) + passive carbon plate wing—Variable camber DOF (≈3% → 9–12% of chord)	Shkarayev, Null & Wagner (2004) [223]	Wind-tunnel testing + theoretical performance analysis + flight tests (MAV)	• Camber range tested: 3, 6, 9, 12% • Minimum flight speed reduced ≈6.5 → 4.5 m/s (−30%) via camber increase • Max flight speed ≈10.3 m/s at 6% camber • Best endurance camber: ≈6%	• Extremely simple, lightweight actuation (single added micro-servo) • Large aerodynamic benefit at very low Reynolds numbers • Enables in-flight optimisation of endurance vs. speed • Flight-demonstrated feasibility	• Actuation authority limited by wing flexibility • Increased structural weight and complexity (inner fuselage, linkages) • Pitching-moment management required (elevator coupling) • Flight results sensitive to gusts; limited quantitative validation
Macro-fibre composite (MFC) piezoelectric bimorph with pinned–pinned supports—Continuous camber morphing DOF (±4–5% chord camber)	Bilgen et al. (2010) [224]	Wind-tunnel experiments + coupled FSI analysis (Re ≈ 1.27×10^5)	• Peak-to-peak $\Delta C_L \approx 1.46$ via voltage actuation alone • Max 2D L/D ≈ 17.8 • Camber change ≈ ±4–5% at ±1400 V • Sustained loads up to 15 m/s without aeroelastic instability	• High-bandwidth, solid-state actuation • Smooth, hingeless OML → low drag penalty • Significant lift change without control surfaces • Actuation effective at low Reynolds numbers	• High voltage required (≈1–1.5 kV) • Limited actuation force → thin, low-load airfoils only • Piezo hysteresis requires feedback control • Scalability to higher dynamic pressure uncertain
Load-bearing electromechanical linear actuators driving segmented morphing ribs—True-scale variable-camber aileron DOF (continuous camber, no chord extension)	Rea et al. (2017) [225]	High-fidelity FEM-DLM aeroelastic analysis + wind-tunnel validation (CRIAQ MDO-505)	• Flutter clearance >1.2 × VM (VM = 85 m/s) for all actuator stiffness cases • Flutter speed range ≈110–146 m/s depending on actuator stiffness • Morphing achieved with continuous monotonic camber and no chord change	• Load-bearing actuators integrated into structure (no external hinges) • Continuous camber improves aerodynamic efficiency without gaps • Actuator stiffness can be tuned to manage aeroelastic stability • Architecture scalable to CS-25 aircraft class	• High mechanical and control complexity (segmented ribs, multi-box structure) • Aeroelastic behaviour strongly sensitive to actuator stiffness • Primarily quasi-static morphing (not high-bandwidth control) • System weight and reliability challenges for certification

Table A1. *Cont.*

Actuation Mechanism	Key Investigation	Investigation Type	Performance Output	Actuation Advantages	Actuation Limitations
Manually set, segmented hinged flap elements sealed with elastomer (VCCTEF)—Spanwise & chordwise continuous-camber morphing DOFs (15 independently shaped flap segments)	Precup, Mor & Livne (2014) [226]	Aeroelastic wind-tunnel testing + NASTRAN FEM/DLM correlation	• Lift increase up to ≈3× clean-wing lift at low AoA • Continuous camber shapes ("smiling/sad") significantly alter lift & twist distributions • Good test–NASTRAN correlation (lift error ≈ 3–14%) • Flutter-free up to q = 30 psf, flutter speed ≈ 280 ft/s	• Highly flexible, continuous-camber control authority • Eliminates discrete flap gaps → improved aerodynamic efficiency • Demonstrates rich shape control beyond single-hinge flaps • Architecture scalable to transport-class wings	• No active in-flight actuation (manual preset only) • Mechanically complex (15 segments, elastomer seals) • High sensitivity to hinge stiffness & manufacturing tolerances • Actuation system feasibility, weight & reliability not addressed
Passive/semi-active free-folding wingtip hinge with flare angle (Semi-Aeroelastic Hinge); actuator + lock for release/recovery—Out-of-plane wingtip fold DOF for gust & manoeuvre load alleviation	Wilson et al. (2019) [227]	Wind-tunnel tests + first-ever flight tests of free-folding wingtips (small-scale demonstrator)	• Wing-root bending moment reduction ≈13–17% (WT & flight correlation) • Stable free-folding with flapping frequencies ≈3–6 Hz, well separated from wing bending modes • Coasting (fold) angles up to ≈45° without flutter • Demonstrated in-flight stability and load alleviation	• Very low actuation power (loads drive motion) • Exploits aeroelasticity instead of fighting it • Enables span increase without proportional load/weight penalty • Flight-demonstrated stability of a morphing concept	• Not continuous geometric morphing (hinged, discrete DOF) • Control authority indirect and condition-dependent • Recovery actuator/lock system not yet flight-demonstrated • Results qualitative (not dynamically scaled to transport aircraft)
Servo-driven torque rod coupled with programmable ultralight lattice (architected cellular metamaterial). Passive + active aeroelastic twist & camber morphing DOFs	Cramer et al. (2019) [228]	Full-scale wind-tunnel experiments (NASA LaRC 14×22) + FEM -VLM correlation	• Wingspan: 4.27 m • Ultralight stiffness: ≈2.6–8.4 MPa at ~5.6 mg/cm^3 • Global stiffness reduction: ≈43% torsion, ≈46% bending via programmed assembly • L/D efficiency gain ≈ 5–8% vs. homogeneous wing • Active twist doubled: ±0.25° → ±0.5° with same actuator	• Actuator authority amplified by structural programmability (system-level gain) • Very low actuation power (loads do most work) • Extremely mass-efficient load-bearing morphing structure • Combines passive morphing + simple active actuation	• Not fast morphing (quasi-static, low-bandwidth) • Assembly currently labour-intensive (manual build) • Actuation authority limited to small twist angles • Durability, fatigue, and flight certification not yet demonstrated
Hybrid electro-active trailing-edge: surface-embedded SMA wires (low-frequency camber) + piezoelectric MFC vibrating trailing edge (HFVTE)—Camber (±10% chord) + high-frequency TE vibration DOFs	Jodin et al. (2017) [229]	Subsonic wind-tunnel experiments (Re $\leq 1 \times 10^6$) with closed-loop actuation control	• Camber range −5% to +5% chord (±10 mm TE) • Lift change ≈ +23%, drag reduction ≈ 35%, L/D +16% • HFVTE displacement > 0.6 mm up to ≈140 Hz • 20–30% reduction in SMA power via nested control loops	• Combines high force (SMA) + high bandwidth (piezo) in one TE • Continuous, gapless OML • Closed-loop SMA control improves efficiency • Demonstrated aerodynamic benefit in wind tunnel	• Thermal SMA actuation → slow response & hysteresis • SMA training degrades stroke (~15% loss before stabilisation) • High system & control complexity • Low-TRL, small-scale demonstration only

References

1. Wright, O.; Wright, W. IFI CLAIMS Patent Services: US821393A-Flying-Machine. U.S. Patent US821393A, 22 May 1906. Available online: https://patents.google.com/patent/US821393A/en (accessed on 16 January 2023).
2. Concilio, A.; Dimino, I.; Lecce, L.; Pecora, R. *Morphing Wing Technologies: Large Commercial Aircraft and Civil Helicopters*; Butterworth-Heinemann: Cambridge, MA, USA, 2018.
3. Straub, F.; Anand, V.; Birchette, T.; Lau, B. SMART Rotor Development and Wind Tunnel Test. In Proceedings of the 35th European Rotorcraft Forum, Hamburg, Germany, 22–25 September 2009.
4. Dietrich, O.; Enenkl, B.; Roth, D. Trailing Edge Flaps for Active Rotor Control: Aeroelastic Characteristics of the ADASYS Rotor System. In Proceedings of the 62nd American Helicopter Society Forum, Phoenix, AZ, USA, 9–11 May 2006.
5. Roth, D.; Enenkl, B.; Dieterich, O. Active Rotor Control by Flaps for Vibration Reduction—Full Scale Demonstrator and First Flight Test Results. In *Proceedings of the 32nd European Rotorcraft Forum (ERF), Maastricht, The Netherlands, 12–14 September 2006*; National Aerospace Laboratory (NLR): Amsterdam, The Netherlands, 2006; Volume 2, pp. 801–814.
6. Léon, O. Reducing Helicopter Main Rotor Power Requirements Using Multiple Trailing Edge Flaps and Extendable Chord Sections. Master's Thesis, The Pennsylvania State University, University Park, PA, USA, 2009.
7. Chen, P.C.; Chopra, I. Induced Strain Actuation of Composite Beams and Rotor Blades with Embedded Piezoceramic Elements. *Smart Mater. Struct.* **1996**, *5*, 35–48. [CrossRef]
8. Spangler, R. Piezoelectric Actuators for Helicopter Rotor Control. Master's Thesis, Massachusetts Institute of Technology, Cambridge, MA, USA, February 1989.
9. Prechtl, E. Development of a Piezoelectric Servo-Flap Actuator for Helicopter Rotor Control. Master's Thesis, Massachusetts Institute of Technology, Cambridge, MA, USA, May 1994.
10. Hall, S.; Prechtl, E. Development of a Piezoelectric Servo flap for Helicopter Rotor Control. *Smart Mater. Struct.* **1996**, *5*, 26–34. [CrossRef]
11. Samak, D.; Chopra, I. A Feasibility Study to Build a Smart Rotor: Trailing Edge Flap Actuation. In Proceedings of the 1993 North American Conference on Smart Structures and Materials, Albuquerque, NM, USA, 1–4 February 1993; Volume 1917. [CrossRef]
12. Walz, C.; Chopra, I. Design and Testing of a Helicopter Rotor Model with Smart Trailing Edge Flaps. In Proceedings of the 35th Structures, Structural Dynamics, and Materials Conference, Hilton Head, SC, USA, 21–22 April 1994; Adaptive Structures Forum. [CrossRef]
13. Fulton, M.; Ormiston, R. Hover Testing of a Small-Scale Rotor with On-Blade Elevons. In Proceedings of the 53rd American Helicopter Society Forum, Virginia Beach, VA, USA, 29 April–1 May 1997. [CrossRef]
14. Ben-Zeev, O.; Chopra, I. Advances in the Development of an Intelligent Helicopter Rotor Employing Smart Trailing-Edge Flaps. *Smart Mater. Struct.* **1996**, *5*, 11–25. [CrossRef]
15. Fulton, M.; Ormiston, R. Small-Scale Rotor Experiments with On-Blade Elevons to Reduce Blade Vibratory Loads in Forward Flight. In Proceedings of the 54th American Helicopter Society Forum, Washington, DC, USA, 20–22 May 1998.
16. Koratkar, N.; Chopra, I. Analysis and Testing of Mach Scaled Rotor Model with Piezoelectric Bender Actuated Trailing-Edge Flaps for Helicopter Vibration Control. In Proceedings of the 40th AIAA/ASME/ASCE/AHS/ASC Structures, Structural Dynamics, and Materials Conference, St. Louis, MO, USA, 12–15 April 1999. [CrossRef]
17. Koratkar, N. Smart Helicopter Rotor with Piezoelectric Bender Actuated Trailing-Edge Flaps. Ph.D. Thesis, University of Maryland, College Park, MD, USA, 2000.
18. Koratkar, N.; Chopra, I. Wind Tunnel Testing of a Mach-Scaled Rotor Model with Trailing-Edge Flaps. *Smart Mater. Struct.* **2001**, *10*, 1–14. [CrossRef]
19. Spencer, B.; Chopra, I. Design and Testing of a Helicopter Trailing Edge Flap with Piezoelectric Stack Actuators. In Proceedings of the 1996 Symposium on Smart Structures and Materials, San Diego, CA, USA, 25–29 February 1996; Volume 2717. [CrossRef]
20. Lee, T.; Chopra, I. Design of a piezostack-driven trailing-edge flap actuator for helicopter rotors. *Smart Mater. Struct.* **2001**, *10*, 15–24. [CrossRef]
21. Lee, T.; Chopra, I. Design and static testing of a trailing-edge flap actuator with piezostacks for a rotor blade. In Proceedings of the 5th Annual International Symposium on Smart Structures and Materials, San Diego, CA, USA, 1–5 March 1998; Volume 3329. [CrossRef]
22. Lee, T. High Displacement Piezoelectric Trailing-Edge Flap Mechanism for Helicopter Rotors. Ph.D. Thesis, University of Maryland, College Park, MD, USA, 1999.
23. Hall, S.; Prechtl, E. Preliminary Testing of a Mach-Scaled Active Rotor Blade with a Trailing Edge ServoFlap. In Proceedings of the 1999 Symposium on Smart Structures and Materials, Newport Beach, CA, USA, 1 March 1999. [CrossRef]
24. Prechtl, E. Design and Implementation of a Piezoelectric Servo-Flap Actuation System for Helicopter Rotor Individual Blade Control. Ph.D. Thesis, MIT, Cambridge, MA, USA, February 2000.

25. Hall, S.; Tzianetopoulou, T.; Straub, F.; Ngo, H. Design and Testing of a Double X-Frame Piezoelectric Actuator. In Proceedings of the SPIE'S 7th Annual International Symposium on Smart Structures And Materials, Newport Beach, CA, USA, 6–9 March 2000. [CrossRef]
26. Straub, F.K.; Ngo, H.T.; Anand, V.; Domzalski, D.B. Development of a piezoelectric actuator for trailing edge flap control of full scale rotor blades. *Smart Mater. Struct.* **2001**, *10*, 25–34. [CrossRef]
27. Straub, F.; Merkley, D. Design of a Smart Material Actuator for Rotor Control. In Proceedings of the SPIE North American Conference, on Smart Structures and Materials, San Diego, CA, USA, 26 February–3 March 1995. [CrossRef]
28. Straub, F.; Ealey, M.; Schetky, L. Application of Smart Materials to Helicopter Rotor Active Control. In Proceedings of the Smart Structures and Materials '97, San Diego, CA, USA, 3–6 March 1997.
29. Straub, F.; Ngo, H.; Anand, V.; Domzalski, D. Development of a Piezoelectric Actuator for Trailing Edge Flap Control of Full Scale Rotor Blades. In Proceedings of the 1999 Symposium on Smart Structures and Materials, Newport Beach, CA, USA, 1 March 1999; Volume 3668.
30. Straub, F.; Kennedy, D.; Domzalski, D.; Hassan, A.; Ngo, H.; Anand, V.; Birchette, T. Smart Material-Actuated Rotor Technology—SMART. *J. Intell. Mater. Syst. Struct.* **2004**, *15*, 249–260. [CrossRef]
31. Bernhard, A.; Chopra, I. Trailing Edge Flap Activated by a Piezo-Induced Bending-Torsion Coupled Beam. In Proceedings of the 52nd American Helicopter Society Annual Forum, Washington, DC, USA, 4–6 June 1996. [CrossRef]
32. Bernhard, A. Smart Helicopter Rotor with Active Blade Tips. Ph.D. Thesis, University of Maryland, College Park, MD, USA, 2000.
33. Clement, J.; Brei, D.; Moskalik, A.; Barrett, R. Bench-top Characterization of an Active Rotor Blade Flap System Incorporating C-Block Actuators. In Proceedings of the 39th AIAA/ASME/ASCE/AHS/ASC Structures, Structural Dynamics, and Materials Conference, Long Beach, CA, USA, 20–23 April 1998. [CrossRef]
34. Clement, J.; Brei, D.; Barrett, R. Wind Tunnel Testing of a High Authority Airspeed Insensitive Rotor Blade Flap. In Proceedings of the 40th AIAA/ASME/ASCE/AHS/ASC Structures, Structural Dynamics, and Materials Conference, St. Louis, MO, USA, 12–15 April 1999.
35. Centolanza, L.; Smith, E.; Munsky, B. Induced-Shear Piezoelectric Actuators for Rotor Blade Trailing Edge Flaps. *Smart Mater. Struct.* **2002**, *11*, 24–35. [CrossRef]
36. Centolanza, L. Induced Shear Piezoelectric Actuators for Smart Rotor Blades. Ph.D. Thesis, Penn State University, University Park, PA, USA, 2001.
37. Szefi, J.; Mockensturm, E.; Smith, E.; Rehrig, W.K.P.; Centolanza, L. Development of a Novel High Authority Piezo-Electric Actuator for Rotor Blades with Trailing Edge Flaps. In Proceedings of the 62nd American Helicopter Society Annual Forum, Phoenix, AZ, USA, 9–11 May 2006.
38. Hongu, T.; Sato, M.; Yamakawa, E. Elementary Studies of Active Flap Control with Smart Material Actuators. In Proceedings of the 12th European Rotorcraft Forum, Rome, Italy, 14–16 September 1999.
39. Hasegawa, Y.; Katayama, N.; Kobiki, N.; Nakasato, E.; Yamakawa, E.; Okawa, H. Experimental and Analytical Results of Whirl Tower Test of ATIC Full Scale Rotor System. In Proceedings of the 57th American Helicopter Society Annual Forum, Washington, DC, USA, 9–11 May 2001.
40. Mainz, H.; van der Wall, B.; Leconte, P. ABC Rotor Blades: Design, Manufacturing and Testing. In Proceedings of the 31st European Rotorcraft Forum, Florence, Italy, 13–15 September 2005.
41. Leconte, P.; des Rochettes, H.M. Experimental Assessment of an Active Flap Device. In Proceedings of the 58th American Helicopter Society Annual Forum, Montreal, QC, Canada, 11–13 June 2002.
42. Delrieux, Y.; Le Pape, A.; Leconte, P.; Crozier, P.; Gimonet, B.; des Rochettes, H.M. Wind-Tunnel Assessment of the Concept of Active Flaps on a Helicopter Rotor Model. In Proceedings of the 63rd American Helicopter Society Annual Forum, Virginia Beach, VA, USA, 1–3 May 2007.
43. Enenkl, B.; Kloppel, V.; Preissler, D.; Janker, P. Full Scale Rotor with Piezoelectric Actuated Blade Flaps. In Proceedings of the 28th European Rotorcraft Forum, Bristol, UK, 17–21 September 2002.
44. Lee, J.; Kwak, J.; Son, K.; Shin, S. Development of an SNU Intelligent Rotor Blade with an Active Trailing Edge Flap. In Proceedings of the 66th American Helicopter Society Annual Forum, Phoenix, AZ, USA, 11–13 May 2010.
45. Fukami, T.; Kobiki, N.; Komura, T.; Saito, S. Design and Performance Evaluation of Full Scale On-Board Active Flap System. In Proceedings of the 63rd American Helicopter Society Annual Forum, Virginia Beach, VA, USA, 1–3 May 2007.
46. Dawson, S.; Straub, F. Design, Validation and Test of a Model Rotor with Tip Mounted Active Flaps. In Proceedings of the 50th American Helicopter Society Annual Forum, Washington, DC, USA, 11–13 May 1994.
47. Fenn, R.; Downer, J.; Bushko, D.; Gondhalekar, V.; Ham, N. Terfenol-D driven flap for helicopter vibration reduction. *Smart Mater. Struct.* **1996**, *5*, 49–57. [CrossRef]
48. Bowen, J.; Sanders, B.; Cannon, B.; Kudva, J.; Joshi, S.; Weisshaar, T. Development of next generation morphing aircraft structures. In Proceedings of the 48th AIAA/ASME/ASCE/AHS/ASC Structures, Structural Dynamics, and Materials Conference, Honolulu, HI, USA, 23–26 April 2007. [CrossRef]

49. Hyer, M.W.; Dano, M.; Schultz, M.R.; Aimmanee, S.; Jilani, A.B. A summary of several studies with unsymmetric laminates. In *Adaptive Structures: Engineering Applications*; Wiley: Hoboken, NJ, USA, 2007; pp. 191–229.
50. Schultz, M.R. Use of Piezoelectric Actuators to Effect Snap-Through Behaviour of Unsymmetric Composite Laminates. Ph.D. Thesis, Virginia Polytechnic Institute and State University, Blacksburg, VA, USA, 2003.
51. Schultz, M.R.; Hyer, M.W. Snap-through of unsymmetric cross-ply laminates using piezoceramic actuators. *J. Intell. Mater. Syst. Struct.* **2003**, *14*, 795–814. [CrossRef]
52. Schultz, M.; Hyer, M. A morphing concept based on unsymmetric composite laminates and piezoceramic MFC actuators. In Proceedings of the 45th AIAA/ASME/ASCE/AHS/ASC Structures, Structural Dynamics & Materials Conference, Palm Springs, CA, USA, 19–22 April 2004. [CrossRef]
53. Dano, M.-L.; Hyer, M.W. SMA-induced snap-through of unsymmetric fiber-reinforced composite laminates. *Int. J. Solids Struct.* **2003**, *40*, 5949–5972. [CrossRef]
54. Sinapius, M.; Monner, H.P.; Kintscher, M.; Riemenschneider, J. DLR's morphing wing activities within the European network. *Procedia IUTAM* **2009**, *10*, 416–426. [CrossRef]
55. El Sayed, M.Y.; Oswald, P.; Sattler, S.; Kumar, P.; Radespiel, R.; Behr, C.; Sinapius, M.; Petersen, J.; Wierach, P.; Quade, M.; et al. Open- and closed-loop control investigations of unsteady Coanda actuation on a high-lift configuration. In Proceedings of the 2018 Flow Control Conference, Atlanta, GA, USA, 25–29 June 2018. [CrossRef]
56. Woods, B.K.; Friswell, M.I. The adaptive aspect ratio morphing wing: Design concept and low fidelity skin optimization. *Aerosp. Sci. Technol.* **2015**, *42*, 209–217. [CrossRef]
57. Kaygan, E. Development of an Active Morphing Wing with Novel Adaptive Skin for Aircraft Control and Performance. Ph.D. Thesis, Brunel University London, Uxbridge, UK, 2016. Available online: http://bura.brunel.ac.uk/handle/2438/15224 (accessed on 17 June 2023).
58. Cheung, K.; Cellucci, D.; Copplestone, G.; Cramer, N.; Fusco, J.; Jenett, B.; Kim, J.; Langford, A.; Mazhari, A.; Trinh, G.; et al. Development of Mission Adaptive Digital Composite Aerostructure Technologies (MADCAT). In Proceedings of the 17th AIAA Aviation Technology, Integration, and Operations Conference, 5–9 June 2017. [CrossRef]
59. Jenett, B.; Calisch, S.; Cellucci, D.; Cramer, N.; Gershenfeld, N.; Swei, S.; Cheung, K.C. Digital morphing wing: Active wing shaping concept using composite lattice-based cellular structures. *Soft Robot.* **2017**, *4*, 33–48. [CrossRef]
60. Rivas-Padilla, J.R.; Boston, D.M.; Boddapati, K.; Arrieta, A.F. Aero-structural optimization and actuation analysis of a morphing wing section with embedded selectively stiff bistable elements. *J. Compos. Mater.* **2023**, *57*, 737–757. [CrossRef]
61. Wang, C.; Khodaparast, H.H.; Friswell, M.I.; Shaw, A.D.; Xia, Y.; Walters, P. Development of a morphing wingtip based on compliant structures. *J. Intell. Mater. Syst. Struct.* **2018**, *29*, 3293–3304. [CrossRef]
62. Antcliff, R.R.; McGowan, A.R. Active control technology for enhanced performance operational capabilities of military aircraft, land vehicles and sea vehicles/Active Control Technology NASA Langley Research Centre. In Proceedings of the NATO RTO AVT Symposium, Braunschweig, Germany, 8–11 May 2000.
63. Bothwell, C.; Chandra, R.; Chopra, I. Torsional actuation with extension-torsion composite coupling and a magnetostrictive actuator. *AIAA J.* **1995**, *33*, 723–729. [CrossRef]
64. Duvernier, M.; Reithler, L.; Guerrero, J.; Rossi, R. Active control system for a rotor blade trailing-edge flap. In Proceedings of the SPIE'S 7th Annual International Symposium on Smart Structures and Materials, Newport Beach, CA, USA, 6–9 March 2000; Volume 3985. [CrossRef]
65. Woods, B.; Wereley, N.; Kothera, C. Wind tunnel testing of a helicopter rotor trailing edge flap actuated via pneumatic artificial muscles. In Proceedings of the ASME Conference, on Smart Materials, Adaptive Structures and Intelligent Systems, Philadelphia, PA, USA, 28 September–1 October 2010. [CrossRef]
66. Thepvongs, S. Design and Testing of an Active Gurney Flap Actuator for Helicopter Rotor Blade Control. Bachelor's Thesis, The Pennsylvania State University, University Park, PA, USA, 2002.
67. Thiel, M. Actuation of an Active Gurney Flap for Rotorcraft Applications. Master's Thesis, The Pennsylvania State University, University Park, PA, USA, 2006.
68. Woodgate, M.A.; Pastrikakis, V.A.; Barakos, G.N. Method for calculating rotors with active Gurney flaps. *AIAA J.* **2016**, *53*, 605–626. [CrossRef]
69. Gagliardi, A.; Barakos, G.N. Analysis and design of a flap-equipped low-twist rotor for hover. *J. Aircr.* **2009**, *46*, 251–259. [CrossRef]
70. Kim, J.-S.; Wang, K.W.; Smith, E.C. Development of a resonant trailing-edge flap actuation system for helicopter rotor vibration control. *Smart Mater. Struct.* **2007**, *16*, 2275–2285. [CrossRef]
71. Chia, M.H.; Padtke, A.K.; Duraisamy, K.; Friedmann, P.P. An efficient approach for the simulation and on-blade control of helicopter noise and the impact on vibration. *J. Am. Helicopter Soc.* **2017**, *62*, 042004. [CrossRef]
72. Feinerman, J.A.; Koushik, S.; Schmitz, F.H. Effect of leading-edge serrations on helicopter blade–vortex interaction noise. *J. Am. Helicopter Soc.* **2017**, *62*, 032001. [CrossRef]

73. Palacios, J.; Overmeyer, A.; Smith, E.; Maughmer, M.; Kinzel, M.; Szefi, J. Experimental measurement of unsteady lift and pitching moments for MiTEs on a S903 airfoil. In Proceedings of the 67th American Helicopter Society Forum, Virginia Beach, VA, USA, 3–5 May 2011.
74. Wilbur, M.L.; Yeager, W.T., Jr.; Sekula, M.K. Further examination of the vibratory loads reduction results from the NASA/Army/MIT active twist rotor test. In Proceedings of the 58th Annual Forum of the American Helicopter Society, Montreal, QC, Canada, 11–13 June 2002.
75. Sekula, M.; Wilbur, M.; Yeager, W. A parametric study of the structural design for an advanced active twist rotor. In Proceedings of the 61st American Helicopter Society Forum, Grapevine, TX, USA, 1–3 June 2005.
76. Floros, M.; Johnson, W.; Scully, M. Advanced rotor aerodynamics concepts with application to large rotorcraft. In Proceedings of the AHS Aerodynamics, Acoustics, and Test and Evaluation Technical Specialists Meeting, San Francisco, CA, USA, 23–25 January 2002.
77. Keys, C.; Tarzanin, F.; McHugh, F. Effect of twist on helicopter performance and vibratory loads. In Proceedings of the 13th European Rotorcraft Forum, Arles, France, 8–11 September 1987.
78. Bousman, W. Airfoil design and rotorcraft performance. In Proceedings of the 58th American Helicopter Society Forum, Montreal, QC, Canada, 11–13 June 2002.
79. Leishman, G. *Principles of Helicopter Aerodynamics*; Cambridge University Press: Cambridge, UK, 2006.
80. Mistry, M.; Gandhi, F. Twist control of an I-beam through Vlasov bimoment actuation. In Proceedings of the 49th AIAA/ASME/ASCE/AHS/ASC Structures, Structural Dynamics, and Materials Conference, Schaumburg, IL, USA, 7–10 April 2008. [CrossRef]
81. Takeda, S.; Sugiura, M.; Tanabe, Y.; Sugawara, H.; Kanazaki, M.; Harigae, M. Influence of pre-twist distribution at the rotor blade tip on performance during hovering flight. *Trans. Jpn. Soc. Aeronaut. Space Sci.* **2015**, *58*, 39–44. [CrossRef]
82. Proctor, P. Adaptive Rotor Makes First Flight. *Aviat. Week Space Technol.* **1997**, *146*, 47.
83. Barrett, R.M. Adaptive Aerostructures: Improving High Performance Subscale Military UAVs. Presented at the 45th AIAA/ASME/ASCE/AHS/ASC Structures, Structural Dynamics & Materials Conference, Palm Springs, CA, USA, 19–22 April 2004; AIAA Paper 2004-1886. [CrossRef]
84. Barrett, R. Intelligent Rotor Blade and Structures Development Using Directionally Attached Piezoelectric Crystals. Master's Thesis, University of Maryland, College Park, MD, USA, 1990.
85. Jang, J.; Chopra, I. Ground and air resonance of an advanced bearingless rotor in hover. *J. Am. Helicopter Soc.* **1988**, *33*, 20–29. [CrossRef]
86. Chen, P. Development of a Smart Rotor with Induced-Strain Actuation of Blade Twist. Ph.D. Thesis, University of Maryland, College Park, MD, USA, 1996.
87. Chen, P.; Chopra, I. Wind tunnel test of a smart rotor model with individual blade twist control. *J. Intell. Mater. Syst. Struct.* **1997**, *8*, 414–425. [CrossRef]
88. Rodgers, J. Development of an Integral Twist-Actuated Rotor Blade for Individual Blade Control. Ph.D. Thesis, Massachusetts Institute of Technology, Cambridge, MA, USA, 1999.
89. Shin, S. Integral Twist Actuation of Helicopter Rotor Blades for Vibration Reduction. Ph.D. Thesis, Massachusetts Institute of Technology, Cambridge, MA, USA, 2001.
90. Shin, S.; Cesnik, C.; Hall, S. Integral twist actuation of rotor blades. In Proceedings of the 59th American Helicopter Society Forum, Phoenix, AZ, USA, 6–8 May 2003.
91. Derham, R.; Weems, D.; Mathew, M.B.; Bussom, R. The design evolution of an active materials rotor. In Proceedings of the 57th American Helicopter Society Forum, Washington, DC, USA, 9–11 May 2001.
92. Weems, D.; Anderson, D.; Mathew, M.B.; Bussom, R. A large-scale active twist rotor. In Proceedings of the 60th American Helicopter Society Forum, Baltimore, MD, USA, 7–10 June 2004.
93. Kota, S.; Ervin, G.; Osborn, R.; Ormiston, R. Design and fabrication of an adaptive leading edge rotor blade. In Proceedings of the 64th American Helicopter Society Forum, Montreal, QC, Canada, 29 April–1 May 2008.
94. Shin, S.; Cesnik, C.; Wilkie, W.; Wilbur, M. Design and manufacturing of a model-scale active twist rotor prototype blade. *J. Intell. Mater. Syst. Struct.* **2008**, *19*, 1443–1456. [CrossRef]
95. Wierach, P.; Riemenschneider, J.; Opitz, S.; Hoffmann, F. Experimental investigation of an active twist model rotor blade under centrifugal loads. In Proceedings of the 33rd European Rotorcraft Forum, Kazan, Russia, 11–13 September 2007.
96. Monner, H.P.; Opitz, S.; Riemenschneider, J.; Wierach, P. Evolution of active twist rotor designs at DLR. In Proceedings of the 49th AIAA/ASME/ASCE/AHS/ASC Structures, Structural Dynamics and Materials Conference, Schaumburg, IL, USA, 7–10 April 2008. [CrossRef]
97. Hoffmann, F.; Opitz, S.; Riemenschneider, J. Validation of active twist modeling based on whirl tower tests. In Proceedings of the 65th Annual American Helicopter Society Forum, Grapevine, TX, USA, 27–29 May 2009.

98. Riemenschneider, J.; Opitz, S.; Wierach, P.; des Rochettes, H.M.; Buchaniek, L.; Joly, D. Structural design and testing of active twist blades—A comparison. In Proceedings of the 35th European Rotorcraft Forum, Hamburg, Germany, 22–25 September 2009.
99. Opitz, S.; Riemenschneider, J.; Hoffmann, F.; Schneider, O. Measurement of the dynamic tip twist angle of an active twist model scale rotor blade. In Proceedings of the 36th European Rotorcraft Forum, Paris, France, 7–9 September 2010.
100. Opitz, S.; Riemenschneider, J.; Schulz, M. Prerequisites for the closed loop control of an active twist rotor blade. In Proceedings of the 67th American Helicopter Society Forum, Virginia Beach, VA, USA, 3–5 May 2011.
101. Monner, H.P.; Riemenschneider, J.; Opitz, S.; Schulz, M. Development of active twist rotors at the German Aerospace Center (DLR). In Proceedings of the 52nd AIAA/ASME/ASCE/AHS/ASC Structures, Structural Dynamics and Materials Conference, Denver, CO, USA, 4–7 April 2011. [CrossRef]
102. Sekula, M.K.; Wilbur, M.; Yeager, W. Aerodynamic design study of an advanced active twist rotor, American Helicopter Society. In Proceedings of the 4th Decennial Specialists Conference on Aeromechanics, San Francisco, CA, USA, 21–23 January 2004.
103. Wilbur, M.; Sekula, M. The effect of tip geometry on Active-twist rotor response. In Proceedings of the 61st American Helicopter Society Forum, Grapevine, TX, USA, 1–3 June 2005.
104. Thornburgh, R.; Kreshock, A.; Wilbur, M. Structural optimization of active-twist rotor blades. In Proceedings of the 67th American Helicopter Society Forum, Virginia Beach, VA, USA, 3–5 May 2011.
105. Cesnik, C.; Mok, J.; Morillo, J.; Parikh, A. Design optimization of active twist rotor blades. In Proceedings of the 30th European Rotorcraft Forum, Marseille, France, 14–16 September 2004.
106. Kreshock, A.; Thornburgh, R.; Wilbur, M.; Langston, C.W. Experimental bench testing of an active-twist rotor blade. In Proceedings of the 53rd AIAA/ASME/ASCE/AHS/ASC Structures, Structural Dynamics and Materials Conference, Honolulu, HI, USA, 23–26 April 2012. [CrossRef]
107. Thakkar, D.; Ganguli, R. Induced shear actuation of helicopter rotor blade for active twist control. *J. Thin-Walled Struct.* **2007**, *45*, 111–121. [CrossRef]
108. Bernhard, A.P.F.; Chopra, I. Hover test of Mach-scale active twist rotor using piezo-bending–torsion actuators. *J. Aircr.* **2002**, *39*, 678–688. [CrossRef]
109. Bernhard, A.; Chopra, I. Analysis of a bending-torsion coupled actuator for a smart rotor with active blade tips. *Smart Mater. Struct.* **2001**, *10*, 35–52. [CrossRef]
110. Rochettes, H.M.D.; Joly, D.; Buchaniek, L.; Leconte, P. A new concept of active twist rotor blade applied to main rotor of helicopter. In Proceedings of the RTO Applied Vehicle Technology Panel (AVT) Symposium, Evora, Portugal, 20–24 April 2009.
111. Riemenschneider, J.; Keye, S.; Wierach, P.; des Rochetter, H. Review of the common DLR/ONERA project Active Twist Blade (ATB). In Proceedings of the 30th European Rotorcraft Forum, Marseille, France, 14–16 September 2004; pp. 22.1–22.9.
112. Lake, R.; Nixon, M.; Wilbur, M.; Singleton, J. A demonstration of passive blade twist control using extension-twist coupling. In Proceedings of the 33rd AIAA/ASME/ASCE/AHS/ASC Structures, Structural Dynamics and Materials Conference, Dallas, TX, USA, 13–15 April 1992. [CrossRef]
113. Lake, R.; Nixon, M.; Wilbur, M.; Singleton, J.; Mirick, P. Demonstration of an elastically coupled twist control concept for tilt rotor blade application. In Proceedings of the 33rd AIAA/ASME/ASCE/AHS/ASC Structures, Structural Dynamics and Materials Conference, Dallas, TX, USA, 13–15 April 1992. [CrossRef]
114. Nampy, S. Structural Behavior and Design of Flexible Matrix Composite Box Beams with Extension Twist Coupling. Master's Thesis, The Pennsylvania State University, University Park, PA, USA, August 2005.
115. Kosmatka, J.; Lake, R. Extension-twist behavior of initially twisted composite spars for tilt-rotor applications. In Proceedings of the 37th AIAA/ASME/ASCE/AHS/ASC Structures, Structural Dynamics and Materials Conference, Salt Lake City, UT, USA, 15–17 April 1996. [CrossRef]
116. DiOttavio, J.; Friedmann, D. Operational benefits of an optimal, widely variable speed rotor. In Proceedings of the 66th American Helicopter Society Forum, Phoenix, AZ, USA, 11–13 May 2010.
117. Guo, W. Flight Control Design for Rotorcraft with Variable Rotor Speed. Ph.D. Thesis, The Pennsylvania State University, University Park, PA, USA, December 2009.
118. Steiner, J.; Gandhi, F.; Yoshizaki, Y. An investigation of variable rotor RPM on performance and trim. In Proceedings of the AHS 64th Annual Forum, Montreal, QC, Canada, 29 April–1 May 2008.
119. Mistry, M.; Gandhi, F. Performance improvement with variable rotor span and RPM. In Proceedings of the 66th Annual AHS Forum, Phoenix, AZ, USA, 11–13 May 2010.
120. Bowen-Davies, G.; Chopra, I. Aeromechanics of a variable-speed rotor. In Proceedings of the 67th American Helicopter Society Forum, Virginia Beach, VA, USA, 3–5 May 2011.
121. Berry, B.; Chopra, I. Wind tunnel testing for performance and vibratory loads of a variable-speed mach-scale rotor. In Proceedings of the 67th American Helicopter Society Forum, Virginia Beach, VA, USA, 3–5 May 2011.
122. Datta, A.; Yeo, H.; Norman, T. Experimental investigation and fundamental understanding of a slowed UH-60A rotor at high advance ratios. In Proceedings of the 67th American Helicopter Society Forum, Virginia Beach, VA, USA, 3–5 May 2011.

123. Berry, B.; Chopra, I. Performance and vibratory load measurements of a slowed-rotor at high advance ratios. In Proceedings of the 68th American Helicopter Society Forum, Fort Worth, TX, USA, 1–3 May 2012.
124. Clingman, D.J.; Jacot, D. Shape memory alloy consortium and demonstration. In Proceedings of the SPIE Smart Structures and Materials Conference, Newport Beach, CA, USA, 7 March 2000. [CrossRef]
125. Ruggeri, R.; Jacot, D.; Clingman, D. Shape memory actuator systems and the use of thermoelectric modules. In Proceedings of the SPIE Smart Structures and Materials Conference, San Diego, CA, USA, 18 March 2002. [CrossRef]
126. Caldwell, N.; Gutmark, E. Performance predictions of a blade twist actuator system. In Proceedings of the 45th AIAA Aerospace Sciences Meeting and Exhibit, Reno, NV, USA, 8–11 January 2007. [CrossRef]
127. Arbogast, D.; Ruggeri, R.; Bussom, R. Development of a 1/4th -scale NiTinol actuator for reconfigurable structures. In Proceedings of the SPIE Industrial and Commercial Applications of Smart Structures Technologies, San Diego, CA, USA, 9–13 March 2008; Volume 6930. [CrossRef]
128. Ruggeri, R.; Arbogast, D.; Bussom, R. Wind tunnel testing of a lightweight 1/4th -scale actuator utilizing shape memory alloy. In Proceedings of the 49th AIAA/ASME/ASCE/AHS/ASC Structures, Structural Dynamics, and Materials Conference, Schaumburg, IL, USA, 7–10 April 2008. [CrossRef]
129. Prahlad, H.; Chopra, I. Design of a variable twist tiltrotor blade using shape memory alloys (SMA) actuators. In Proceedings of the SPIE Smart Structures and Materials Conference, Newport Beach, CA, USA, 5 March 2001. [CrossRef]
130. Prahlad, H. Development of Shape Memory Alloy (SMA) Torsional Actuators for Variable Twist Tilt Rotor (VTTR) Blades. Ph.D. Thesis, University of Maryland, College Park, MD, USA, 2002.
131. Park, J.; Kim, S.; Jung, S.N. Application of shape memory alloy hybrid composites for variable-twist proprotors. In Proceedings of the 66th American Helicopter Society Forum, Phoenix, AZ, USA, 11–13 May 2010.
132. Mistry, M. Induced Warp Systems to Obtain Active Twist of Rotor Blades. Master's Thesis, The Pennsylvania State University, University Park, PA, USA, 2008.
133. Van Weddingen, Y.; Bauchau, O.; Kottapalli, S.; Ozbay, S.; Mehrotra, Y. Application of out-of-plane warping to control rotor blade twist. In Proceedings of the American Helicopter Society Aeromechanics Specialists Conference, San Francisco, CA, USA, 20–22 January 2010.
134. Linden, A.W.; Beck, D.; D'Onofrio, M.; Flemming, R.; Hibyan, E.; Johnston, R.A.; Murrill, R.J.; Unsworth, D.K.; Bausch, W.E. *Variable Diameter Rotor Study*; Tech. Rep. AFFDL-TR-71-170; Air Force Flight Dynamics Laboratory, Wright-Patterson AFB: Dayton, OH, USA, 1972.
135. Fenny, C. Mechanism for varying the diameter of rotors using compound differential rotary transmissions. In Proceedings of the 61st American Helicopter Society Forum, Grapevine, TX, USA, 13 June 2005.
136. Segel, R.M.; Fradenburgh, E.A. Development of the TRAC variable diameter rotor concept. In Proceedings of the AIAA/AHS VTOL Research, Design, and Operations Meeting, Atlanta, GA, USA, 17–19 February 1969. [CrossRef]
137. Fradenburgh, E.A.; Murrill, R.J.; Kiely, E. *Dynamic Model Wind Tunnel Tests of a Variable Diameter, Telescoping-Blade Rotor System (TRAC Rotor)*; Tech. Rep. USAAMRDL-TR-73-32; Sikorsky Aircraft: Newport News, VA, USA, 1973. [CrossRef]
138. Fradenburgh, E.A. Application of a variable diameter rotor system to advanced VTOL aircraft. In Proceedings of the 31st American Helicopter Society Forum, Washington, DC, USA, 13–15 May 1975.
139. Fradenburgh, E.A.; Hager, L.; Kefford, N. *Evaluation of the TRAC Variable-Diameter Rotor: Preliminary Design of a Full-Scale Rotor and Parametric Mission Analysis Comparison*; Tech. Rep. USAAMRDL-TR-75-54; Sikorsky Aircraft: Newport News, VA, USA, 1976.
140. Frint, H. *Design Selection Tests for TRAC Retraction Mechanism*; Tech. Rep. USAAMRDL-TR-76-43; Sikorsky Aircraft: Newport News, VA, USA, 1977.
141. Fradenburgh, E.A.; Matuska, D.G. dvancing tiltrotor state-of-the-art with variable diameter rotors. In Proceedings of the 48th American Helicopter Society Forum, Washington, DC, USA, 3–5 June 1992.
142. Studebaker, K.; Matuska, D.G. Variable diameter tiltrotor wind tunnel test results. In Proceedings of the 49th American Helicopter Society Forum, St. Louis, MO, USA, 19–21 May 1993.
143. Turmanidze, R.S.; Khutsishvili, S.N.; Dadone, L. Design and experimental investigation of variable geometry rotor concepts. In Proceedings of the Adaptive Structures and Materials Symposium, IMECE, New York, NY, USA, 11–16 November 2001.
144. Turmanidze, R.S.; Dadone, L. New design of a variable geometry prop-rotor with cable and hydraulic system actuation. In Proceedings of the 66th American Helicopter Society Forum, Phoenix, AZ, USA, 11–13 May 2010.
145. Prabhakar, T.; Gandhi, F.; Steiner, J.; McLaughlin, D. A centrifugal force actuated variable span morphing helicopter rotor. In Proceedings of the AHS 63rd Annual Forum, Virginia Beach, VA, USA, 1–3 May 2007.
146. Prabhakar, T. A Centrifugal Force Actuated Morphing Rotor. Master's Thesis, The Pennsylvania State University, University Park, PA, USA, 2007.
147. Mistry, M. Quasi-Static Rotor Morphing Concepts for Rotorcraft Performance Improvements. Ph.D. Thesis, The Pennsylvania State University, University Park, PA, USA, 2012.

148. Wang, J.M.; Jones, C.T.; Nixon, M.W. A variable diameter short haul civil tiltrotor. In Proceedings of the 55th Annual Forum of the American Helicopter Society, Montreal, QC, Canada, 25–27 May 1999.
149. Vocke, R.D., III; Kothera, C.S.; Wereley, N.M. Development of a span-extending blade tip system for a reconfigurable helicopter rotor. In Proceedings of the 53rd AIAA/ASME/ASCE/AHS/ASC Structures, Structural Dynamics, and Materials Conference, Honolulu, HI, USA, 23–26 April 2012. AIAA Paper 2012-1664. [CrossRef]
150. Léon, O.; Hayden, E.; Gandhi, F. Rotorcraft operating envelope expansion using extendable chord sections. In Proceedings of the American Helicopter Society 65th Annual Forum, Grapevine, TX, USA, 27–29 May 2009.
151. Moser, P.R.; Barbarino, S.; Gandhi, F. Helicopter rotor blade chord extension morphing using a centrifugally actuated bi-stable von-Mises truss. *J. Aircr.* **2014**, *51*, 1422–1431. [CrossRef]
152. Barbarino, S.; Gandhi, F.; Webster, S. Design of extendable chord sections for morphing helicopter rotor blades. *J. Intell. Mater. Syst. Struct.* **2011**, *22*, 891–905. [CrossRef]
153. Khoshlahjeh, M.; Gandhi, F. Extendable chord rotors for helicopter envelope expansion and performance improvement. *J. Am. Helicopter Soc.* **2014**, *59*, 012007. [CrossRef]
154. Hayden, E. Design and Testing of a Helicopter Rotor Blade Chord Extension System. Master's Thesis, The Pennsylvania State University, University Park, PA, USA, 2012.
155. Barbarino, S.; Gandhi, F.S.; Visdeloup, R. A bi-stable von-Mises truss for morphing applications actuated using shape memory alloys. In Proceedings of the ASME 2013 Conference, on Smart Materials, Adaptive Structures and Intelligent Systems (SMASIS2013), Snowbird, UT, USA, 16–18 September 2013; Paper No. SMASIS2013-3062. [CrossRef]
156. Barbarino, S.; Gandhi, F.S. A cellular frame for morphing applications based on bi-stable von-Mises trusses actuated using shape memory alloys. In Proceedings of the AIAA SciTech Forum and Exposition, National Harbor, MD, USA, 13–17 January 2014; p. 1736921. [CrossRef]
157. Buter, A.; Ehlert, C.; Sachau, U.D.; Breitbach, E. Adaptive rotor blade concepts—Direct twist and camber variation. In Proceedings of the RTO AVT Symposium on Active Control Technology for Enhanced Performance Operational Capabilities of Military Aircraft, Land Vehicles and Sea Vehicles, Braunschweig, Germany, 8–11 May 2000.
158. Anusonti-Inthra, P.; Sarjeant, R.; Frecker, M.; Gandhi, F. Design of a conformable rotor airfoil using distributed piezoelectric actuators. *AIAA J.* **2005**, *43*, 1684–1695. [CrossRef]
159. Nissly, A.; Anusonti-Inthra, P.; Gandhi, F.; Frecker, M. Design optimization of a controllable camber rotor airfoil. In Proceedings of the 61st American Helicopter Society Forum, Grapevine, TX, USA, 1–3 July 2005.
160. Kammegne, M.J.T.; Grigorie, L.T.; Botez, R.M.; Koreanschi, A. Design and wind tunnel experimental validation of a controlled new rotary actuation system for a morphing wing application. *Proc. Inst. Mech. Eng. Part G J. Aerosp. Eng.* **2016**, *230*, 132–145. [CrossRef]
161. Martin, P.; McAlister, K.; Chandrasekhara, M.; Geissler, W. Dynamic stall measurements and computations for a VR-12 airfoil with a variable droop leading edge. In Proceedings of the 59th American Helicopter Society Forum, Phoenix, AZ, USA, 6–8 May 2003.
162. Shaner, M.; Chopra, I. Design and testing of a piezostack actuated leading-edge flap. In Proceedings of the SPIE Symposium on Smart Structures and Materials, Newport Beach, CA, USA, 1 March 1999; Volume 3668.
163. Fink, D.; Reinhardt, N.; Severance, R.; Phillips, R.; Gaudreau, M.; Ormiston, R. Deformable leading edge electromagnetic airfoil. In Proceedings of the 63rd American Helicopter Society Forum, Virginia Beach, VA, USA, 1–3 May 2007.
164. Guo, W.; Horn, J. Helicopter flight control with variable rotor speed and torque limiting. In Proceedings of the 65th Annual American Helicopter Society Forum, Grapevine, TX, USA, 27–29 May 2009.
165. Rauleder, J.; Wall, B.; Abdelmoula, A.; Komp, D.; Kumar, S.; Ondra, V.; Titurus, B.; Woods, B. Aerodynamic performance of morphing blades and rotor systems. In Proceedings of the 74th Annual American Helicopter Society International Forum and Technology Display 2018 (FORUM 74): The Future of Vertical Flight, Phoenix, AZ, USA, 14–17 May 2018. [CrossRef]
166. Woods, B.K.S.; Bilgen, O.; Friswell, M.I. Wind tunnel testing of the Fish Bone Active Camber morphing concept. *J. Intell. Mater. Syst. Struct.* **2014**, *25*, 772–785. [CrossRef]
167. Barbarino, S.; Bilgen, O.; Ajaj, R.M.; Friswell, M.I.; Inman, D.J. A review of morphing aircraft. *J. Intell. Mater. Syst. Struct.* **2011**, *22*, 823–877. [CrossRef]
168. Martin, S.; Hall, G. Rotor Will Retract in Flight to Improve V/STOL Cruise Performance. *Space Aeronaut.* **1969**, *52*, 72.
169. Spangler, R.L.; Hall, S.R. Piezoelectric actuators for helicopter rotor control. In Proceedings of the 31st AIAA/ASME/ASCE/AHS/ASC Structures, Structural Dynamics and Materials Conference, Long Beach, CA, USA, 24 April 1990; AIAA1990-1076. [CrossRef]
170. Fenn, R.C.; Downer, J.R.; Bushko, D.A.; Gondhalekar, V.; Ham, N.D. Terfenol-D-Driven Flaps for Helicopter Vibration Reduction. In Proceedings of the Smart Structures and Materials 1993: Smart Structures and Intelligent Systems, Bellingham, WA, USA, 8 September 1993; Proc. SPIE 1917. [CrossRef]
171. Barrett, R. Active aeroelastic tailoring of an adaptive Flexspar stabilator. *Smart Mater. Struct.* **1996**, *5*, 723–730. [CrossRef]

172. Brender, S.; Mark, H.; Aguilera, F. *The Attributes of a Variable-Diameter Rotor System Applied to Civil Tiltrotor Aircraft*; NASA Contractor Report, NASA-CR-203092; Ames Research Center: Mountain View, CA, USA, 1997.
173. Barrett, R.M. Convertible Vertical Take-Off and Landing Miniature Aerial Vehicle. US Patent 6,502,787,22, 22 February 2002.
174. Barbarino, S.; Gandhi, F.; Webster, S.D. Design of Extendable Chord Sections for Morphing Helicopter Rotor Blades. In Proceedings of the ASME 2010 Conference on Smart Materials, Adaptive Structures and Intelligent Systems, Philadelphia, PA, USA, 28 September–1 October 2010; pp. 323–336. [CrossRef]
175. Khoshlahjeh, M.; Bae, E.S.; Gandhi, F. Helicopter Performance Improvement with Variable Chord Morphing Rotors. In Proceedings of the 36th European Rotorcraft Forum, Paris, France, 7–9 September 2010.
176. Xiong, J.; Nguyen, N.; Cramer, N.B. Acoustic optimization for anti-phase asymmetric rotor. In *Proceedings of the 2020 AIAA SciTech Forum, Orlando, FL, USA, 6–10 January 2020*; American Institute of Aeronautics and Astronautics: Reston, VA, USA, 2020; Paper No. 2020-1496.
177. Koning, W.J.F.; Perez Perez, N.; Cummings, H.V.; Nagata, T.; Kanzaki, Y.; Kasai, M.; Miyagi, M.; Nonomura, T.; Asai, K.; Caros, L.; et al. *Experimental Results for Mars Rotorcraft Airfoils (roamx-0201 and clf5605) at Low Reynolds Number and Compressible Flow in a Mars Wind Tunnel*; NASA Technical Memorandum; NASA: Washington, DC, USA, 2024; NASA/TM-20240004230.
178. Ajaj, R.M.; Parancheerivilakkathil, M.S.; Amoozgar, M.; Friswell, M.I.; Cantwell, W.J. Recent Developments in the Aeroelasticity of Morphing Aircraft. *Prog. Aerosp. Sci.* **2021**, *120*, 100682. [CrossRef]
179. Bent, A.; Hagood, N. Piezoelectric fiber composites with interdigitated electrodes. *J. Intell. Mater. Syst. Struct.* **1997**, *8*, 903–919. [CrossRef]
180. Huang, Q.; Abdelmoula, A.; Chourdakis, G.; Rauleder, J.; Uekermann, B. CFD/CSD coupling for an isolated rotor using precice. In Proceedings of the 14th World Congress on Computational Mechanics (WCCM), ECCOMAS Congress, Virtual, 11–15 January 2021. [CrossRef]
181. Crawley, E.F.; De Luis, L. Use of piezoelectric actuators as elements of intelligent structures. *AIAA J.* **1987**, *25*, 10. [CrossRef]
182. Szyszko, S. Feasibility of FishBAC Morphing Camber Technology in Fixed Wing UAV Applications. Master's Thesis, School of Civil, Aerospace and Design Engineering, University of Bristol, Bristol, UK, 23 January 2024.
183. Wong, A.; Bil, C.; Marino, M. Design and Aerodynamic Performance of a FishBAC Morphing Wing. In *Proceedings of the AIAA SCITECH 2022 Forum, San Diego, CA, USA, 3–7 January 2022*; American Institute of Aeronautics and Astronautics: Reston, VA, USA, 2022; Paper No. AIAA-2022-1298. [CrossRef]
184. Fincham, J.H.S.; Ajaj, R.M.; Friswell, M.I. Aerodynamic performance of corrugated skins for spanwise wing morphing. In *Proceedings of the AIAA AVIATION 2014 – 14th AIAA Aviation Technology, Integration, and Operations Conference, Atlanta, GA, USA, 16–20 June 2014*; American Institute of Aeronautics and Astronautics: Reston, VA, USA, 2014; Paper No. AIAA-2014-2724. [CrossRef]
185. Skillen, M.D.; Crossley, W.A. *Modeling and Optimization for Morphing Wing Concept Generation II Part I: Morphing Wing Modeling and Structural Sizing Techniques*; NASA Report, NASA/CR-2008-214902; NASA: Washington, DC, USA, 2008.
186. Bourdin, P.; Gatto, A.; Friswell, M.I. Potential of Articulated Split Wingtips for Morphing-Based Control of Flying Wing. In Proceedings of the 25th AIAA Applied Aerodynamics Conference, Miami, FL, USA, 25–28 June 2007; Paper No. AIAA 2007-4443.
187. Bourdin, P.; Gatto, A.; Friswell, M.I. Aircraft Control via Variable Cant-Angle Winglets. *J. Aircr.* **2008**, *45*, 414–423. [CrossRef]
188. Bourdin, P.; Gatto, A.; Friswell, M.I. Performing Co-Ordinated Turns with Articulated Wing Tips as Multi-Axis Control Effectors. *Aeronaut. J.* **2010**, *114*, 35–47. [CrossRef]
189. Liao, Y.; Krishnan, S. Deployable Scissor Structures: Classification of Modifications and Applications. *Autom. Constr.* **2024**, *165*, 105547. [CrossRef]
190. Andersen, G.R.; Cowan, D.L.; Piatak, D.J. Aeroelastic Modeling, Analysis and Testing of a Morphing Wing Structure. In *Proceedings of the 48th AIAA/ASME/ASCE/AHS/ASC Structures, Structural Dynamics and Materials Conference, Honolulu, HI, USA, 23–26 April 2007*; AIAA: Reston, VA, USA, 2007; Paper No. AIAA-2007-1734. [CrossRef]
191. Manzo, J.; Garcia, E. Demonstration of an In Situ Morphing Hyperelliptical Cambered Span Wing Mechanism. *Smart Mater. Struct.* **2010**, *19*, 025012. [CrossRef]
192. Bharti, S.; Frecker, M.I.; Lesieutre, G.; Browne, J. Tendon Actuated cellular Mechanisms for Morphing Aircraft Wing. In Proceedings of the SPIE Modeling, Signal Processing, and Control for Smart Structures, San Diego, CA, USA, 19 March 2007; Volume 6523. [CrossRef]
193. Supekar, A.H. Design, Analysis and Development of a Morphable Wing Structure for Unmanned Aerial Vehicle Performance Augmentation. Master's Thesis, University of Texas, Arlington, TX, USA, 2007.
194. Gamboa, P.; Vale, J.; Lau, F.J.P.; Suleman, A. Optimization of a Morphing Wing Based on Coupled Aerodynamic and Structural Constraints. *AIAA J.* **2009**, *47*, 2087–2104. [CrossRef]
195. Kress, R.W. Variable Sweep Wing Design. In *Proceedings of the Aircraft Prototype and Technology Demonstrator Symposium, Dayton, OH, USA, 23–24 March 1983*; AIAA: Reston, VA, USA, 1983; Paper No. AIAA-1983-1051.

196. Mattioni, F.; Gatto, A.; Weaver, P.M.; Friswell, M.I.; Potter, K.D. The Application of Residual Stress Tailoring of Snap-through Composites for Variable Sweep Wings. In *Proceedings of the 47th AIAA/ASME/ASCE/AHS/ASC Structures, Structural Dynamics, and Materials Conference, Newport, RI, USA, 1–4 May 2006*; AIAA: Reston, VA, USA, 2006; Paper No. AIAA 2006-1972.
197. Amprikidis, M.; Cooper, J.E. Development of Smart Spars for Active Aeroelastic Structures. In Proceedings of the 44th AIAA/ASME/ASCE/AHS Structures, Structural Dynamics, and Materials Conference, Norfolk, VA, USA, 7–10 April 2003; AIAA 2003 1799. [CrossRef]
198. Arrison, L.; Birocco, K.; Gaylord, C.; Herndon, B.; Manion, K.; Metheny, M. *2002–2003 AE/ME Morphing Wing Design*; Virginia Tech Aerospace Engineering Senior Design Project Final Report; Virginia Tech: Blacksburg, VA, USA, 2003. Available online: https://archive.aoe.vt.edu/mason/Mason_f/AEMEMorph03FinalRpt.pdf (accessed on 16 January 2023).
199. Blondeau, J.; Richeson, J.; Pines, D.J. Design, Development and Testing of a Morphing Aspect Ratio Wing Using an Inflatable Telescopic Spar. In *Proceedings of the 44th AIAA/ASME/ASCE/AHS/ASC Structures, Structural Dynamics and Materials Conference, Norfolk, VA, USA, 7–10 April 2003*; AIAA: Reston, VA, USA, 2003. [CrossRef]
200. Sullivan, J.; Watkins, W. *Obliquing Wing with Extendable Span Critical Design Review*; Critical Design Review, AAE 490T/590T AT 490D Tech 581N Design/Build/Test; Purdue University: West Lafayette, IN, USA, 2003.
201. Neal, D.A.; Good, M.G.; Johnston, C.O.; Robertshaw, H.H.; Mason, W.H.; Inman, D.J. Desing and Wind-Tunnel Analysis of a Fully Adaptive Aircraft Configuration. In Proceedings of the 45th AIAA/ASME/ASCE/AHS/ASC Structures, Structural Dynamics, and Materials Conference, Palm Springs, CA, USA, 19–22 April 2004; AIAA 2004-1727. [CrossRef]
202. Neal, D.A.; Farmer, J.; Inman, D.J. Development of a Morphing Aircraft Model for Wind Tunnel Experimentation. In Proceedings of the 47th AIAA/ASME/ASCE/AHS/ASC Structures, Structural Dynamics, and Materials Conference, Newport, RI, USA, 1–4 May 2006; AIAA 2006-2141. [CrossRef]
203. Bae, J.-S.; Seigler, T.M.; Inman, D.J. Aerodynamic and Static Aeroelastic Characteristics of a Variable-Span Morphing Wing. *J. Aircr.* **2005**, *42*, 528–534. [CrossRef]
204. Heryawan, Y.; Park, H.C.; Goo, N.S.; Yoon, K.J.; Byun, Y.H. Design and Demonstration of a Small Expandable Morphing Wing. In Proceedings of the SPIE 12th Annual International Symposium on Smart Structures and Materials, San Diego, CA, USA, 6–10 March 2005; Volume 5764, pp. 224–231. [CrossRef]
205. Vale, J.; Lau, F.; Suleman, A.; Gamboa, P. Multidisciplinary Design Optimization of a Morphing Wing for an Experimental UAV. In Proceedings of the 11th AIAA/ISSMO Multidisciplinary Analysis and Optimization Conference, Portsmouth, VA, USA, 6–8 September 2006; AIAA 2006-7131. [CrossRef]
206. Gamboa, P.; Aleixo, P.; Vale, J.; Lau, F.; Suleman, A. *Design and Testing of a Morphing Wing for an Experimental UAV*; RTO-MP-AVT-146; NATO Research and Technology Organization: Neuilly-sur-Seine, France, 2007.
207. Bye, D.R.; McClure, P.D. Design of a Morphing Vehicle. In Proceedings of the 48th AIAA/ASME/ASCE/AHS/ASC Structures, Structural Dynamics, and Materials Conference, Honolulu, HI, USA, 23–26 April 2007; AIAA 2007-1728; p. 16. [CrossRef]
208. Ivanco, T.G.; Scott, R.C.; Love, M.H.; Zink, S.; Weisshaar, T.A. Validation of the Lockheed Martin Morphing Concept with Wind Tunnel Testing. In Proceedings of the 48th AIAA/ASME/ASCE/AHS/ASC Structures, Structural Dynamics, and Materials Conference, Honolulu, HI, USA, 23–26 April 2007; AIAA 2007-2235; p. 17. [CrossRef]
209. Love, M.H.; Zink, P.S.; Stroud, R.L.; Bye, D.R.; Rizk, S.; White, D. Demonstration of Morphing Technology through Ground and Wind Tunnel Tests. In Proceedings of the 48th AIAA/ASME/ASCE/AHS/ASC Structures, Structural Dynamics, and Materials Conference, Honolulu, HI, USA, 23–26 April 2007; AIAA 2007-1729. p. 12. [CrossRef]
210. Yu, Y.; Li, X.; Zhang, W.; Leng, J. Investigation on Adaptive Wing Structure based on Shape Memory Polymer Composite Hinge. In Proceedings of the SPIE International Conference on Smart Materials and Nanotechnology in Engineering, Harbin, China, 1 July 2007; Volume 6423. [CrossRef]
211. Grady, B. Multi-Objective Optimization of a Three Cell Morphing Wing Substructure. Master's Thesis, University of Dayton, Dayton, OH, USA, 2010.
212. Perkins, D.A.; Reed, J.L.; Havens, E. Morphing Wing Structures for Loitering Air Vehicles. In Proceedings of the 45th AIAA/ASME/ASCE/AHS/ASC Structures, Structural Dynamics & Materials Conference, Palm Springs, CA, USA, 19–22 April 2004; AIAA 2004-1888; p. 10. [CrossRef]
213. Miller, G.D. *Active Flexible Wing (AFW) Technology*; AFWAL-TR-87-3096; Rockwell International North American Aircraft Operations: Los Angeles, CA, USA, 1988.
214. Kuzmina, S.; Gennadi, A.; Schweiger, J.; Cooper, J.; Amprikidis, M.; Sensberg, O. Review and Outlook on Active and Passive Aeroelastic Design Concepts for Future Aircraft. In Proceedings of the International Congress of the Aeronautical Sciences (ICAS 2002), Toronto, ON, Canada, 8–13 September 2002; pp. 432.1–432.10.
215. Florance, J.R.; Heeg, J.; Spain, C.V.; Lively, P.S. Variable Stiffness Spar Wind-Tunnel Modal Development and Testing. In Proceedings of the 45th AIAA/ASME/ASCE/AHS/ASC Structures, Structural Dynamics and Materials Conference, Palm Springs, CA, USA, 19–22 April 2004; AIAA 2004-1588; p. 11. [CrossRef]

216. Sahoo, D.; Cesnik, C.E.S. Roll Maneuver Control for UCAV Wing Using Anisotropic Piezoelectric Actuators. In Proceedings of the 43rd AIAA/ASME/ASCE/AHS/ASC Structures, Structural Dynamics and Materials Conference, Denver, CO, USA, 22–25 April 2002; AIAA 2002-1720; p. 11. [CrossRef]
217. Martin, C.A.; Kudva, J.; Austin, F.; Jardine, A.P.; Scherer, L.B.; Lockyer, A.J.; Carpenter, B.F. *Smart Materials and Structures-Smart Wing Volumes I, II, III, and IV*; AFRL-ML-WP-TR-1999-4162; Northrop Corporation: Hawthorne, CA, USA; Grumman: West Falls Church, VA, USA, 1998.
218. Gatto, A. Development of a morphing UAV for optimal multi-segment mission performance. *Aeronaut. J.* **2023**, *127*, 1320–1352. [CrossRef]
219. Elzey, D.M.; Sofla, A.Y.N.; Wadley, H.N.G. A Bio Inspired, High-Authority Actuator for Shape Morphing Structures. In *Proceedings of SPIE, Smart Structures and Materials 2003: Active Materials: Behavior and Mechanics, San Diego, CA, USA, 13 August 2003*; Logoudas, D.C., Ed.; SPIE: Bellingham, WA, USA, 2003; Volume 5053, pp. 92–100. [CrossRef]
220. Abdulrahim, M.; Lind, R. Flight Testing and Response Characteristics of a Variable Gull-Wing Morphing Aircraft. In Proceedings of the AIAA Guidance, Navigation, and Control Conference and Exhibit, Providence, RI, USA, 16–19 August 2003; AIAA 2004-5113; pp. 1664–1679. [CrossRef]
221. Gatto, A.; Bourdin, P.; Friswell, M.I. Experimental Investigation into Articulated Winglet Effects on Flying Wing Surface Pressure Aerodynamics. *J. Aircr.* **2010**, *47*, 1811–1815. [CrossRef]
222. Garcia, H.M.; Abdulrahim, M.; Lind, R. Roll Control for a Micro Air Vehicle Using Active Wing Morphing. In Proceedings of the AIAA Guidance, Navigation, and Control Conference Exhibit, Austin, TX, USA, 11–14 August 2003; p. 10. [CrossRef]
223. Shkarayev, S.; Null, W.; Wagner, M. *Development of Micro Air Vehicle Technology with In-Flight Adaptive Wing Structure*; Contractor Report; NASA/CR-2004-213271; NASA Langley Research Center: Hampton, VA, USA, 2004.
224. Bilgen, O.; Kochersberger, K.B.; Inman, D.J. Macro Fiber Composite Actuated Simply-Supported Thin Morphing Airfoils. *Smart Mater. Struct.* **2010**, *19*, 055010. [CrossRef]
225. Rea, F.; Pecora, R.; Amoroso, F.; Arena, M.; Noviello, M.C.; Amendola, G. Aeroelastic stability analysis of a wind tunnel wing model equipped with a true scale morphing aileron. *Int. J. Mech. Eng. Robot. Res.* **2017**, *6*, 440–450. [CrossRef]
226. Livne, E.; Precup, N.; Mor, M. Design, construction, and tests of an aeroelastic wind tunnel model of a variable camber continuous trailing edge flap (VCCTEF) concept wing. In Proceedings of the 32nd AIAA Applied Aerodynamics Conference, Atlanta, GA, USA, 16–20 June 2014. [CrossRef]
227. Wilson, T.; Kirk, J.; Hobday, J.; Castrichini, A. Small scale flying demonstration of semi aeroelastic hinged wing tips. In Proceedings of the International Forum on Aeroelasticity and Structural Dynamics, IFASD 2019, Savannah, GA, USA, 9–13 June 2019.
228. Cramer, N.B.; Cellucci, D.W.; Formoso, O.B.; Gregg, C.E.; Jenett, B.E.; Kim, J.H.; Lendraitis, M.; Swei, S.S.; Trinh, G.T.; Trinh, K.V. Elastic Shape Morphing of Ultralight Structures by Programmable Assembly. *Smart Mater. Struct.* **2019**, *28*, 055006. [CrossRef]
229. Jodin, G.; Scheller, J.; Duhayon, E.; Rouchon, J.F.; Braza, M. Implementation of a hybrid electro-active actuated morphing wing in wind tunnel. *Solid State Phenom.* **2017**, *260*, 85–91. [CrossRef]